AD-A077 292 UTAH UNIV SALT LAKE CITY DEPT OF METEOROLOGY F/G 4/2
ANALYZE, CALCULATE, AND DEVELOP TECHNIQUES FOR WEATHER SATELLIT--ETC(U)
JUN 79 E G ASTLING , K LIOU F19628-78-C-0130
UNCLASSIFIED AFGL-TR-79-0140 NL

1 OF 2
AD
A077292

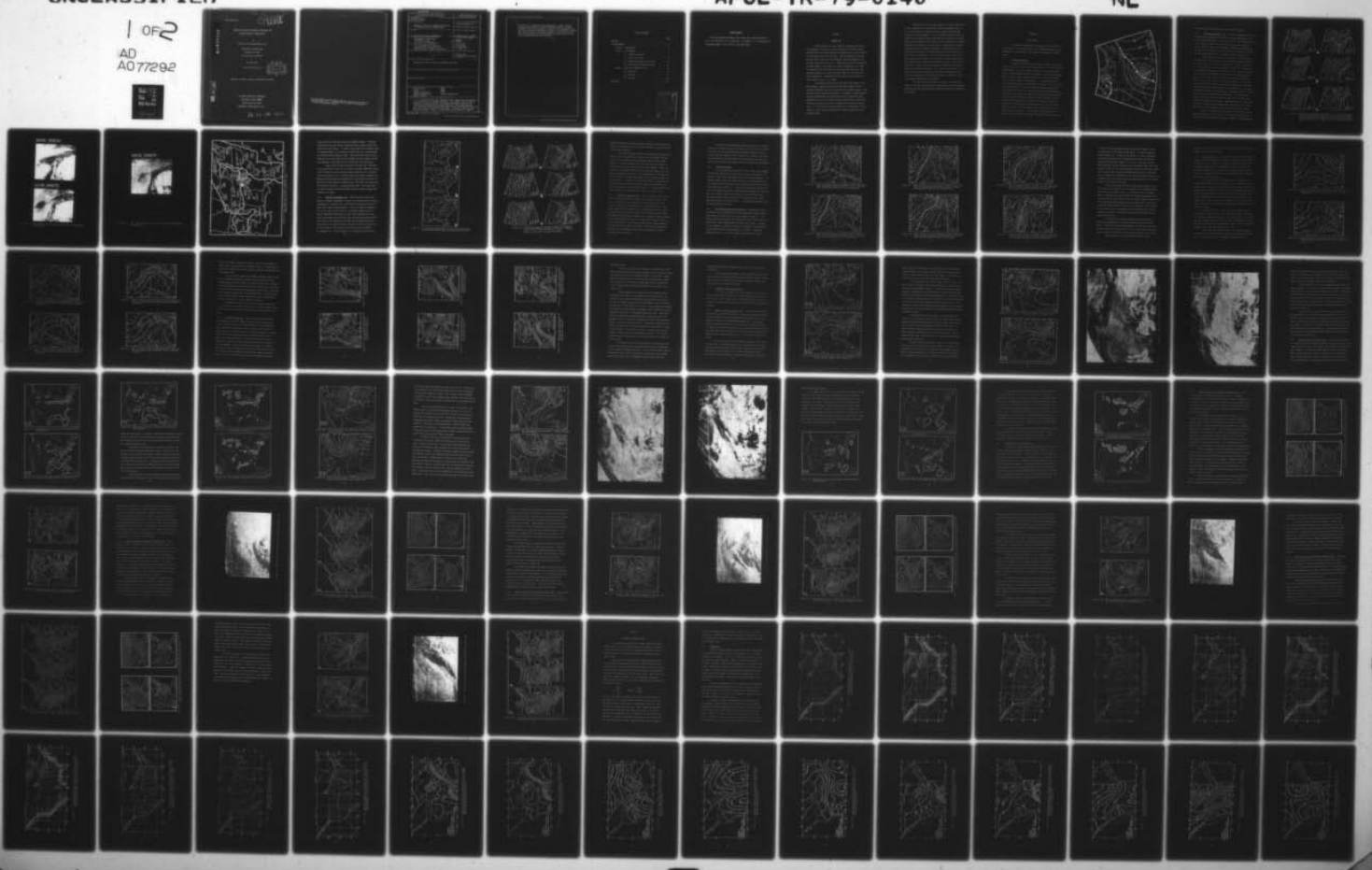

AFGL-TR-79-0140

(12) LEVEL II

AD A077292

ANALYZE, CALCULATE AND DEVELOP TECHNIQUES FOR WEATHER SATELLITE IMAGERY DATA

by

Elford G. Astling and Kuo-Nan Liou

Department of Meteorology

University of Utah

Salt Lake City, Utah 84112

15 June 1979

Scientific Report No. 1

Approved for public release; distribution unlimited

AIR FORCE GEOPHYSICS LABORATORY

AIR FORCE SYSTEMS COMMAND

UNITED STATES AIR FORCE

HANSCOM AFB, MASSACHUSETTS 01731

Unclassified

SECURITY CLASSIFICATION OF THIS PAGE (When Data Entered)

REPORT DOCUMENTATION PAGE	READ INSTRUCTIONS BEFORE COMPLETING FORM
1. REPORT NUMBER: AFGL-TR-79-0140	2. GOVT ACCESSION NO. / 3. RECIPIENT'S CATALOG NUMBER
4. TITLE (and Subtitle): Analyze, Calculate, and Develop Techniques for Weather Satellite Imagery Data.	5. TYPE OF REPORT & PERIOD COVERED: Scientific Report No. 1
	6. PERFORMING ORG. REPORT NUMBER
7. AUTHOR(s): Elford G. Astling, Kuo-Nan Liou	8. CONTRACT OR GRANT NUMBER(s): F19628-78-C-0130
9. PERFORMING ORGANIZATION NAME AND ADDRESS: Department of Meteorology, University of Utah, Salt Lake City, Utah 84112	10. PROGRAM ELEMENT, PROJECT, TASK AREA & WORK UNIT NUMBERS: 62101F, 667008AC
11. CONTROLLING OFFICE NAME AND ADDRESS: Air Force Geophysics Laboratory, Hanscom AFB, Massachusetts 01731, Contact Monitor: James T. Bunting/LYU	12. REPORT DATE: 15 June 1979
	13. NUMBER OF PAGES: 132
14. MONITORING AGENCY NAME & ADDRESS (if different from Controlling Office)	15. SECURITY CLASS. (of this report): Unclassified
	15a. DECLASSIFICATION/DOWNGRADING SCHEDULE

16. DISTRIBUTION STATEMENT (of this Report)

Approved for public release; distribution unlimited

17. DISTRIBUTION STATEMENT (of the abstract entered in Block 20, if different from Report)

18. SUPPLEMENTARY NOTES

19. KEY WORDS (Continue on reverse side if necessary and identify by block number)

Remote Sensing	ESMR
Clouds	SCAMS
Nimbus VI Satellite	THIR
Satellite Meteorology	Synoptic Meteorology
Weather Sensing	

20. ABSTRACT (Continue on reverse side if necessary and identify by block number)

In conjunction with the inference of cloud composition and structure from satellites in all weather conditions, four synoptic cases including severe local storms, tropical disturbances, summertime convection and wintertime mid-latitude cyclones were selected. These cases occurred over the United States during periods when microwave and infrared satellite data from Nimbus VI satellite were available. Detailed studies of some dynamic and synoptic aspects of these cases were carried out. ESMR

DD FORM 1 JAN 73 1473 EDITION OF 1 NOV 65 IS OBSOLETE

401 103

SECURITY CLASSIFICATION OF THIS PAGE (When Data Entered)

(Electronically Scanning Microwave Radiometer), SCAMS (Scanning Microwave Spectrometer) and THIR (Temperature Humidity Infrared Radiometer) data from the Nimbus VI satellite were documented along with the conventional atmospheric parameters. The organized microwave and infrared data and corresponding synoptic, radiosonde and cloud data are fundamental to the understanding and verification of the cloud sounding technique from satellites.

TABLE OF CONTENTS

ACKNOWLEDGMENTS

Charts and graphs presented in this report were largely prepared by Ms. F. M. Chen and Mr. A. G. Peyrefitte. We thank Mr. J. T. Bunting for his continuous support of our satellite sensing program.

SECTION 1

INTRODUCTION

During the past few years, under the sponsorship of the Air Force Geophysics Laboratory, we have developed an infrared radiative transfer model for cloudy atmospheres with applications to the inference of cloud compositions from satellites. We have applied the infrared transfer model to VTPR (Vertical Temperature Profile Radiometer) for the NOAA 4 satellite (Liou, et al., 1978), and to HIRS (High Resolution Infrared Sounder) of the Nimbus VI satellite (Feddes and Liou, 1978), to investigate the cloud effect on these temperature and water vapor sounding channels and to explore feasible means for the inference of cloud compositions. Highlights of these studies were summarized in a final report by Liou, et al. (1978).

Since nonprecipitating and precipitating low clouds are normally opaque to thermal infrared radiation. their composition and structure information may best be derived from microwave sensors. Thus, we have recently focused our attention to the Nimbus VI SCAMS (Scanning Microwave Spectrometer) and ESMR (Electronically Scanning Microwave Radiometer) data for the purpose of deriving quantitative liquid water contents and rainfall rates for low clouds and precipitation, respectively. In line with our infrared studies, use of SCAMS data to infer mesoscale liquid water content has been recently demonstrated (Liou and Duff, 1979).

On the basis of our previous studies it is quite evident that a proper combination of infrared and microwave measurements could result in operationally significant data for vertical and horizontal liquid water content mapping. It is also apparent that the success of determining cloud/precipitation composition and structure in disturbed weather systems depends on the availability and completeness of synoptic, radiosonde and cloud data. We feel that it is imperative to document comprehensively the atmospheric parameters in conjunction with the co-located satellite data so that analysis and empirical retrieval could be carried out successfully. For this reason, we have selected four cases where detailed studies of the dynamic and synoptic aspects have been conducted for different types of weather systems. These include severe local storms, tropical disturbances, summertime convection and wintertime mid-latitude cyclones. All of these cases occurred in the United States during periods when infrared and microwave satellite data from the Nimbus VI satellite were available in addition to the conventional meteorological observations.

The objective of this scientific report is to present and discuss in an organized and coherent manner the conventional atmospheric parameters and the associated SCAMS, ESMR and THIR data from the Nimbus VI satellite.

SECTION 2

CASE STUDIES

The synoptic situations are discussed in this section for all the cases. The relevant weather charts and GOES imagery are presented for the observational times nearest to the Nimbus VI orbital passes.

2.1 Tropical Disturbance

A synoptic system with Nimbus VI data coverage occurred when cloud remnants of hurricane Eloise (1975) moved across the southeastern United States. This system reached landfall near Fort Walton Beach, Florida at approximately 1200 GMT 23 September as shown on the surface map in Figure 2.1 with strongest winds of 110 kt reported at Panama City. Hurricane Eloise rapidly weakened as it progressed northward into southeastern Alabama. By 1600 GMT 23 September, it was classified as a tropical storm as its central pressure increased and the winds diminished to less than 35 kt. Heavy precipitation continued around the center of the surface low as the system merged with a weak stationary front that had previously extended northeast-southwest from the Virginia coastal region to the central Gulf of Mexico (Figure 2.1). The moisture sources for the precipitation appeared to be low level residual moisture from the stationary front and convective activity around Eloise's low center. For this study, detailed analyses and numerical computations were carried out for three successive map times

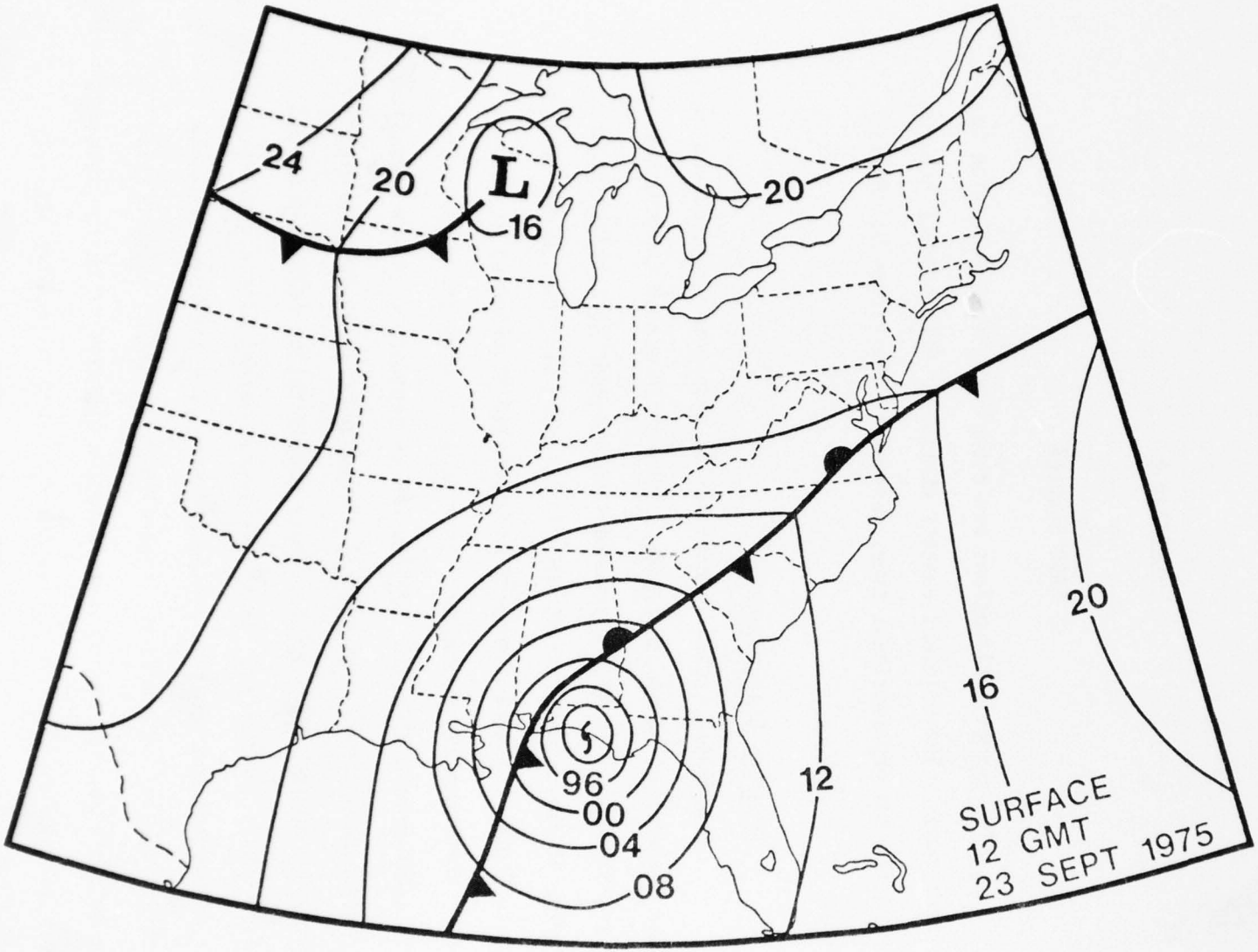

Figure 2.1 Synoptic surface analysis at 1200 GMT 23 September 1975.

at twelve hour intervals beginning at 0000 GMT 24 September.

2.1.1 0000 GMT 24 September 1975. Eloise was downgraded to a tropical depression twelve hours after landfall and was centered over the Georgia--Tennessee border as shown in Figure 2.2a. Warm core characteristics, that are typical of many tropical storms, were evident by a clearly defined maximum in the 500-1000 mb thickness of approximately 581 dm over the surface center at this map time. The warm core feature was also suggested by the -4°C isotherm at 500 mb in Figure 2.2a.

GOES satellite pictures were very useful in determining the distribution and evolution of the cloud field associated with Eloise. Infrared images (10.5 to 12.6 μm) from SMS-1 are shown in Figure 2.3 for three synoptic times that correspond to Figure 2.2. Grade shades are assigned to temperatures between 29° and -75°C according to the ZA enhanced gray scale described in the GOES/SMS User's Guide (Corbell, et al., 1977). White areas in Figure 2.3a correspond to middle and high level clouds, particularly in the region ahead of the cold front and also north of the surface low center over Kentucky and Tennessee. Coldest tops were located around the surface cyclone and in the convective region southeast of the storm center, although they were not easily discernible in the photographs reproduced here. Other interesting features that were barely discernible included areas with dark gray shades over Alabama and Mississippi. These represented low level stratus clouds with warm cloud top temperatures that were not much colder than the warmer land temperatures in the adjacent cloud free areas.

Intense convective activity was present in the radar summary that was nearest to the first map time. Figure 2.4 shows echo tops at 1135 GMT extended above 35,000 ft and were imbedded in two thunderstorm

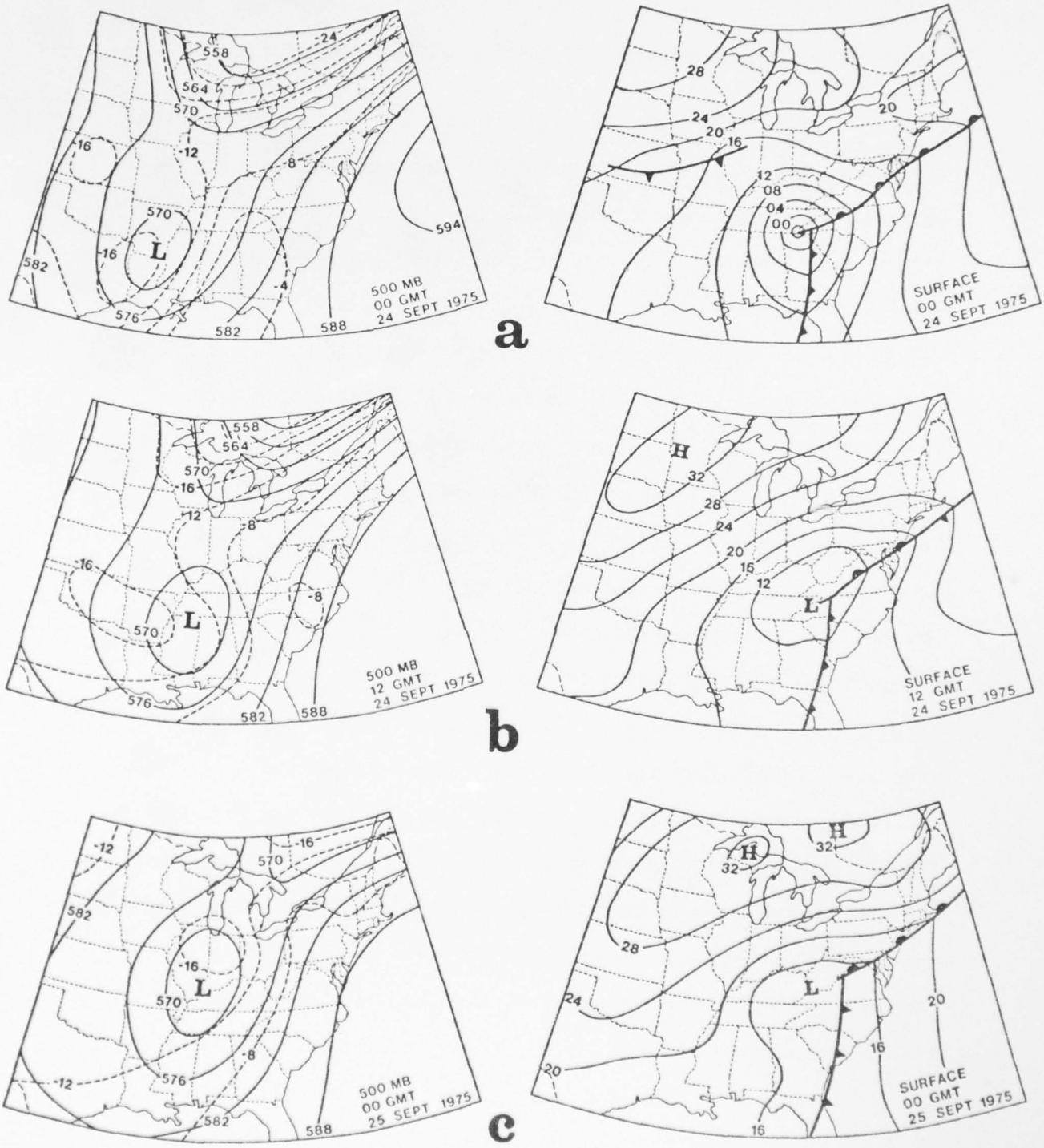

Figure 2.2 Maps of sea level pressure and 500 mb level for three synoptic times (a) 0000 GMT 24 September 1975, (b) 1200 GMT 24 September 1975 and (c) 0000 GMT 25 September 1975. Solid lines represent isobars (mb) and contour heights (dm) and dashed lines isotherms (°C).

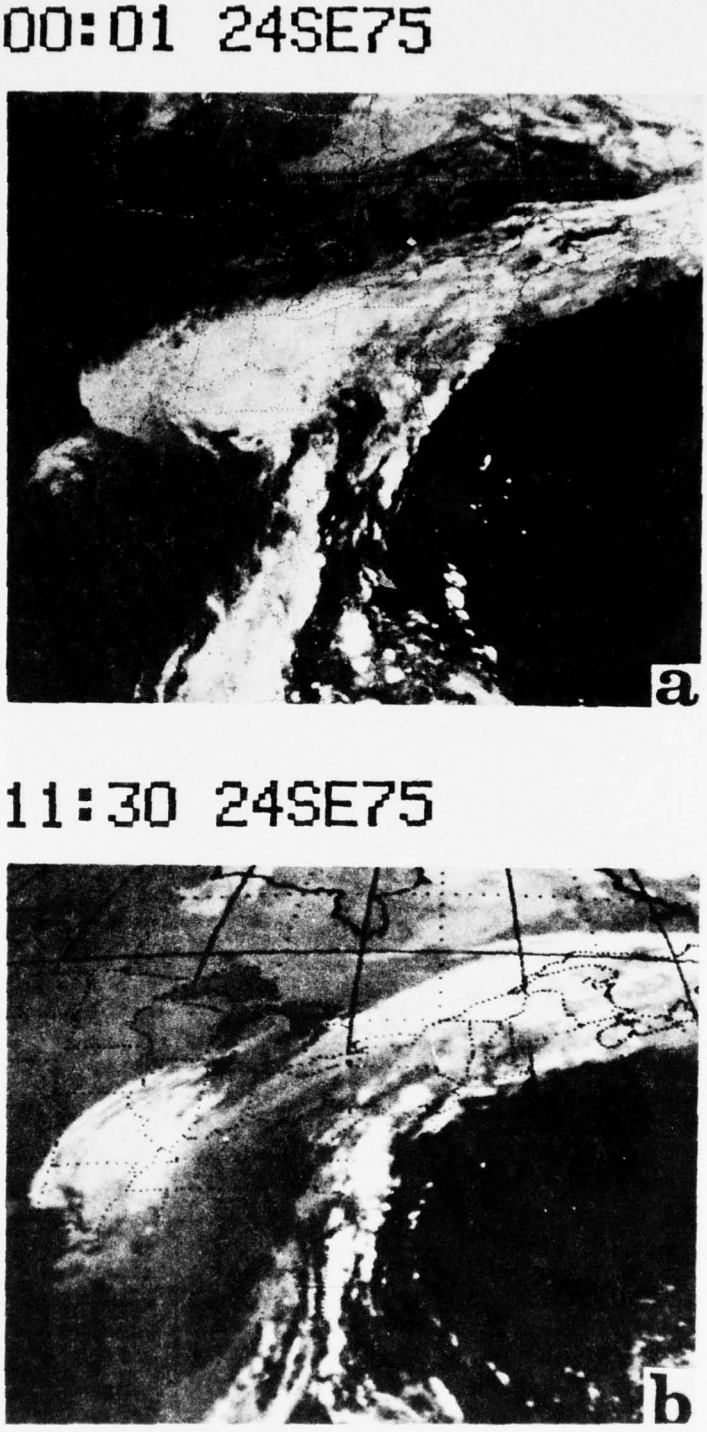

Figure 2.3. SMS-1 infrared satellite pictures for map times corresponding to Figure 2.2

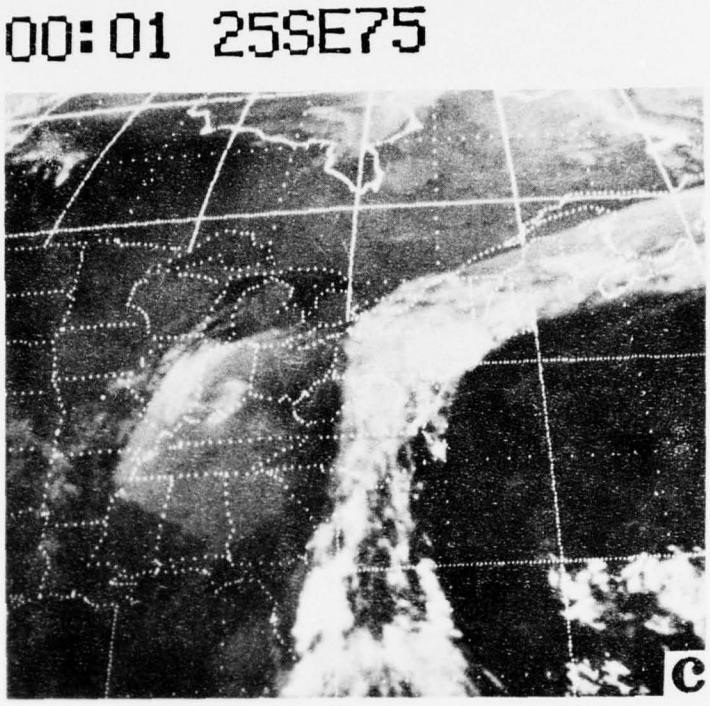

Figure 2.3. SMS-1 infrared satellite pictures for map times corresponding to Figure 2.2

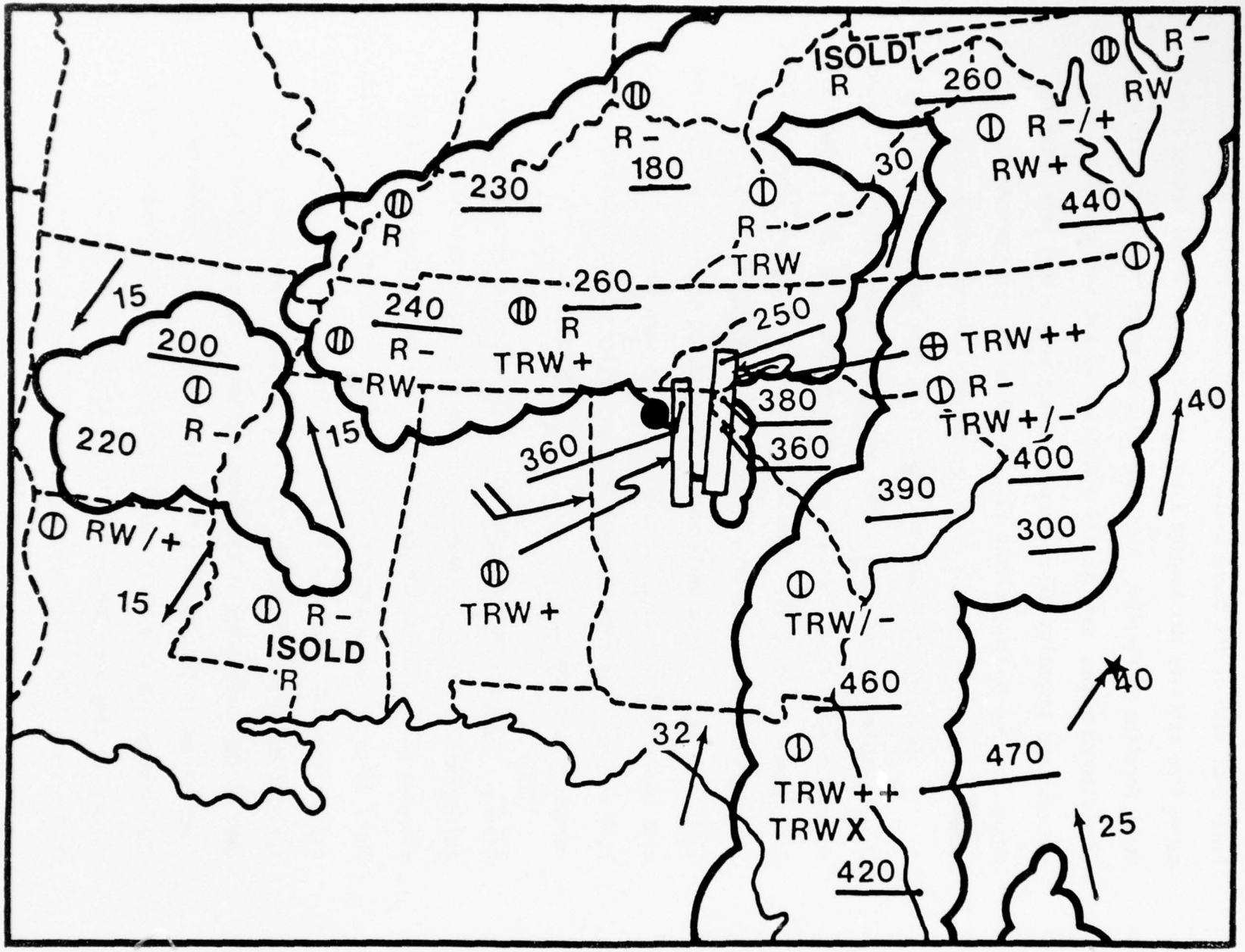

Figure 2.4. Radar summary for 2335 GMT 23 September 1975. The large dot denotes the location of the surface low center.

lines just east of the storm center over northern Georgia. Scattered convective activity was located along the Atlantic coastal region from North Carolina to Florida. It should also be noted that a separate area of scattered echoes was located over Arkansas and was associated with the eastward advancing 500 mb trough. These weak echoes were rotating around the low in the cyclonic flow at 500 mb and later merged with the cloud remnants of hurricane Eloise as the 500 mb trough moved east.

Heavy rainfall amounts occurred at this map time. Precipitation accumulations for the six hour period, centered at 0000 GMT, showed values in excess of an inch, and one station (Asheville, N.C.) reported 2.26 inches (Figure 2.5a). The heavy amounts over eastern Tennessee and Kentucky were associated with warm, moist air overrunning cool, moist air behind the frontal zone while amounts east of the center were associated with convective activity. It should be noted that in this study rainfall data included only National Weather Service stations equipped with recording rain gages.

2.1.2 1200 GMT 24 September 1975. Within the twelve hour period ending at 1200 GMT 24 September, the warm core characteristics of Eloise disappeared as a tongue of dry air moved over the surface low and the upper level trough advanced eastward. Figure 2.6 shows the movement of dry air into this system at 700 mb. For example, maximum values of specific humidities (more than 2.5 g kg^{-1}) were centered just to the east of the surface low at the first map time and were replaced by much lower values in the southerly flow within the following twelve hours. The moisture and streamline fields at 500 mb (not shown) indicated dry air was already over the surface low at higher levels at 0000 GMT 24 September 1975. This dry tongue of air separated the convectively

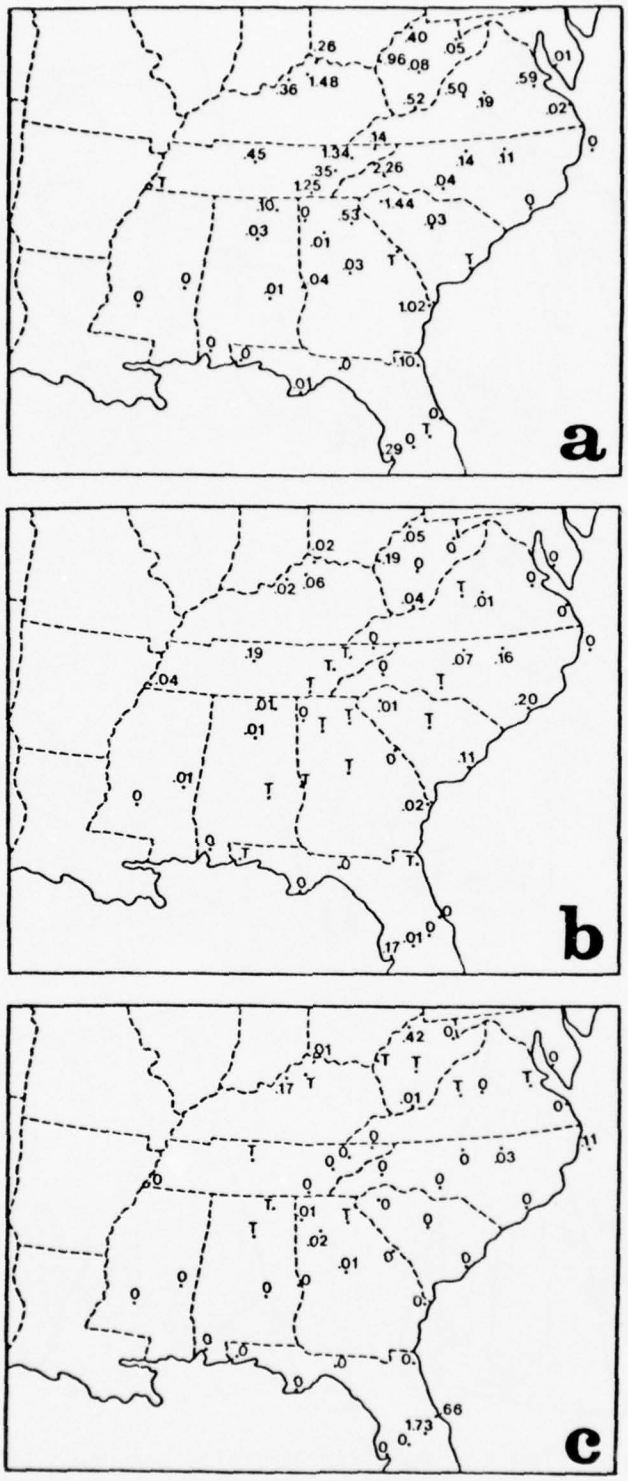

Figure 2.5. Precipitation accumulations in inches for 6 hour periods centered about the map times corresponding to Figure 2.

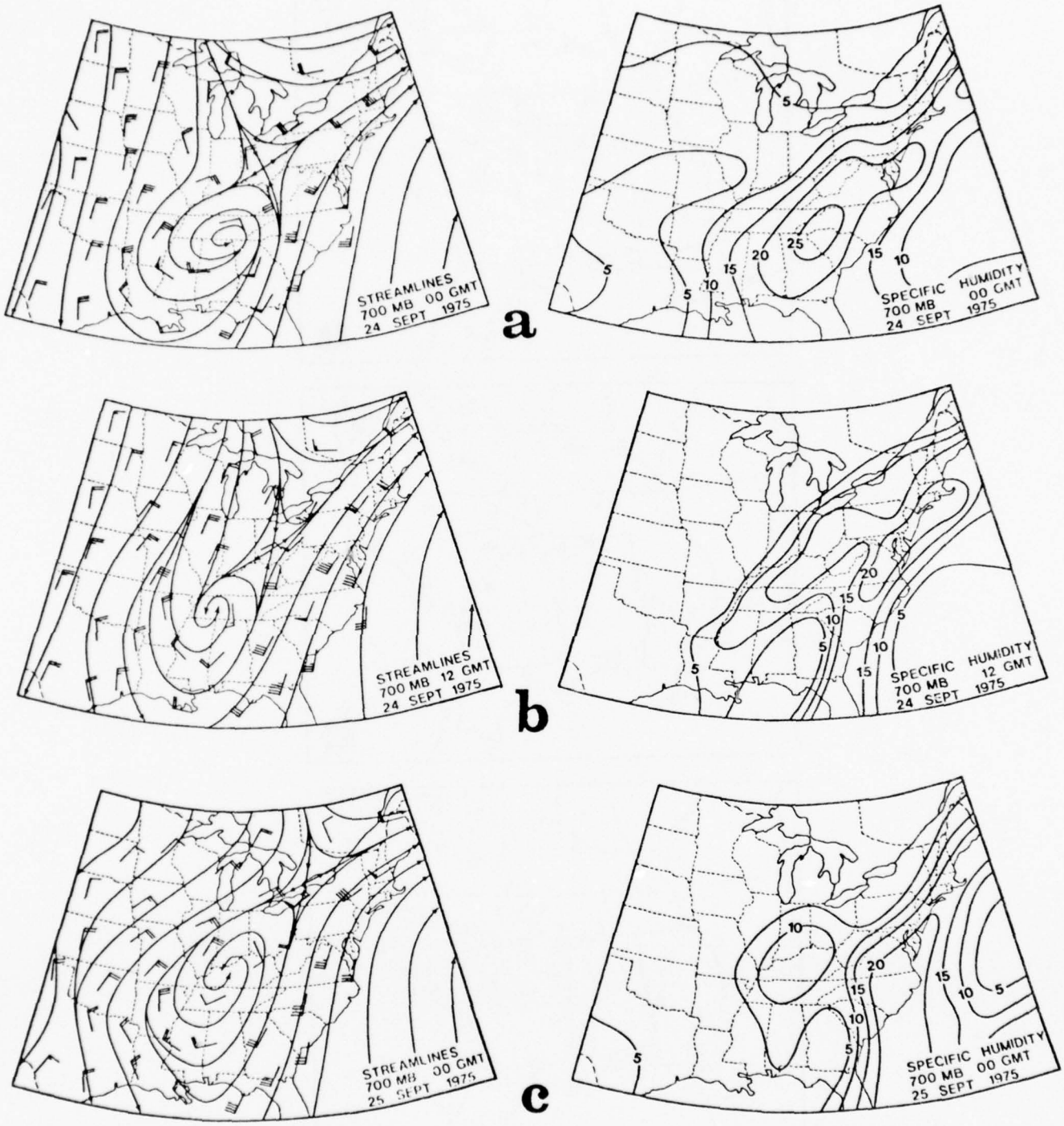

Figure 2.6. Streamline and specific humidity analyses of the 700 mb level for map times corresponding to Figure 2. Isopleth interval is 0.5 g kg^{-1} for specific humidity.

unstable moisture source over the coastal region of the eastern United States from the moist air circling around the 500 mb cyclonic vortex to the west over Tennessee.

There was a dramatic decrease in precipitation around the low center by this second map time. Radar reports (not shown) indicated this area was covered by widely scattered echoes with tops below 20,000 ft. Convective precipitation continued only in the warm air sector ahead of the cold front and was absent elsewhere. Figure 2.5b shows six hour rainfall amounts were less than 0.20 inches at all the recording precipitation stations in the southeastern United States, and only 0.01 inches or traces were observed near the surface cyclonic circulation center. In Figure 2.3b, stratiform clouds coincided with the low level cyclonic circulation and were centered approximately over central Tennessee beneath the 500 mb trough. It is apparent that light, stable precipitation was predominant around this cyclonic flow.

2.1.3 0000 GMT 25 September 1975. During the next 12 hours the remnants of Eloise continued to separate into two cloud systems. One moved northeastward in the southwesterly flow ahead of the 500 mb trough. The other system remained west of the Appalachians as a low level cloud field and continued to circulate about the cyclonic vortex as the surface low filled by another 4 mb and slowly moved north near the Kentucky--Virginia border (Figure 2.2c). The SMS-1 infrared picture at this time (Figure 2.3c) shows a circular, cut-off feature in the low level cloud field with a small area of higher level clouds imbedded in the 500 mb low over Illinois and Indiana. The cold front continued to move east, and it extended from the surface low through the central Carolinas and into Florida.

Precipitation accumulations for the six hour period, centered around the third map time, were less than 0 03 inches at a few stations in northern Georgia; otherwise the precipitation around the surface cyclone center had ended as shown in Figure 2.5c. However, some convective precipitation persisted ahead of the cold front to the south over central Florida and off the southeastern coastal region over the Atlantic.

2.2 Severe Local Storm

On the afternoon and evening of 14 April 1976, severe thunderstorm activity developed over the Central states and continued on the next day. During this period there was data coverage by Nimbus VI. The synoptic weather pattern was characterized by low level confluent flow in a frontal boundary with warm, moist southerly flow ahead of the front and dry westerly flow behind it. Difluent, anticyclonic motion was present in the upper levels and provided favorable conditions for convective activity to develop within very unstable air near the frontal zone. In this section these synoptic features will be traced from the period 0000 GMT 13 April to 0000 GMT 16 April, using the 700 and 200 mb charts and the 850 mb moisture field.

2.2.1 700 Millibar Winds and Surface Fronts. On 0000 GMT 13 April a stationary front extended from the Florida peninsula through the Gulf Coast states to a warm front over Texas as shown in Figure 2.7. This frontal system was very weak and it dissipated on the following day as a high pressure ridge developed over the Great Plains states. Evolution of these features is evident in Figures 2.7 through 2.12 which show the surface frontal positions superimposed on the 700 mb height and temperature fields. A low level ridge was well defined at 700 mb

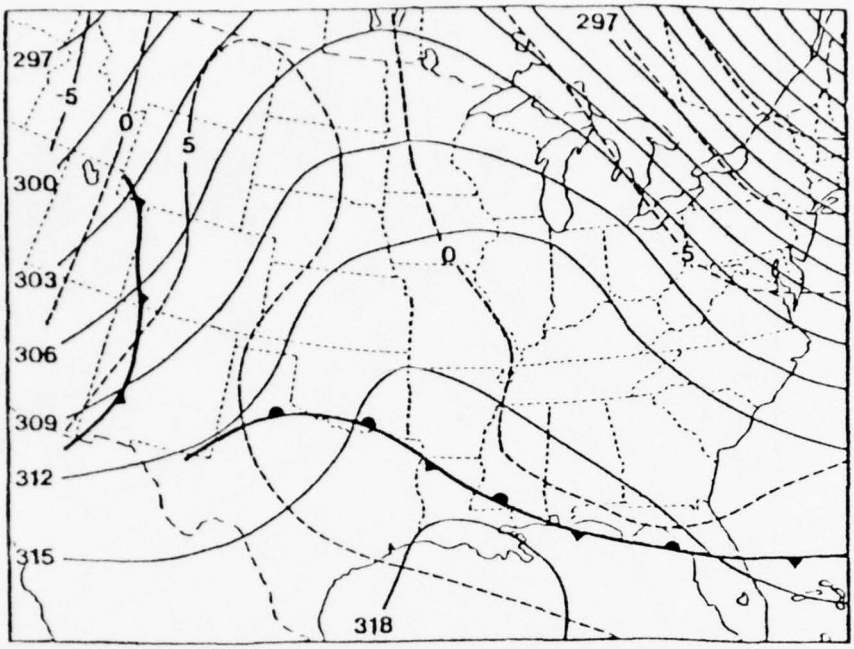

Figure 2.7. Chart of 700 mb surface for 0000 GMT 13 April 1976; solid lines are contours (gpm) and dashed lines are isotherms (°C); surface frontal positions are superimposed.

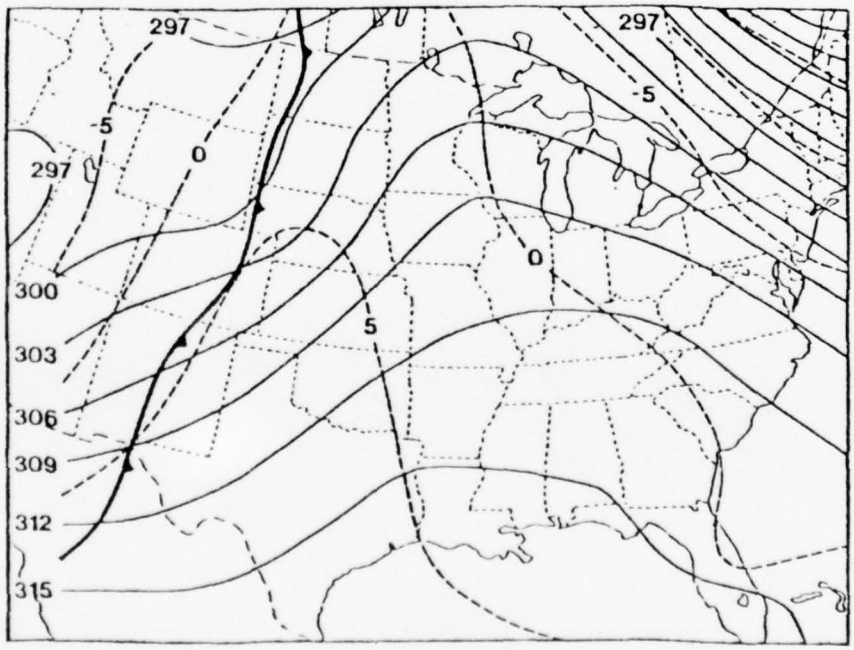

Figure 2.8. Chart of 700 mb surface for 0000 GMT 14 April 1976; solid lines are contours (gpm) and dashed lines are isotherms (°C); surface frontal position is superimposed.

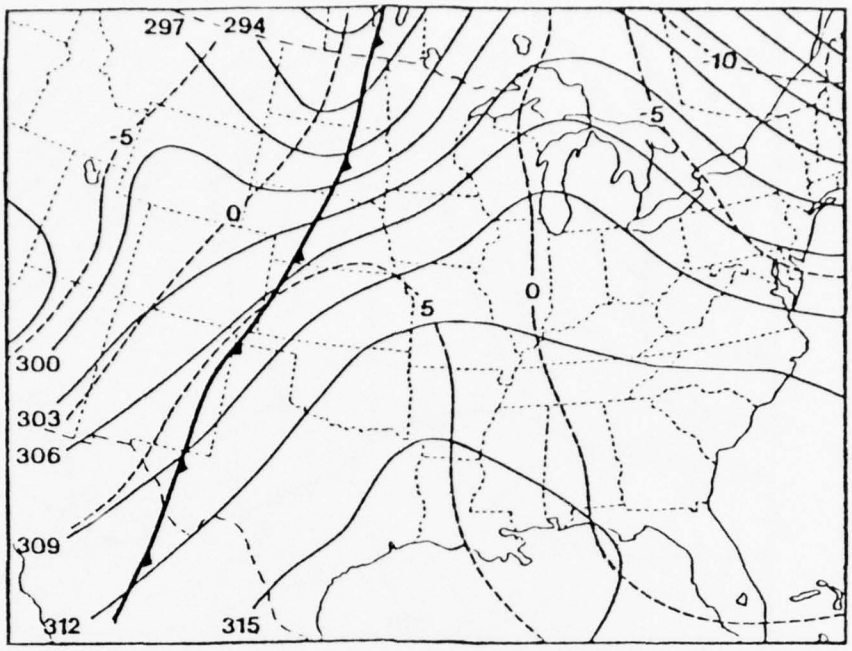

Figure 2.9. Chart of 700 mb surface for 1200 GMT 14 April 1976; solid lines are contours (gpm) and dashed lines are isotherms (°C); surface frontal position is superimposed.

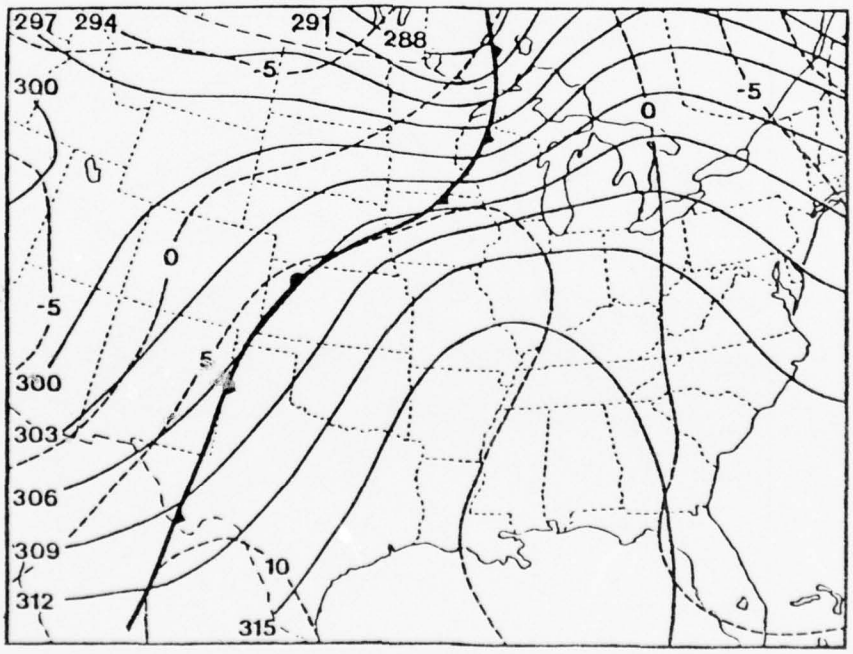

Figure 2.10. Chart of 700 mb surface for 0000 GMT 15 April 1976; solid lines are contours (gpm) and dashed lines are isotherms (°C); surface frontal position is superimposed.

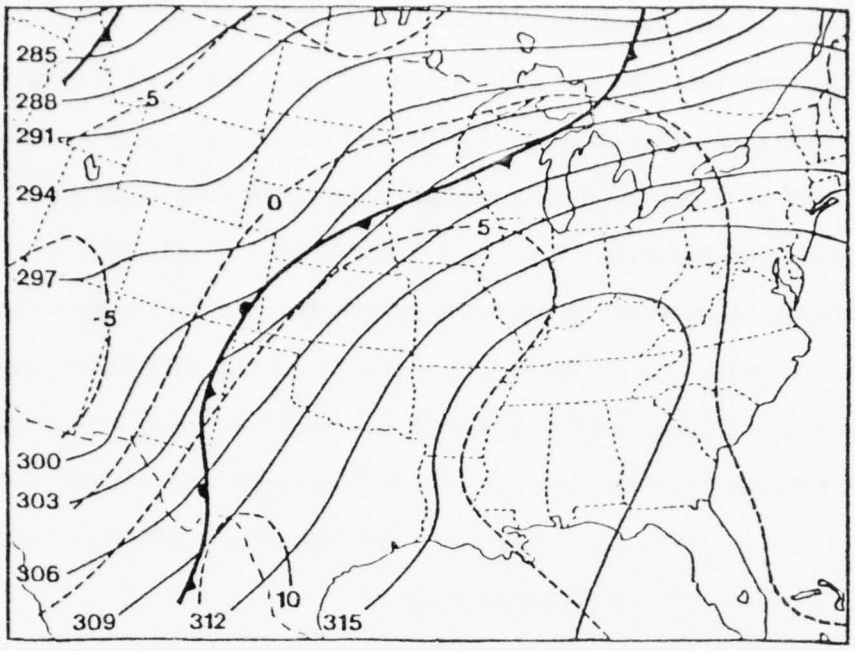

Figure 2.11. Chart of 700 mb surface for 1200 GMT 15 April 1976; solid lines are contours (gpm) and dashed lines are isotherms (°C); surface frontal positions are superimposed.

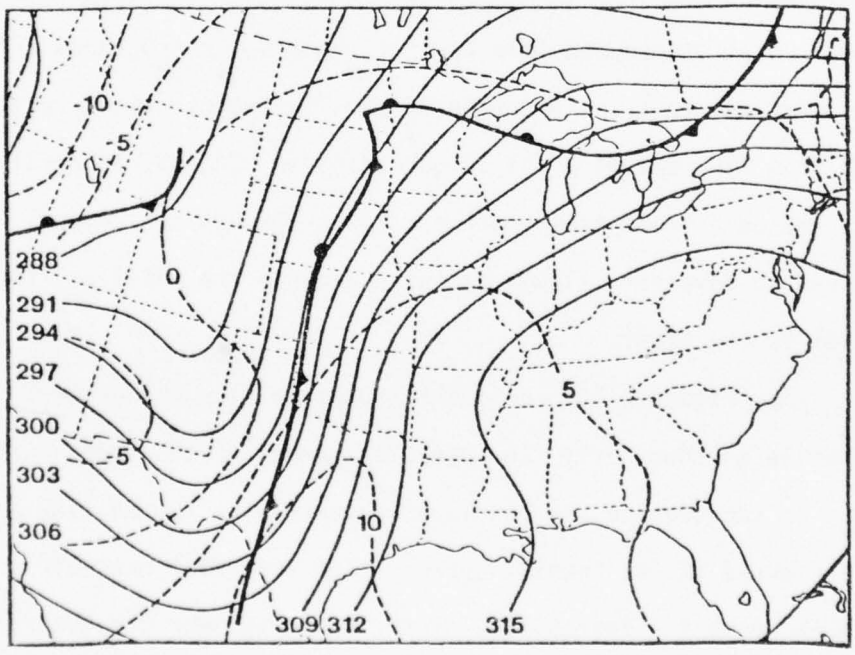

Figure 2.12. Chart of 700 mb surface for 0000 GMT 16 April 1976; solid lines are contours (gpm) and dashed lines are isotherms (°C); surface frontal positions are superimposed.

in Figure 2.8 and extended northward from the Gulf of Mexico, across Louisiana and into the central United States. The entire ridge was moving eastward, as a trough over the western U.S. and an associated cold front were moving slowly eastward across Arizona and Utah into New Mexico and Colorado (Figures 2.7 and 2.8). On 14 April a short wave trough moved rapidly eastward across the northern Great Plains and southern Canada. By 15 April the eastward moving cold front was located over the Great Lakes region and extended southward across the western Plains through eastern Colorado and into eastern New Mexico (Figure 2.11). On 0000 GMT 14 April convective activity developed ahead of this frontal system in the northern Plain states.

Within this period, the 700 mb ridge moved eastward into the Mississippi River Valley, and low level southerly flow advected moisture northward into the Central states. By 1200 GMT 14 April, pronounced warm air advection over Texas retarded the eastward ridge movement over the Gulf Coast states, and this part of the ridge retrograded (Figure 2.9). On the next day this system began to move eastward again. During the period from 1200 GMT 14 April (Figure 2.9) to 0000 GMT 15 April (Figure 2.10), the cold front from southwest Texas through the central Plains continued to move very slowly eastward because the mid-level flow was parallel to the front.

In Figure 2.10, confluent southerly flow was present over Texas while southwesterly flow prevailed ahead of the front further north. In addition to the confluent pattern, the 700 mb flow was warm and dry ahead of the frontal system. The low level warm air advection helped increase the instability of the air mass over the Central states.

Intense convective activity continued through 15 April.

Figures 2.11 and 2.12 show the shift of the 700 mb wind flow and surface frontal position during this time.

2.2.2 200 Millibar Winds. In the upper levels at 0000 GMT 13 April (Figure 2.13), relatively high wind speeds extended across the Southern and Eastern states. Figures 2.13 through 2.18 show the 200 mb height field and isotach analysis. At 0000 GMT 13 April an extensive ridge covered the Central U.S. and Canada while a trough was located over the West Coast. Between 0000 GMT 13 April and 0000 GMT 14 April, both the ridge and trough moved eastward.

By 0000 GMT 14 April wind speeds of 35 ms^{-1} weakened over Oklahoma and northern and western Texas, but still continued over the Southwestern, Southeastern, and Gulf Coast states as shown in Figure 2.14. Between 0000 and 1200 GMT 14 April, the area of high wind speeds over the Southwestern states began to separate with the northern branch moving steadily northeastward, while the southern branch moved eastward and merged with the high wind speeds over southern Texas. This resulted in pronounced difluent flow over the area where severe thunderstorms subsequently developed.

By 1200 GMT 14 April (Figure 2.15), the northern branch of strong winds in excess of 45 ms^{-1} was located over central New Mexico in a northeast-southwest orientation. The southern branch over southern Texas was somewhat stronger with 55 ms^{-1} wind speeds and was oriented east-west across Mexico and the Gulf Coast states. An area of difluence extended between these two branches of the flow.

Figure 2.16 shows that by the next day the core of maximum wind speeds in the northern branch extended from Mexico and New Mexico to Iowa. Wind speeds of 55 ms^{-1} extended into New Mexico while

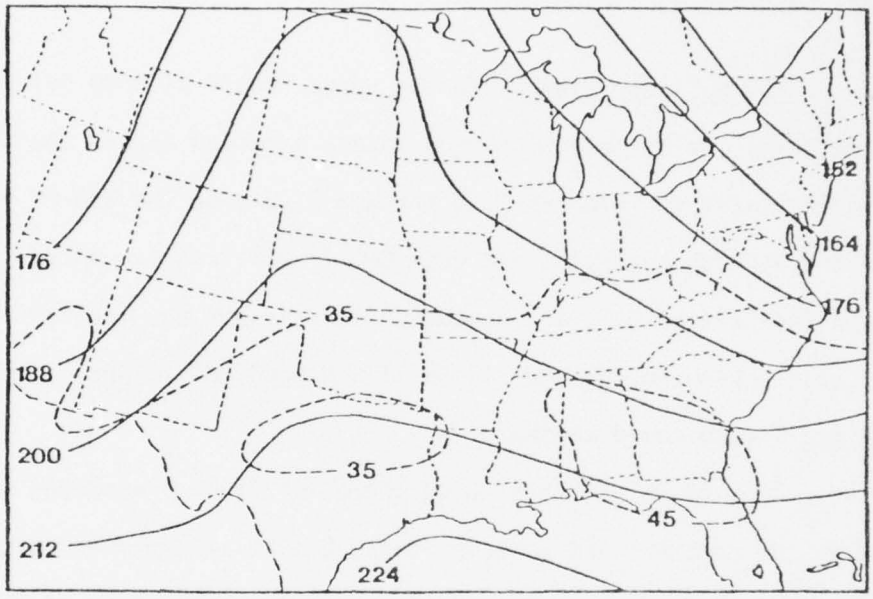

Figure 2.13. Chart of 200 mb surface for 0000 GMT 13 April 1976; solid lines are contours (gpm) and dashed lines are isotachs ($\geq$ 35 ms^{-1}).

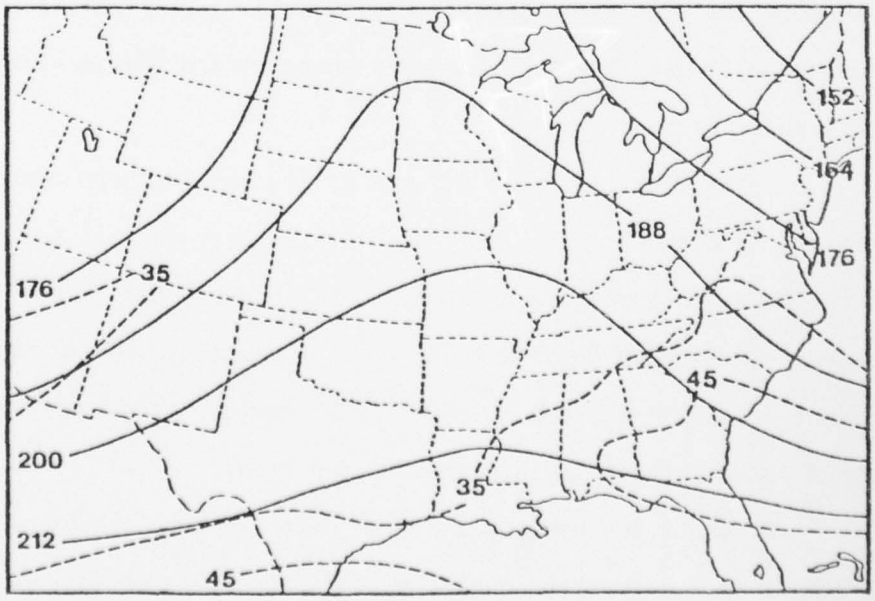

Figure 2.14. Chart of 200 mb surface for 0000 GMT 14 April 1976; solid lines are contours (gpm) and dashed lines are isotachs ($\geq$ 35 ms^{-1}).

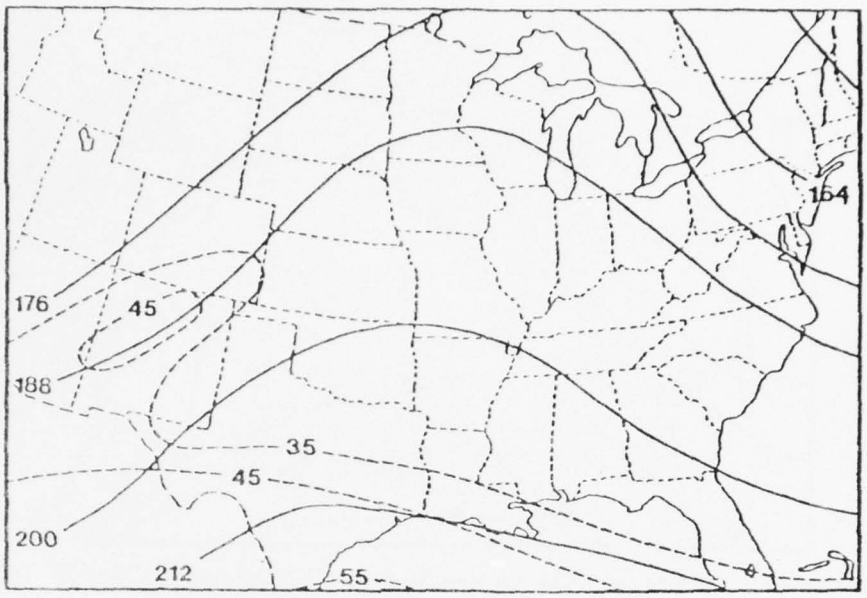

Figure 2.15. Chart of 200 mb surface for 1200 GMT 14 April 1976; solid lines are contours (gpm) and dashed lines are isotachs ($\geq$ 35 ms^{-1}).

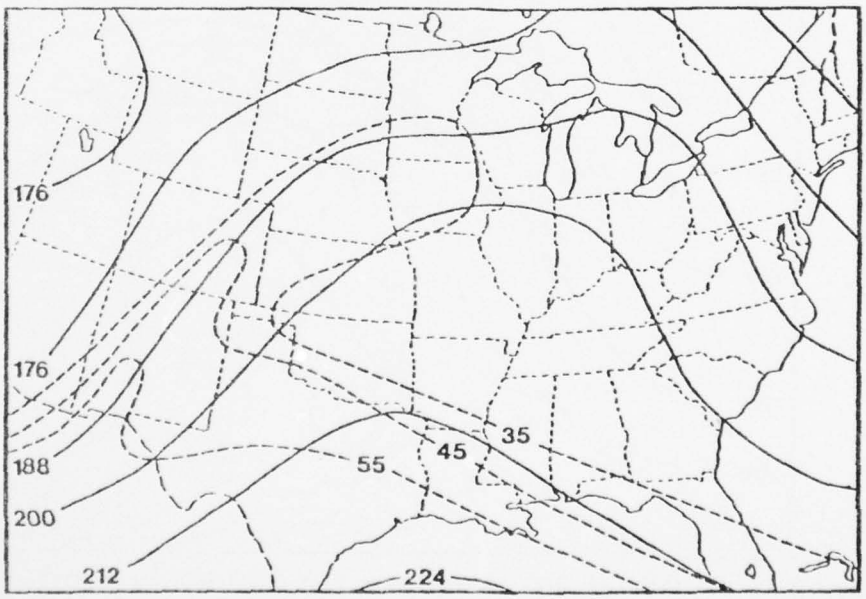

Figure 2.16. Chart of 200 mb surface for 0000 GMT 15 April 1976; solid lines are contours (gpm) and dashed lines are isotachs ($\geq$ 35 ms^{-1}).

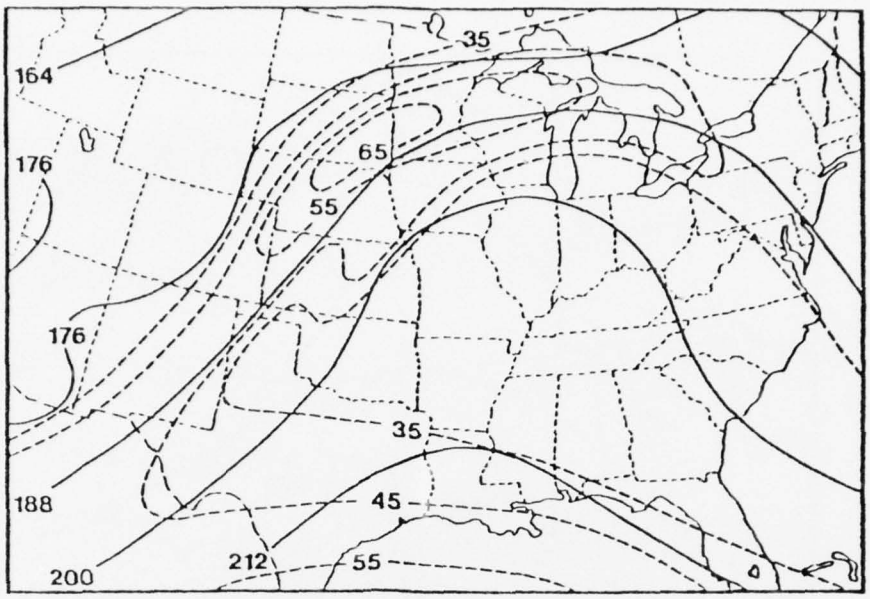

Figure 2.17. Chart of 200 mb surface for 1200 GMT 15 April 1976; solid lines are contours (gpm) and dashed lines are isotachs ($\geq$ 35 ms^{-1}).

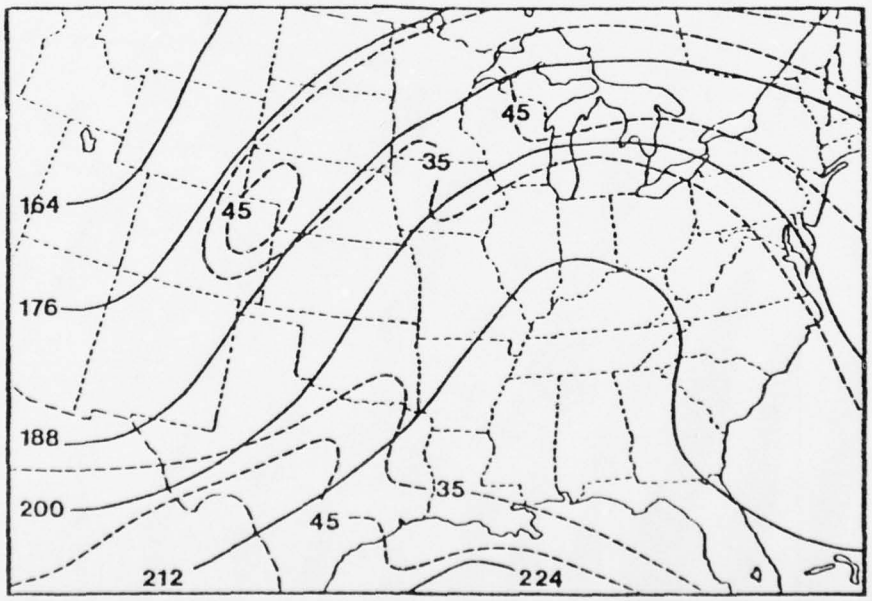

Figure 2.18. Chart of 200 mb surface for 0000 GMT 16 April 1976; solid lines are contours (gpm) and dashed lines are isotachs ($\geq$ 35 ms^{-1}).

50 ms^{-1} wind speeds covered most of Texas. The area of difluence extended across a major portion of the Great Plains. The significance of this type of motion field in severe weather situations has been described by MacDonald (1977).

During the next twelve hours (0000 to 1200 GMT 15 April), the core of maximum wind speed of the northern branch continued to move northeastward to the Great Lakes, and crossed the ridge axis, and began to move southeastward into New York as shown in Figure 2.17. This speed core north of the difluence area produced anticyclonic shear in addition to anticyclonic curvature over the thunderstorm area. High wind speeds in the southern branch shifted southward with the core center moving from south central Texas to the southern tip of Texas.

By 0000 GMT 16 April, the ridge was building northward over the Great Lakes and into Canada (Figure 2.18). High wind speeds in the northern branch had diminished considerably and moved eastward by this time.

2.2.3 850 Millibar Moisture. Another important synoptic feature associated with this severe weather case was the low level moisture field. Detailed analyses of relative humidities from rawinsonde data were carried out for the 850 mb level. Figures 2.19 to 2.24 show these analyses with contours drawn in ten percent increments. Southerly flow ahead of the trough began to advect moisture from the Gulf of Mexico into the Central states in the low levels on 13 April 1976. A comparison of Figures 2.7 and 2.19 indicates the moisture advection on 13 April 0000 GMT. At this time moist air was present up to 500 mb over parts of Texas and Oklahoma, but during the next twenty-four hours the mid-level moisture advected eastward and was replaced by dry air from the west (relative humidities less than 10 percent) at the 700

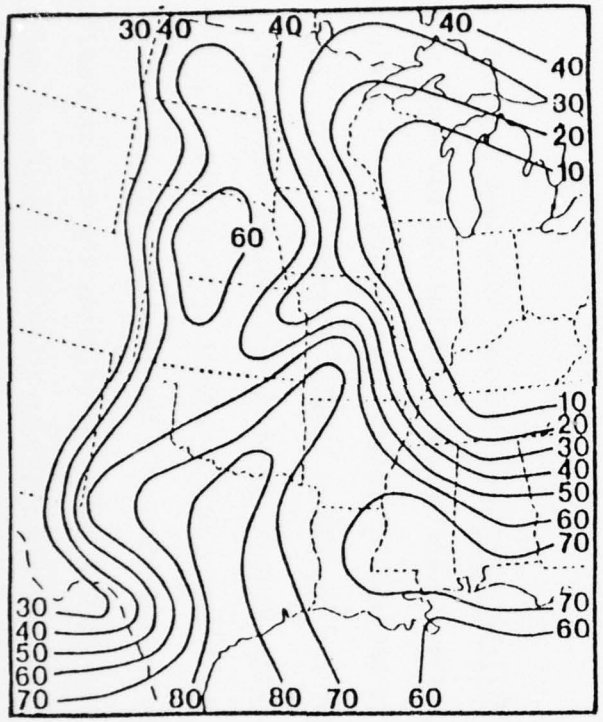

Figure 2.19. Chart of 850 mb relative humidity for 0000 GMT 13 April 1976; isopleths are in percent.

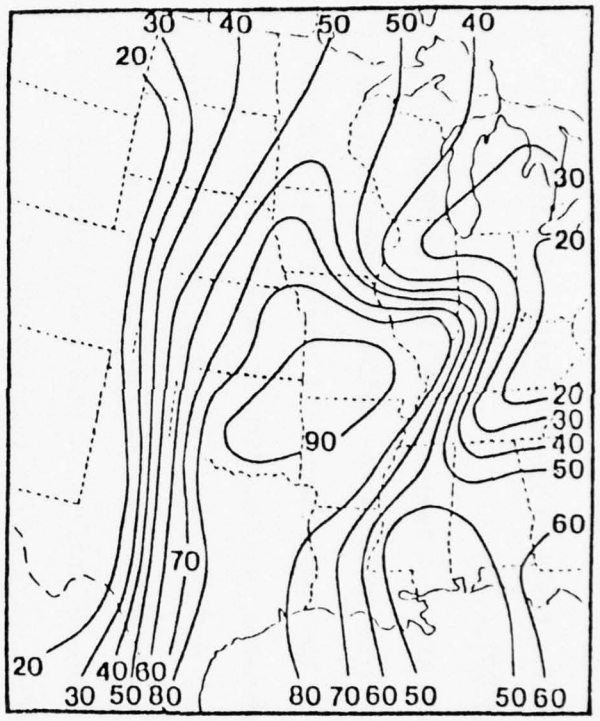

Figure 2.20. Chart of 850 mb relative humidity for 0000 GMT 14 April 1976; isopleths are in percent.

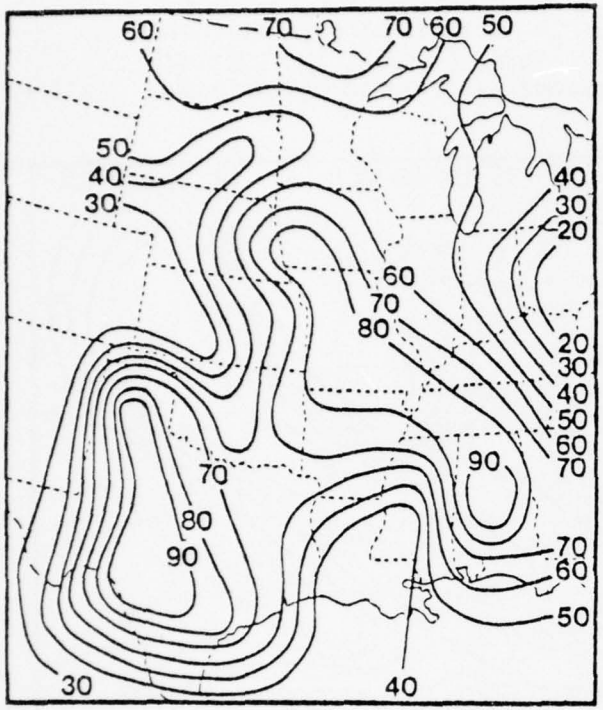

Figure 2.21. Chart of 850 mb relative humidity for 1200 GMT 14 April 1976; isopleths are in percent.

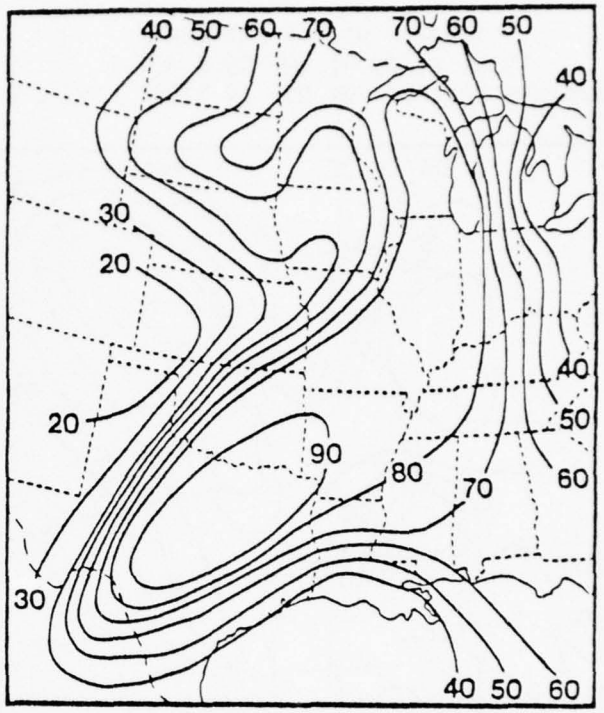

Figure 2.22. Chart of 850 mb relative humidity for 0000 GMT 15 April 1976; isopleths are in percent.

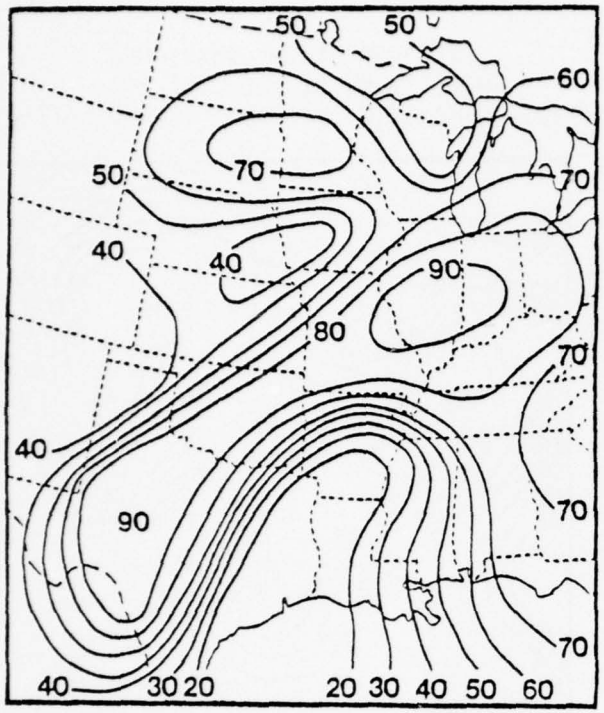

Figure 2.23. Chart of 850 mb relative humidity for 1200 GMT 15 April 1976; isopleths are in percent.

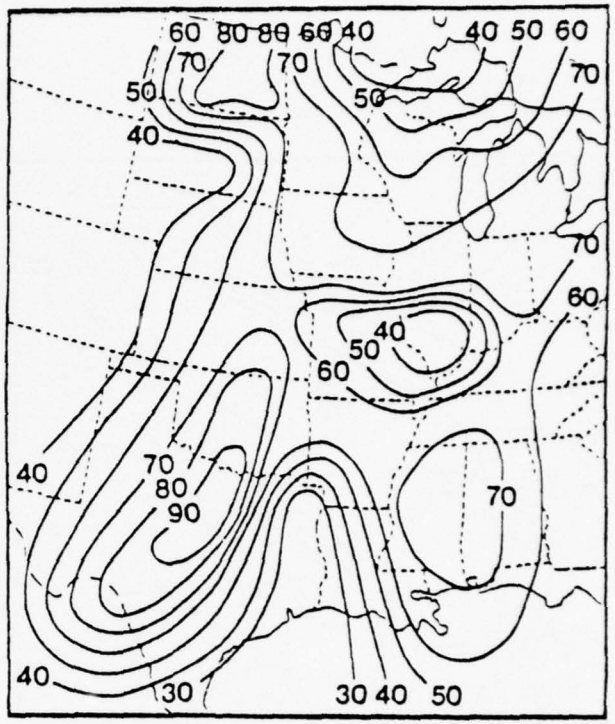

Figure 2.24. Chart of 850 mb relative humidity for 0000 GMT 16 April 1976; isopleths are in percent.

and 500 mb levels.

Moist air at 850 mb, which had been in western Texas at 0000 GMT 13 April and moved into the Texas Panhandle in the following 12 hours, was replaced with dry air by 0000 GMT 14 April (Figure 2.20). Between 0000 and 1200 GMT 14 April a slight pressure rise over Texas, coupled with a weakening in the pressure gradient over New Mexico behind the front, increased the low level moisture advection over western Texas (Figure 2.21).

Surface temperatures and dew points also increased ahead of the frontal system prior to the outbreak of convective activity. By 1800 GMT 14 April surface temperatures along and ahead of the front in the area of intense thunderstorms, from southwestern Texas to northwestern Iowa, were in the high 70's to low 80's. These temperatures averaged 10°F warmer over Texas, Oklahoma, and Kansas, and 5°F warmer over eastern Nebraska and Iowa than in the previous twenty-four hours. The surface dew point temperatures remained essentially constant over Texas and Oklahoma during this period but increased by 5°F over Kansas and eastern Nebraska, and by 10° to 15°F over Iowa. The dew point temperatures decreased rapidly across the front and indicated the presence of a strong moisture gradient. The wind flow ahead of this gradient was moist and southerly while it was dry and southwesterly behind it. This gradient extended through a deep layer and is depicted at 850 mb in Figures 2.21, 2.22, and 2.23.

By 0000 GMT 15 April the 850 mb moisture field decreased over western Texas, eastern Kansas, and eastern Nebraska after thunderstorm activity developed through these areas. More low level moisture advected into eastern Iowa, Illinois, and Wisconsin (Figure 2.22) and provided the moisture source for the thunderstorm activity which moved into

southeastern Minnesota and southern Wisconsin during the following twelve hours.

Moisture returned to western Texas by 1200 GMT 15 April (Figure 2.23) and to the Central Plains states by 0000 GMT 16 April (Figure 2.24) as low level southerly flow moved from the Gulf of Mexico into the Central States through this period.

2.3 Summertime Synoptic Scale Clouds

For this case, interest was focused primarily on convective activity over the north-central U.S. in the afternoon hours of 22 August and 25 August 1975. Synoptic maps and satellite pictures in this discussion are centered around these two times when Nimbus VI provided good coverage.

2.3.1 Synoptic case for 22 August 1975.

The major surface features at 1200 GMT are shown in Figure 2.25. High pressure areas were centered over western Ontario and the southeastern United States and were separated by a frontal system that extended westward from a low pressure center over southeastern Maine to a weak low over southwestern Nebraska. A cyclone with a 1004 mb closed isobar was located over southern Alberta. An occluded front was associated with this low and reached southward into Montana and then extended southwestward as a cold front to northern California.

The 500 mb chart for the corresponding synoptic time is shown in Figure 2.26. The prominent feature was a 500 mb ridge that extended from the central Mississippi Valley to northern Manitoba and indicated the westward tilt with height of the surface high pressure centers. Very weak temperature and height gradients extended across the southern

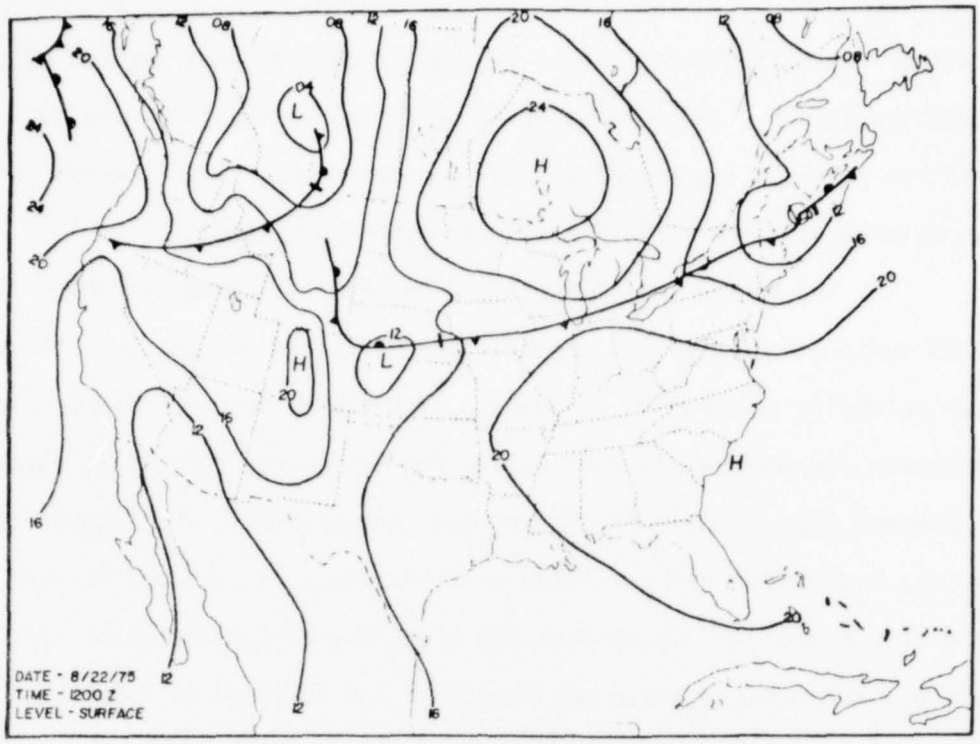

Figure 2.25. Sea level pressure map with fronts. Isobars are drawn at 4 mb intervals.

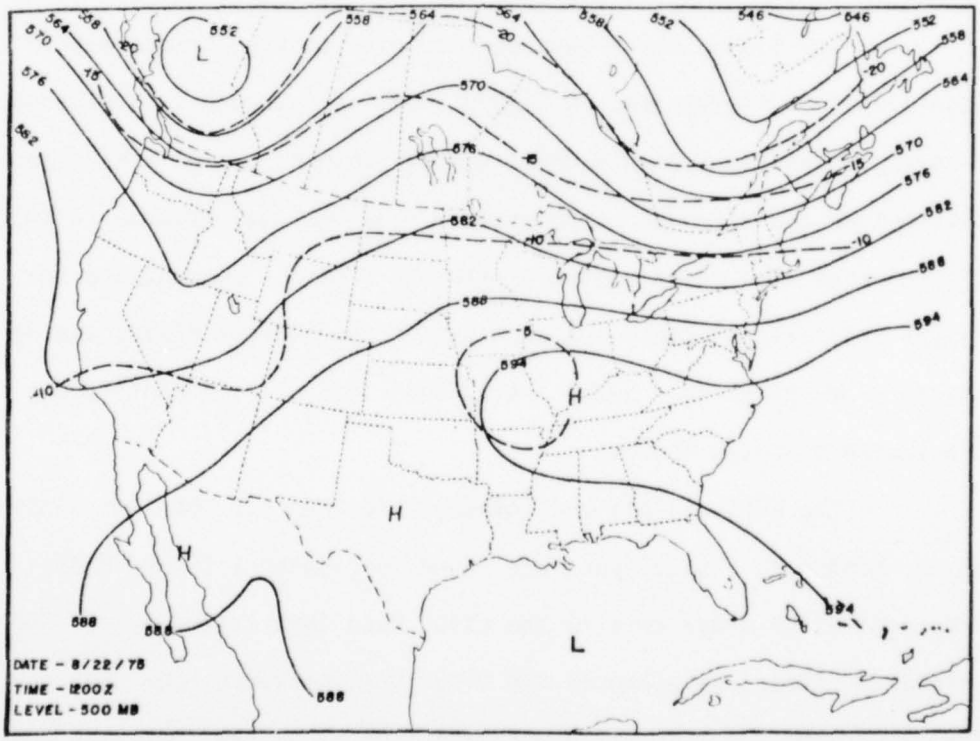

Figure 2.26. Map of the 500 mb level. Solid lines represent contour heights (dm) and dashed lines isotherms (°C).

half of the United States while stronger gradients were located over southern Canada. Two troughs were identified in the flow, one over British Columbia and the other over eastern Quebec. The troughs were associated with the surface lows over Maine and Alberta.

The surface chart for 12 hours later is shown in Figure 2.27. Both surface high pressure centers moved eastward during the 12 hour period ending at 0000 GMT 23 August. The low center over Maine moved eastward and deepened to 1001 mb, and the associated cold front pushed southward into southern New Jersey and Pennsylvania. The frontal system in the Midwest shifted northward while frontolysis occurred further west and only a lee side trough remained along the eastern Rockies. The cyclone over Alberta moved northeastward and deepened to 995 mb and the associated frontal system advanced into Saskatchewan and eastern Montana by 0000 GMT 23 August.

The 500 mb chart that corresponds to the surface map in Figure 2.27 is illustrated in Figure 2.28. The trough systems showed progressive eastward displacement across southern Canada with some amplification and stronger northwesterly flow over New England. The 500 mb ridge also moved eastward with the westerly current, and the height gradients strengthened over the northern Great Plains and upstream from the ridge. Weak, anticyclonic circulation continued over the southern United States.

The GOES visible and infrared pictures for the time closest to the Nimbus VI orbital pass are shown in Figures 2.29 and 2.30. Two prominent cloud areas were: 1) the cloud band that extended from South Dakota to Pennsylvania, and 2) the cloudiness centered over Manitoba. The cloud band was associated with the frontal system that extended

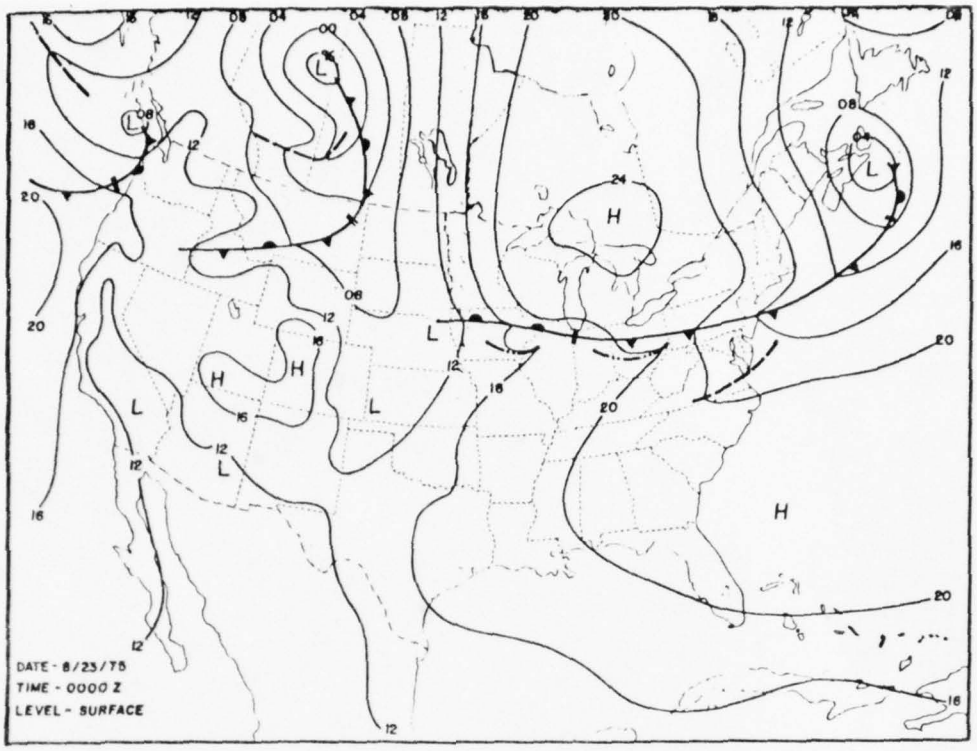

Figure 2.27. Same as Fig. 2.25 except the map is 12 hours later.

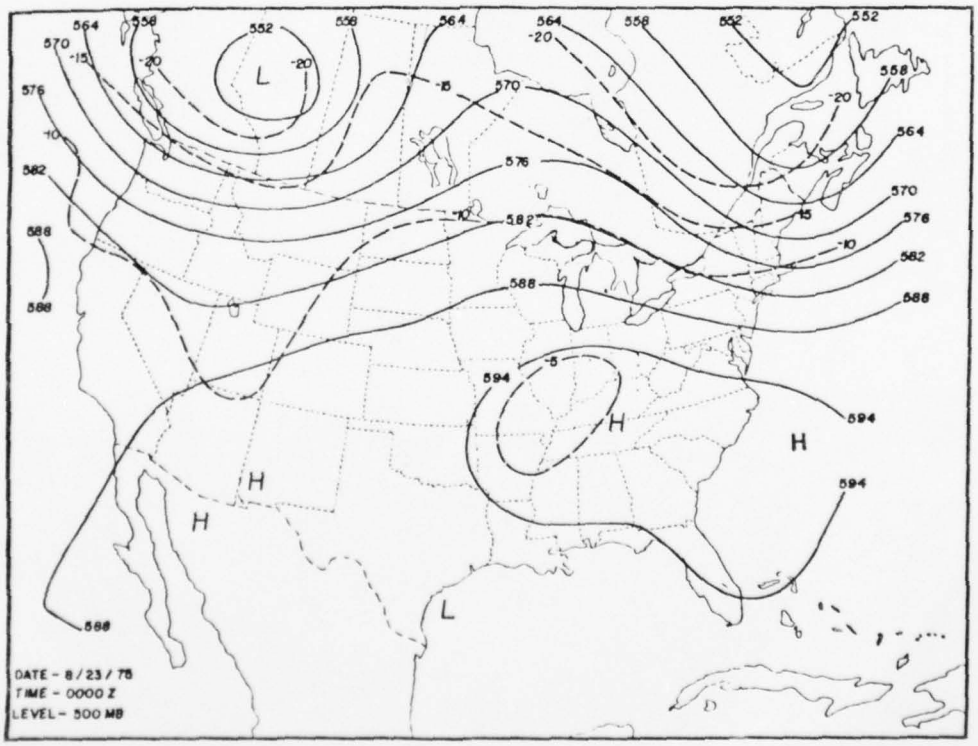

Figure 2.28. Same as Fig. 2.26 except the map is 12 hours later.

Figure 2.29. GOES East visible image for 1800 GMT 22 August 1975.

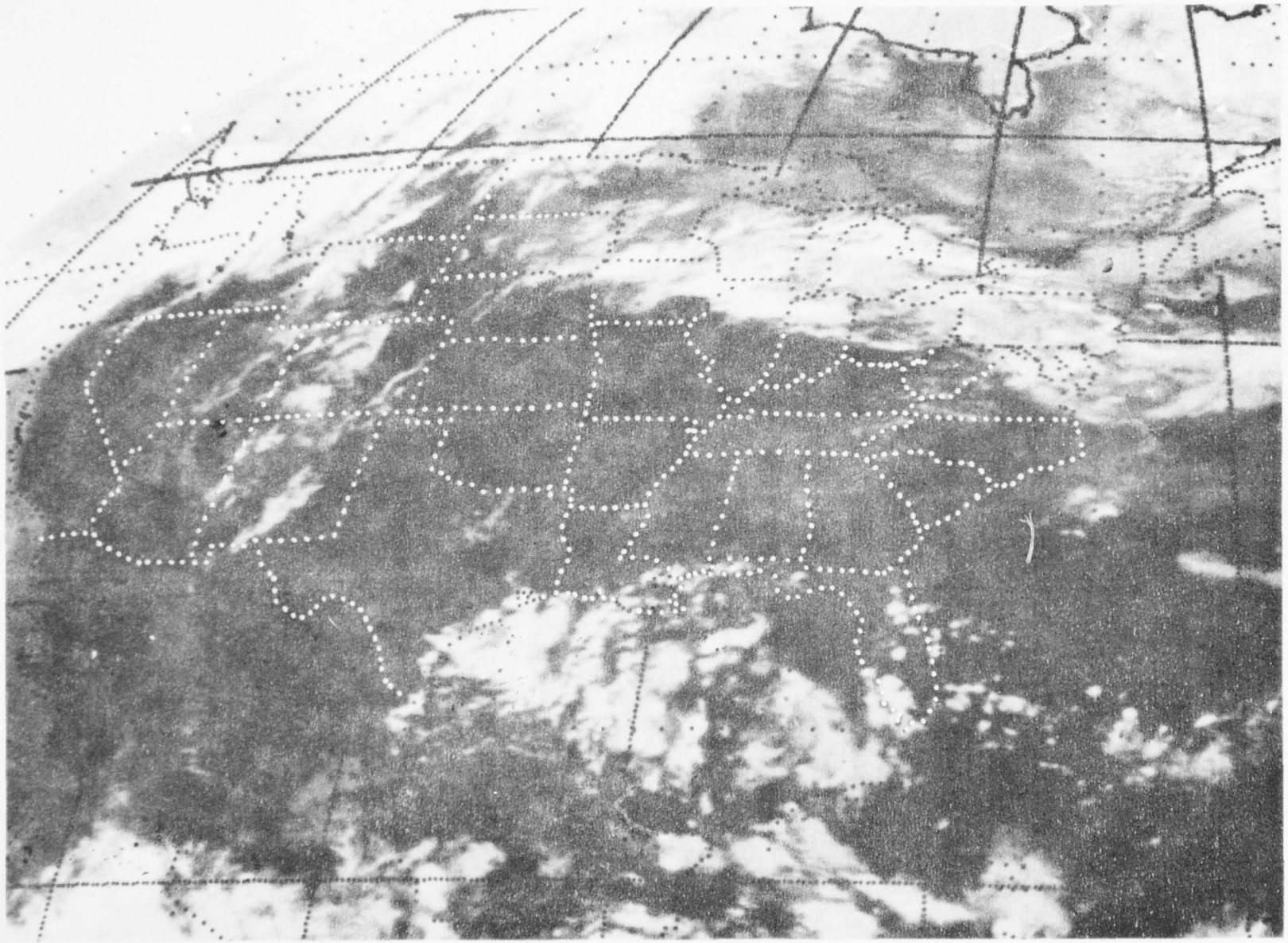

Figure 2.30. GOES East infrared image for 1800 GMT 22 August 1975.

across the northern United States while the second cloud area was related to the prefrontal activity east of the low pressure center over Alberta. The infrared image indicated multi-level cloudiness with some convective activity imbedded in the frontal cloudiness.

The radar summaries for the corresponding synoptic times are shown in Figures 2.31 to 2.33. An east-west band of echoes was located along the front from Lake Ontario to Nebraska at 1235 GMT. Thunderstorms developed within 12 hours along this front and appeared as a line of echoes over southern Wisconsin as shown in Figure 2.33. Another area of echoes occurred along the Gulf Coast at all three radar map times. These echoes were widely scattered as evident in the 1800 GMT GOES imagery (Figures 2.29 and 2.30).

Figures 2.34 and 2.35 show precipitation accumulation for 6 hour periods ending at 1800 GMT 22 August and 0000 GMT 23 August. Precipitation was observed within an elongated region along the frontal zone in the Midwest and East where the amounts were generally less than 0.50 inches. Small areas of precipitation were also observed along the Gulf Coast and over the Rocky Mountains. An extensive area of precipitation occurred over Saskatchewan and Manitoba and North Dakota ahead of the surface low to the west.

2.3.2 Synoptic case for 25 August 1975. The major surface features over the United States and Canada at 1200 GMT are depicted in Figure 2.36. A deep low pressure center with a 984 mb closed isobar was present over central Canada. A cold front extended south of the low into central Ontario and southwestward to Kansas. From there, the front extended across southern Kansas and through a weak low in western Oklahoma and into southern Colorado. A warm front was present over the Great Lakes

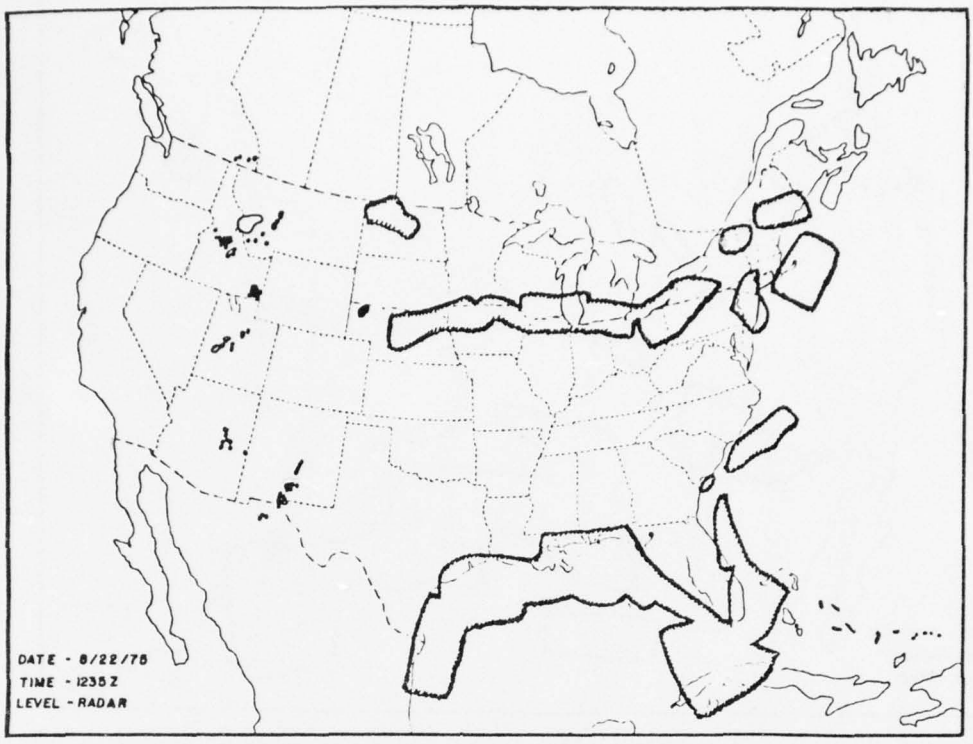

Figure 2.31. Radar summary with areas of radar echoes depicted by scalloped lines.

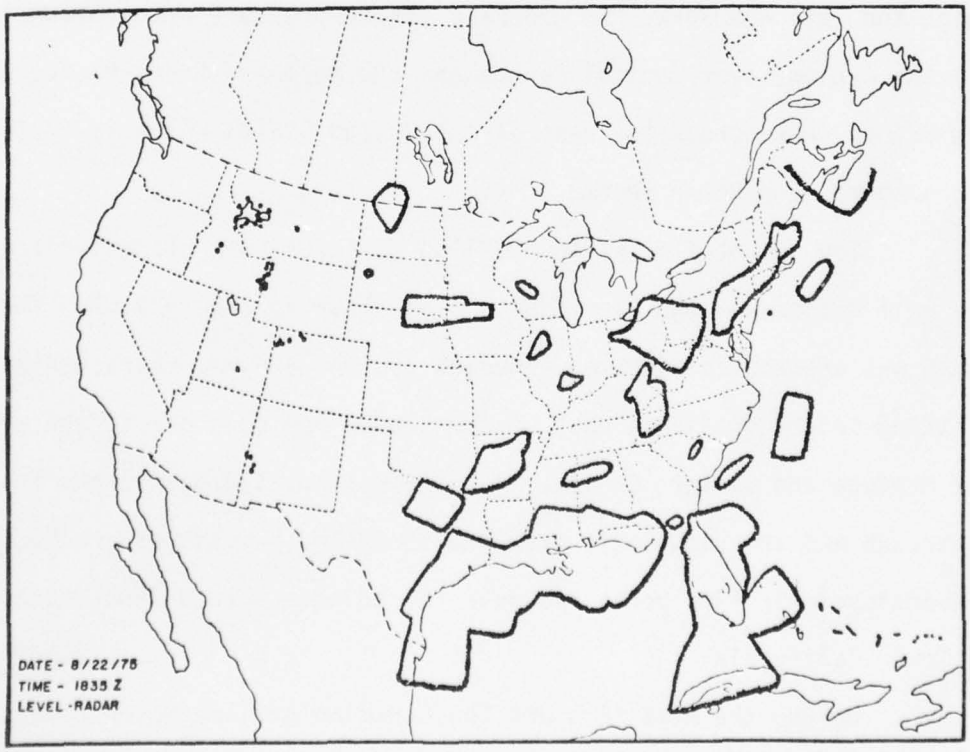

Figure 2.32. Same as above except the time is 6 hours later.

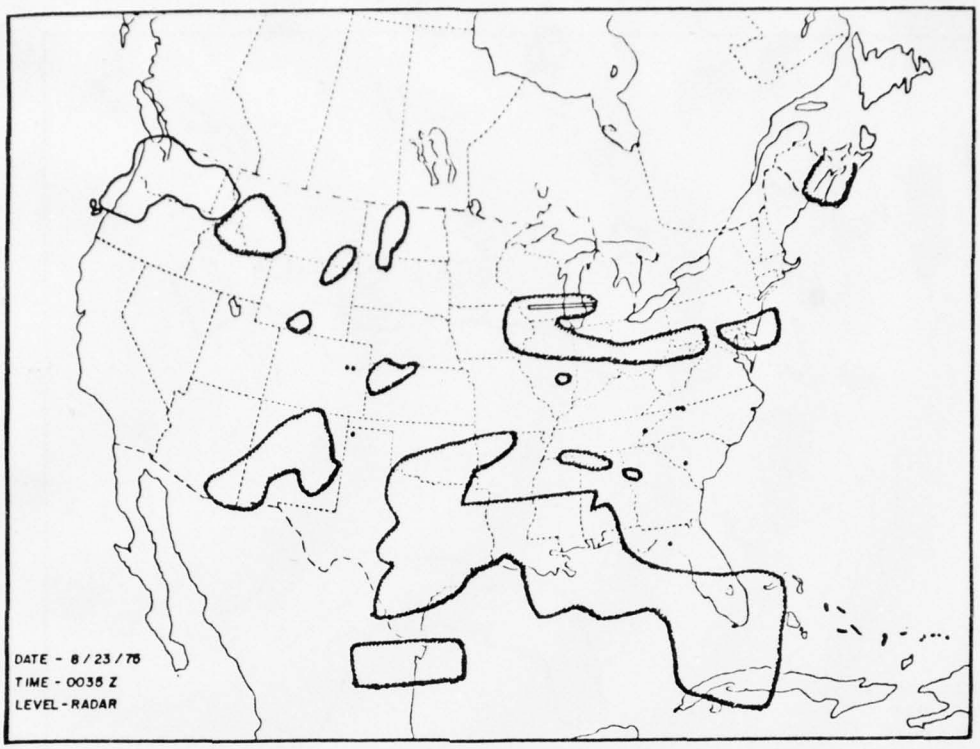

Figure 2.33. Radar summary with areas of radar echoes depicted by scalloped lines.

region and into New York. In general, strong pressure gradients occurred with the cyclone over central Canada and the northern Great Plains but were rather weak across the rest of the United States which is typical of a summertime weather regime.

The 500 mb flow at 1200 GMT on 25 August was characterized by a well defined trough over Manitoba as shown in Figure 2.37. The trough was associated with the Canadian cyclone and was characterized by strong height gradients east of the trough and cold air to the west over Montana and western Canada. A ridge was located downstream from the trough and the ridge axis extended north-south over western Quebec. Weak anticyclonic flow prevailed over the southeastern United States and lower California.

During the next 12 hours the Canadian cyclone moved to Hudson Bay and deepened to 980 mb, and the cold front progressed across Ontario

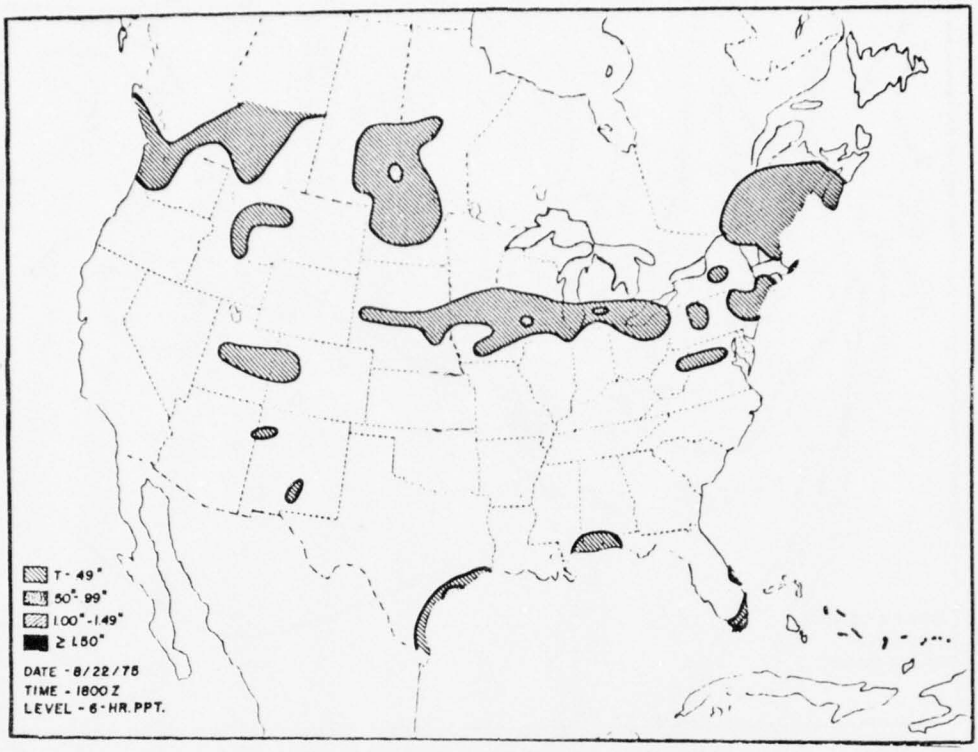

Figure 2.34. Precipitation accumulations in inches for the 6 hour period ending at the map time.

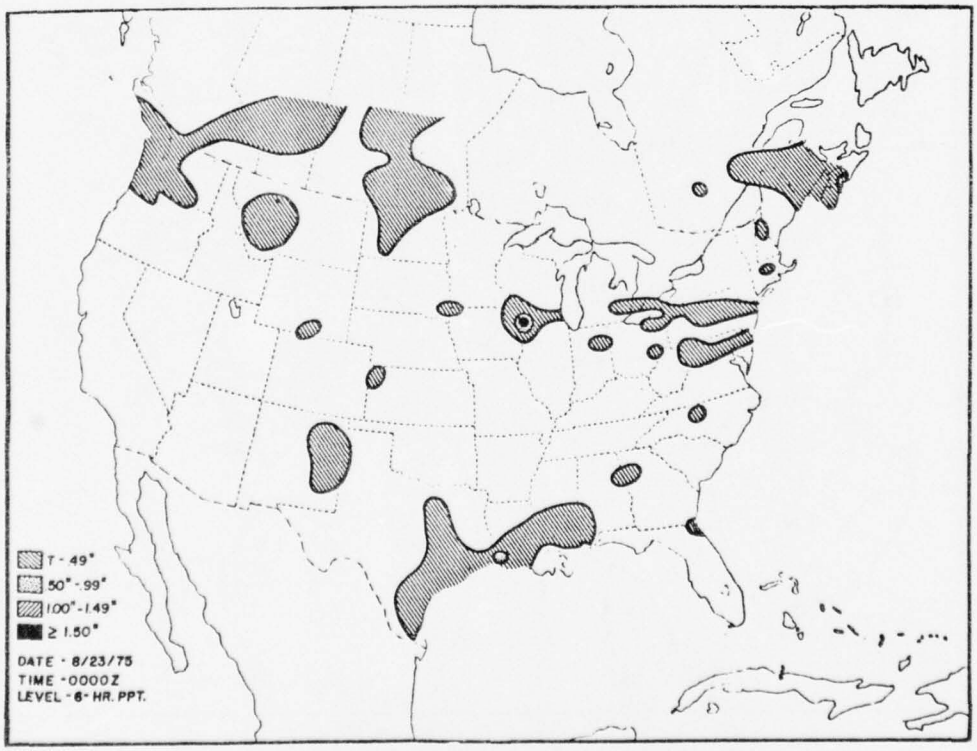

Figure 2.35. Same as above except the time is 6 hours later.

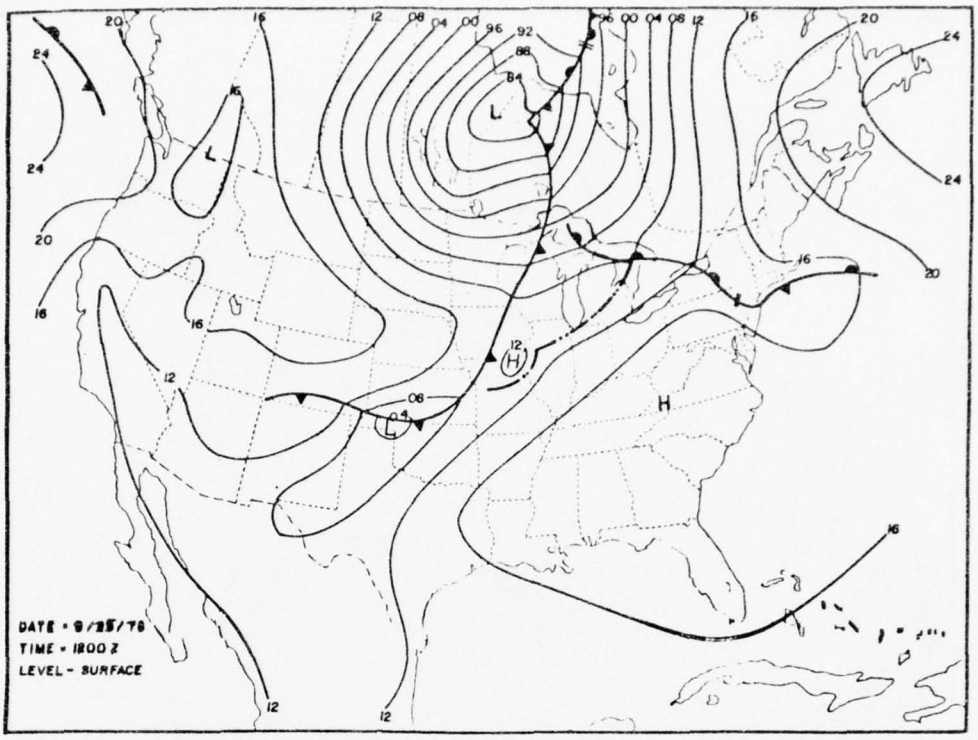

Figure 2.36. Sea level pressure map with fronts. Isobars are drawn at 4 mb intervals.

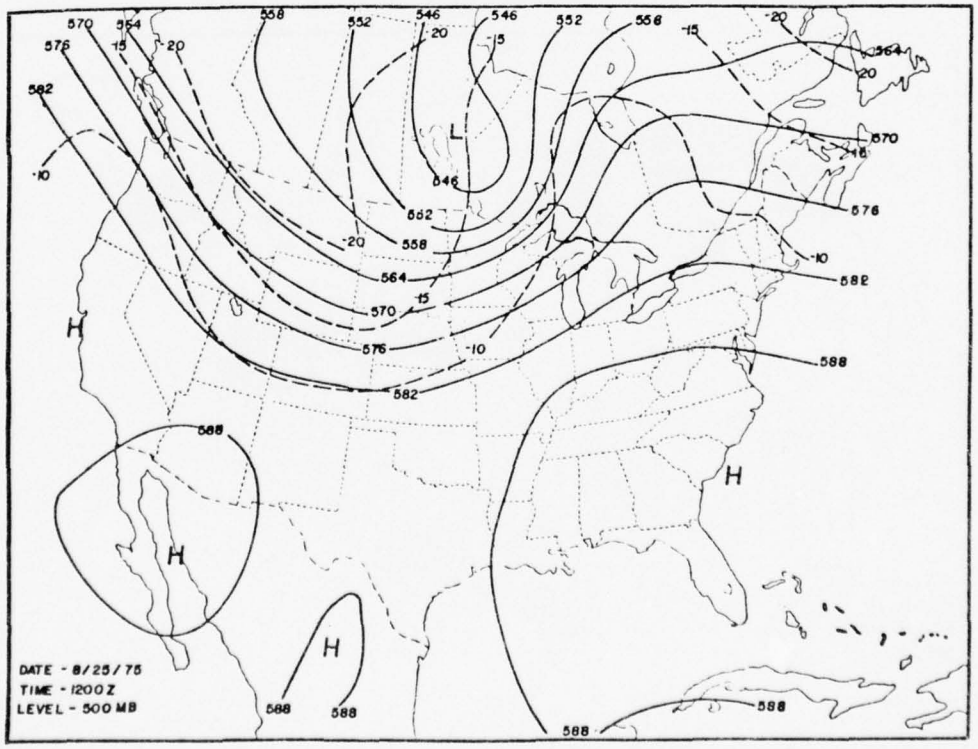

Figure 2.37. Map of the 500 mb level. Solid lines represent contour heights (dm) and dashed lines isotherms (°C).

and into the Great Lakes region as shown in Figure 2.38. Further south in the Midwest, the frontal system moved slowly eastward and remained stationary over Oklahoma and Texas. The sea level pressure gradients at 0000 GMT 26 August were somewhat weaker compared to the previous map time (Figure 2.36) and indicated the Canadian low was beginning to dissipate.

The corresponding 500 mb flow is shown in Figure 2.39. The 500 mb trough, associated with the Canadian cyclone, also progressed eastward and exhibited less vertical tilt with the sea level pressure field than at the previous map time. Anticyclonic flow continued to predominate over eastern Canada, southeastern United States and lower California. There was a pronounced decrease in 500 mb heights over eastern Texas and Louisiana. This was partly due to eastward movement of the major trough to the north and was followed by advection of moist tropical flow from the Gulf of Mexico into Texas.

The GOES visible and infrared satellite imagery that were available at the time of a Nimbus VI orbital pass on 25 August are shown in Figures 2.40 and 2.41. The prominent cloud feature was the cyclone over Canada with a well defined spiral cloud pattern around the surface low center. A frontal cloud band extended from approximately Lake Michigan to Kansas with numerous convective clouds ahead of the front over Missouri. Another area of cloudiness was located over Louisiana and eastern Texas and was associated with moist southerly flow from the Gulf of Mexico. Cumulus cloud lines with anticyclonic curvature were present in the high pressure center over the southeastern United States. Remarkably clear skies were present over the southeastern United States with a cloud free zone stretching northeastward to the Great Lakes

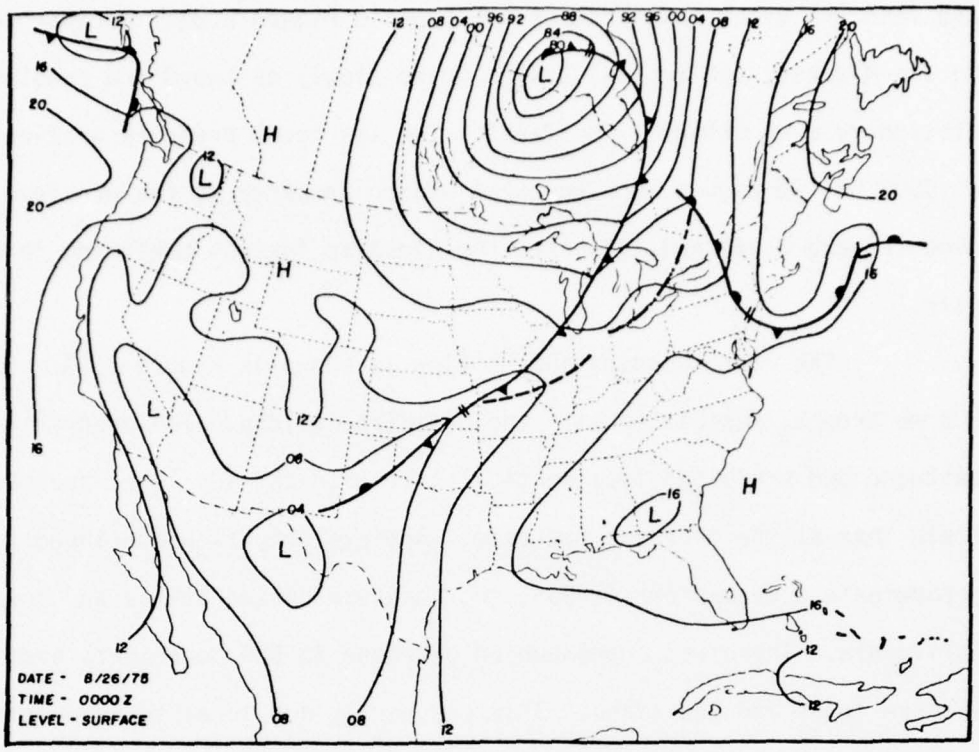

Figure 2.38. Sea level pressure map with fronts. Isobars are drawn at 4 mb intervals.

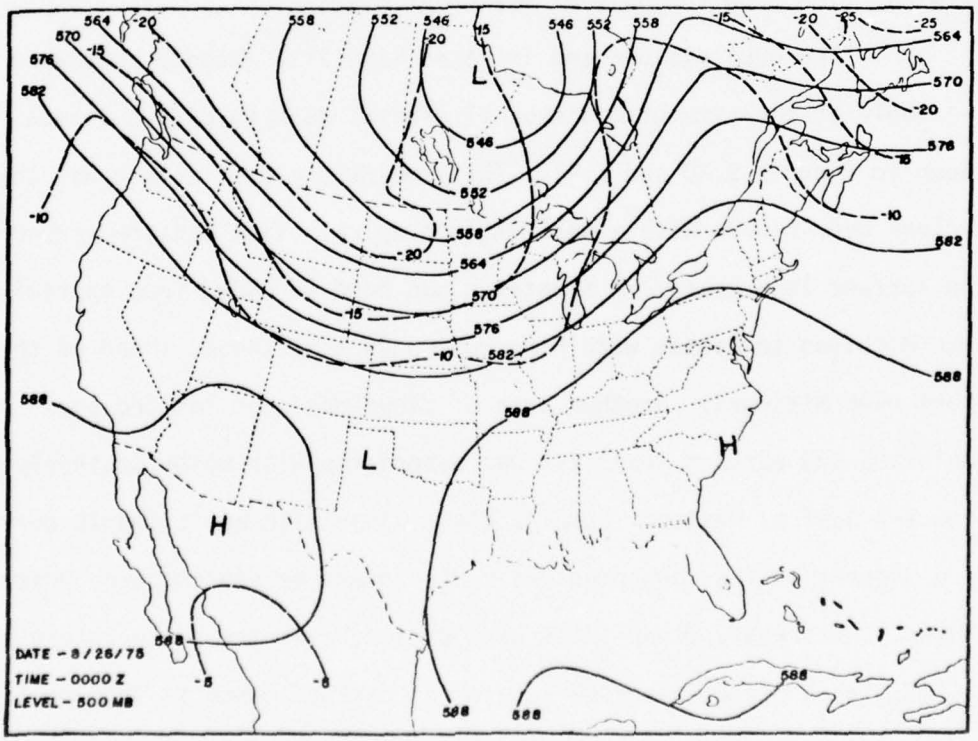

Figure 2.39. Map of the 500 mb level. Solid lines represent contour heights (dm) and dashed lines isotherms (°C).

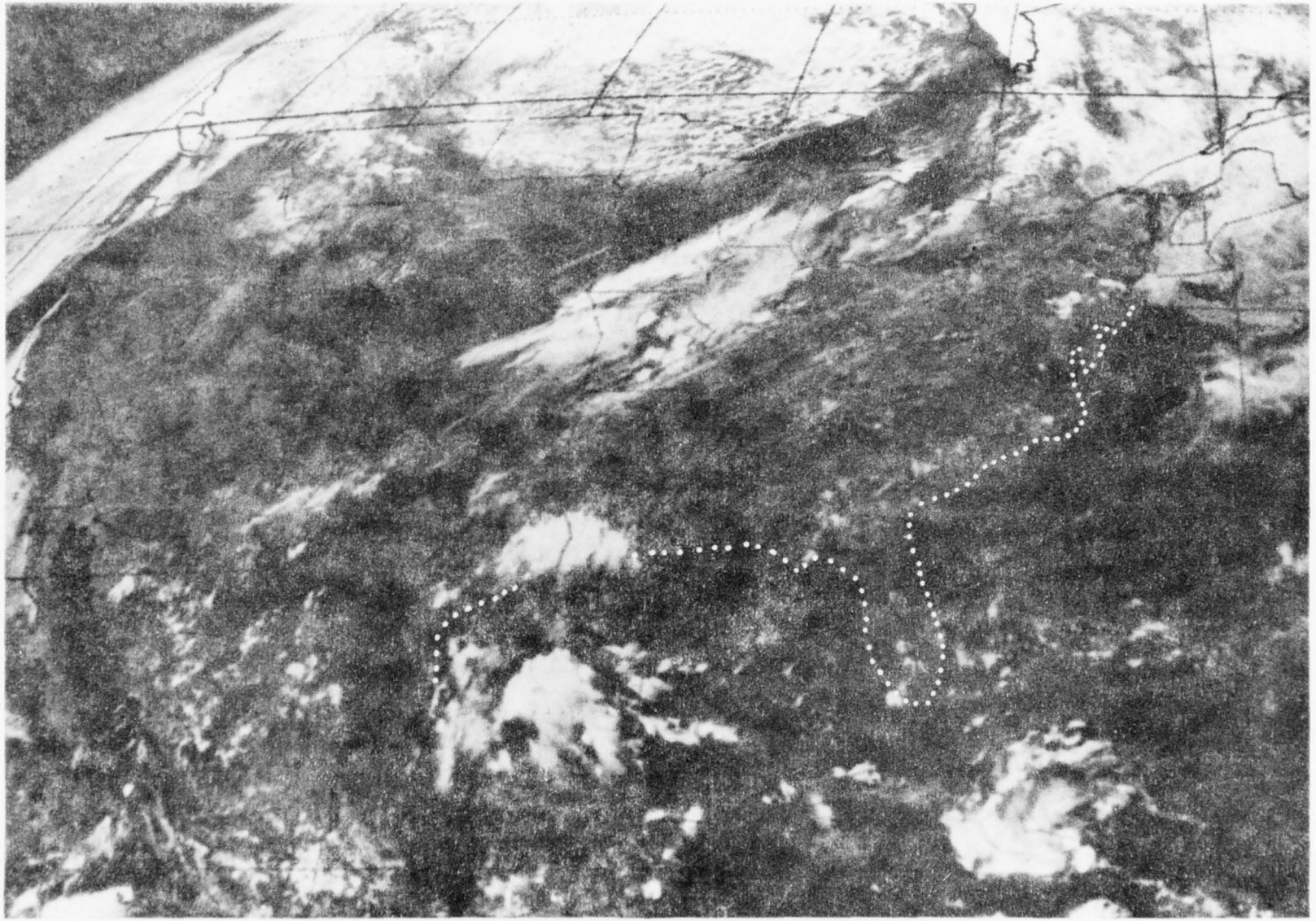

Figure 2.40. GOES visible image for 1900 GMT 25 August 1975.

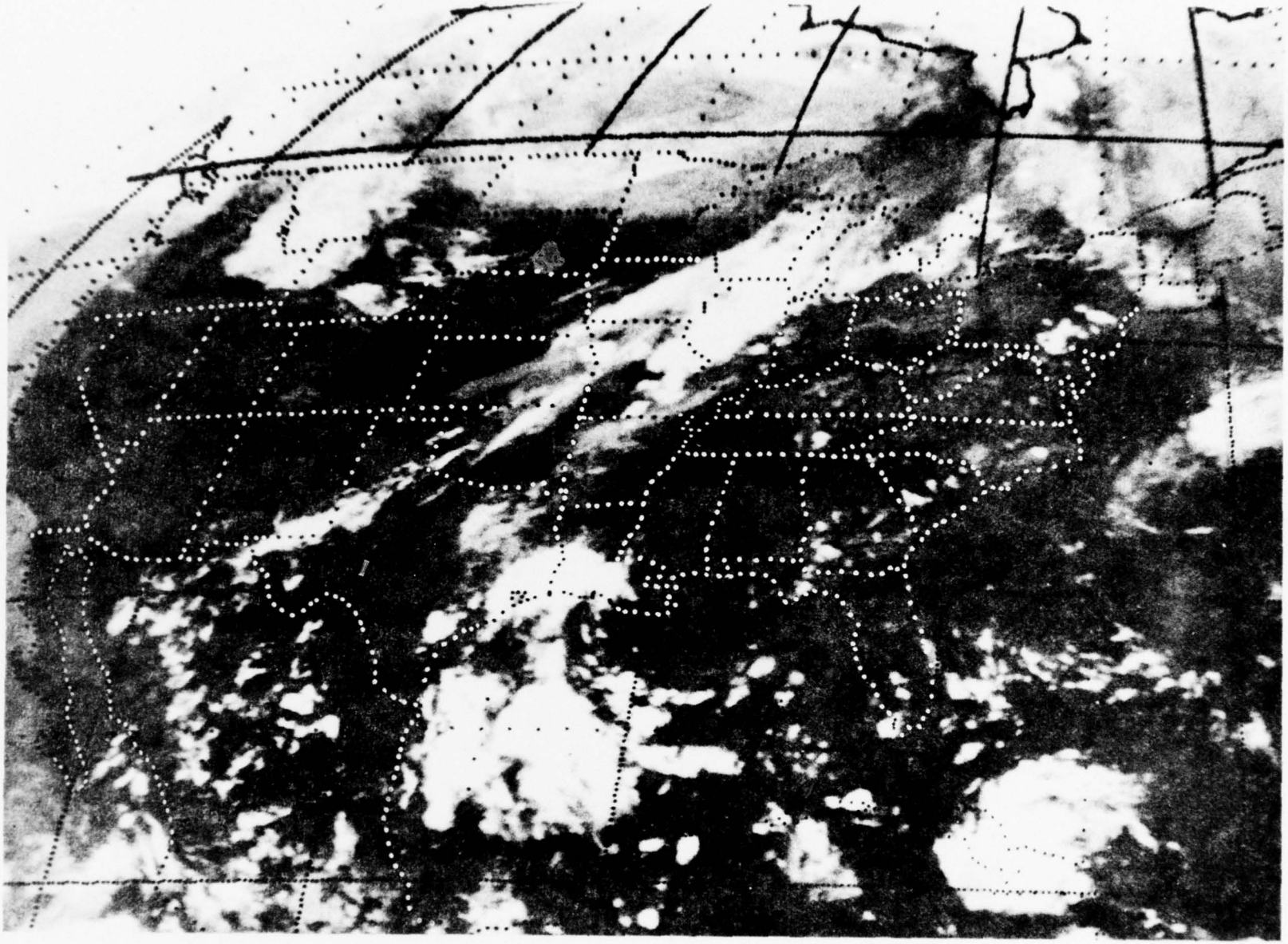

Figure 2.41. GOES infrared image for 1900 GMT 25 August 1975.

region behind the cold front.

The radar summaries for this situation are depicted in Figures 2.42 to 2.44 for three 6 hour time intervals beginning at 1235 GMT 25 August. Radar echoes occurred at all three map times for an area centered over Missouri. These echoes were associated with the cold front as well as prefrontal convective activity and developed up to 64,000 ft. By 0035 GMT 26 August, a line of echoes extended across Missouri and eastern Kansas as shown in Figure 2.44. Prefrontal instability was evident from lifted index values of less than -4 over a large area ahead of the cold front. Echoes were also present along the Gulf coast and the eastern Great Lakes region.

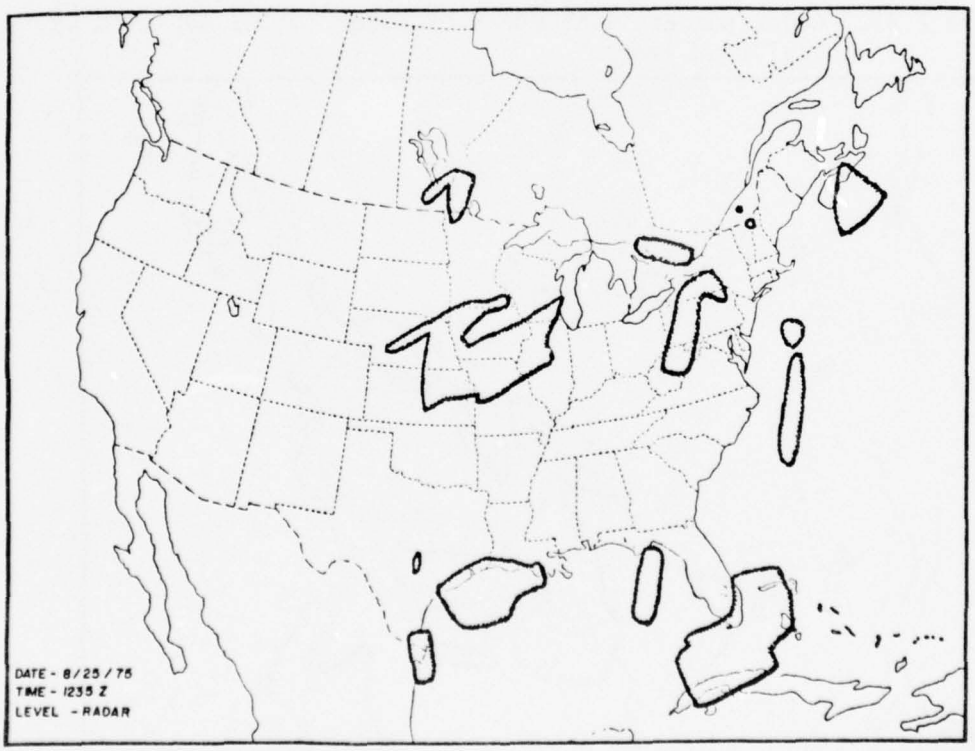

Figure 2.42. Radar summary with areas of radar echoes depicted by scalloped lines.

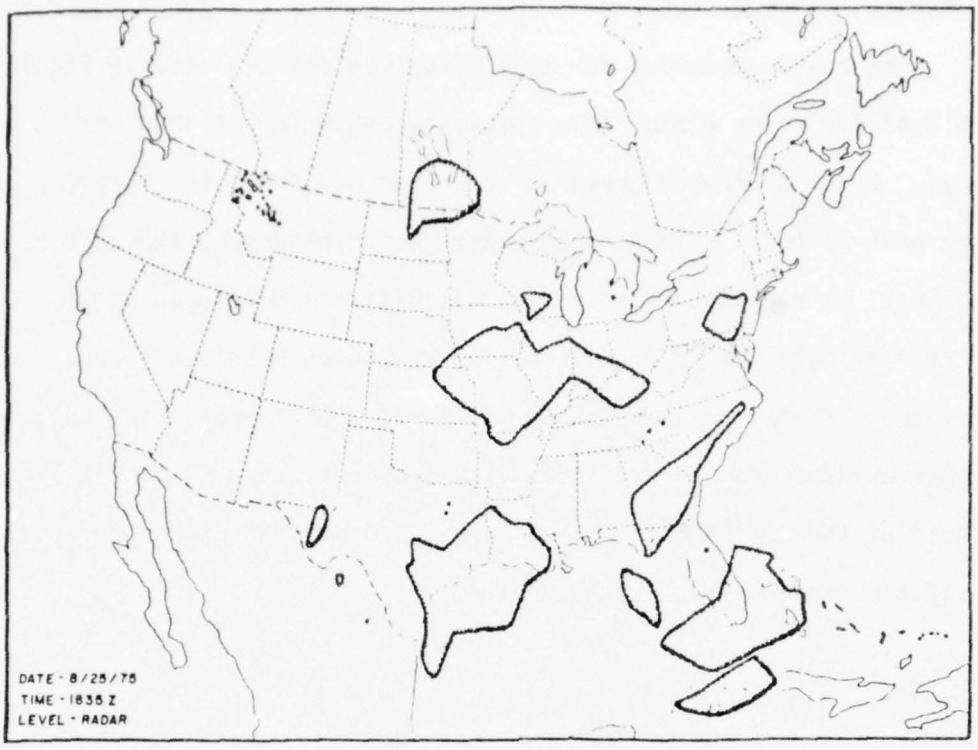

Figure 2.43. Radar summary with areas of radar echoes depicted by scalloped lines.

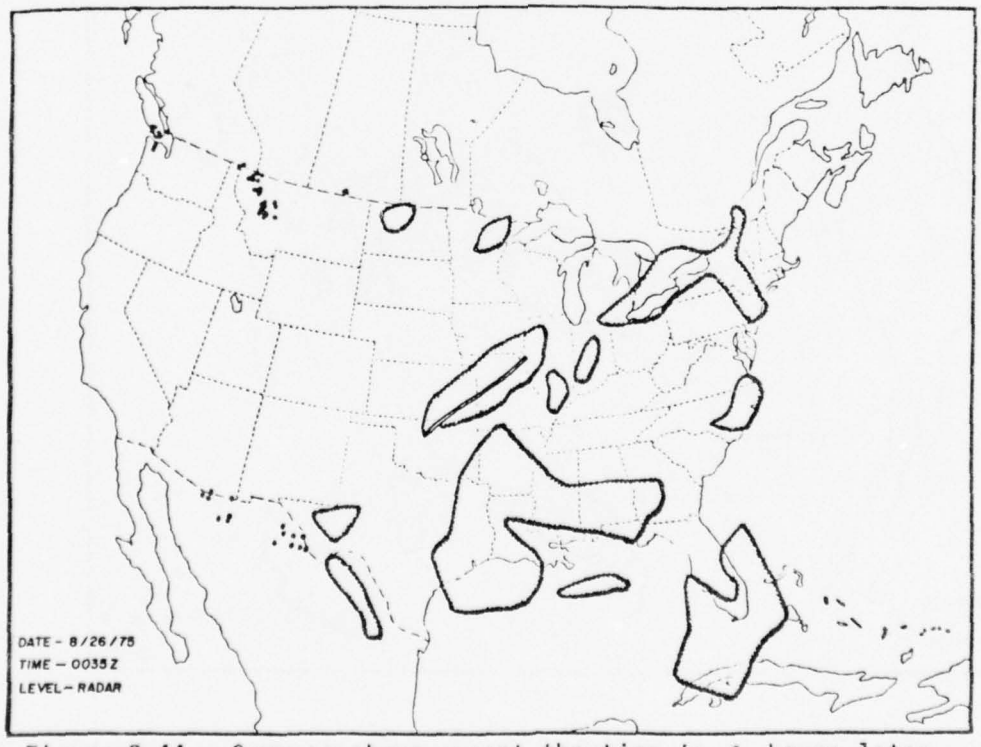

Figure 2.44. Same as above except the time is 6 hours later.

Precipitation amounts for 6 hour periods ending at 1800 GMT 25 August and 0000 GMT 26 August are shown in Figures 2.45 and 2.46. Two extensive areas of precipitation were located in the northern Great Plains along the Canadian border and from the northeastern Great Lakes to New England. Precipitation amounts in the first area were less than 0.50 inches and were associated with the Canadian cyclone and the cold front. It was not possible to determine how far north the precipitation extended because of lack of data. The second precipitation area was associated with the warm front during the first 6 hour period and convective activity later in the day. Several stations in southern Ontario reported over one inch of rain.

An important precipitation area over the United States occurred along the cold front in Iowa, Illinois and Missouri where a line of thunderstorms produced more than 4 inches at one station. Significant precipitation amounts were also produced along the Gulf Coast.

2.4 Wintertime Mid-latitude Cyclone

This case was selected from a February 1976 synoptic situation when a mid-latitude cyclone went through a complete life cycle as it moved across the United States. This cyclone was well defined several days before it entered the U.S. at the Oregon Coast on 18 February. As the system moved across the intermountain region it weakened, particularly in the lower troposphere. By 1200 GMT 20 February, the synoptic system emerged on the lee side of the Rocky Mountains and developed into a major storm in eastern Colorado on the following day. A detailed synoptic investigation was carried out for the period from February 20 to 22 when good satellite data coverage was provided by Nimbus VI.

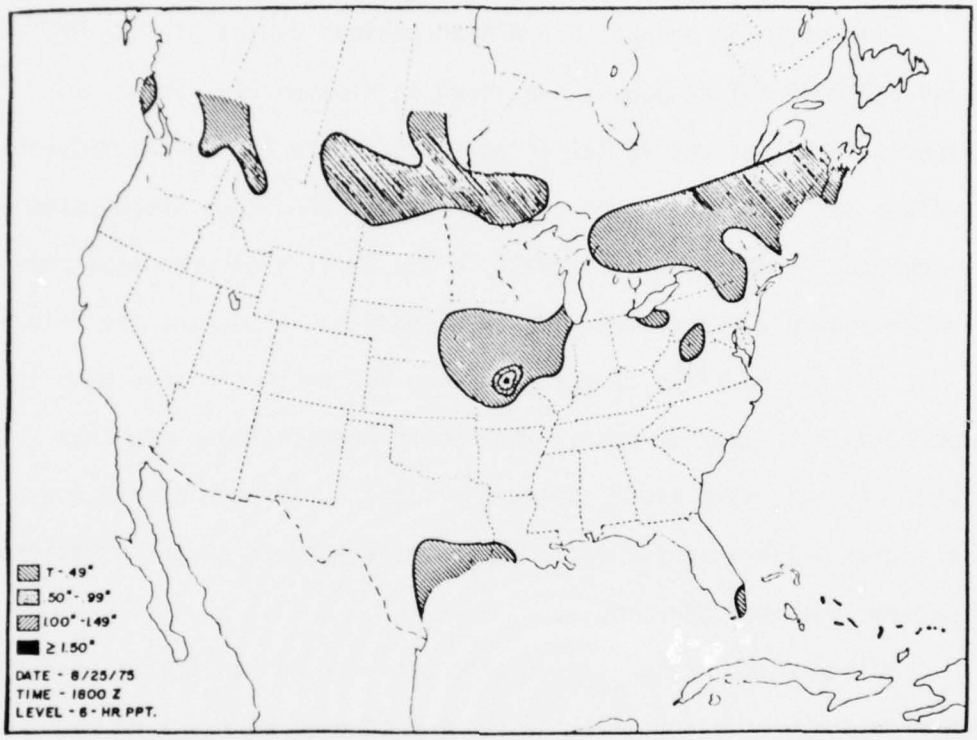

Figure 2.45. Precipitation accumulations in inches for the 6 hour period ending at the map time.

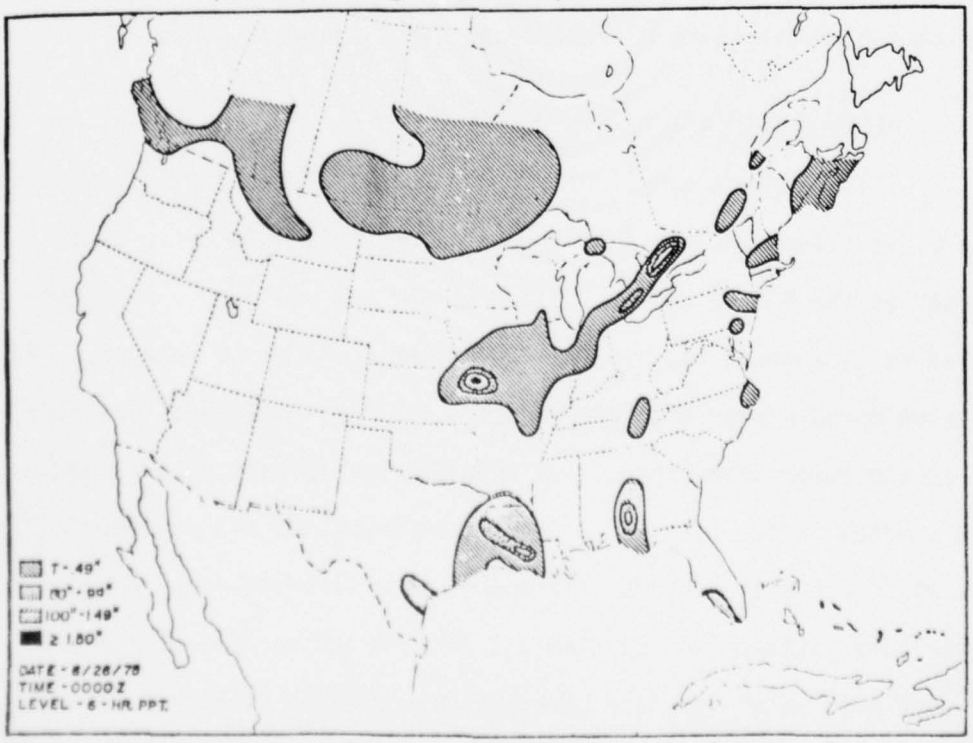

Figure 2.46. Same as above except the time is 6 hours later.

2.4.1 Synoptic Situation at 1200 GMT 20 February 1976. At this first map time, the developing cyclone was present in northeast Colorado with a central low pressure of 996 mb as shown in Figure 2.47. The system tilted west with height with the 500 mb trough centered over the four corners area. Coldest air at 500 mb was located upstream from the trough, and the thermal advection pattern favored further intensification of the cyclone.

The configuration of fronts with this cyclone was somewhat similar to the classical cyclone model. A cold front stretched from the low pressure center across northern Mexico and into the eastern Pacific Ocean. A warm front extended to the southeast across Oklahoma and the lower Mississippi Valley. A noted difference in this case from the classical cyclone model, but typical to this geographic area, was the absence of a well defined pressure trough along the cold front. Instead, the surface trough was located far ahead of the front and was over western Texas and central Mexico. This trough formation was attributed to barrier effects on the westerly flow by the Rocky Mountains.

Figure 2.47 shows the 6 hour precipitation accumulations for the period ending at 1200 GMT. The precipitation area of interest extended across southern Wyoming and northern Colorado and into Utah where the surface pressure gradients were the strongest. Generally, the precipitation occurred in the form of snow with amounts of 1 to 4 inches at lower elevations. Snow was falling along the eastern slopes of the Rockies in northern Colorado and southern Wyoming and was partially detected by radar at 1235 GMT.

Prefrontal weather was characterized by remarkably dry conditions. The 850 and 500 mb relative humidity analyses in Figure 2.48 depict an extensive area with values less than 10% at 500 mb over

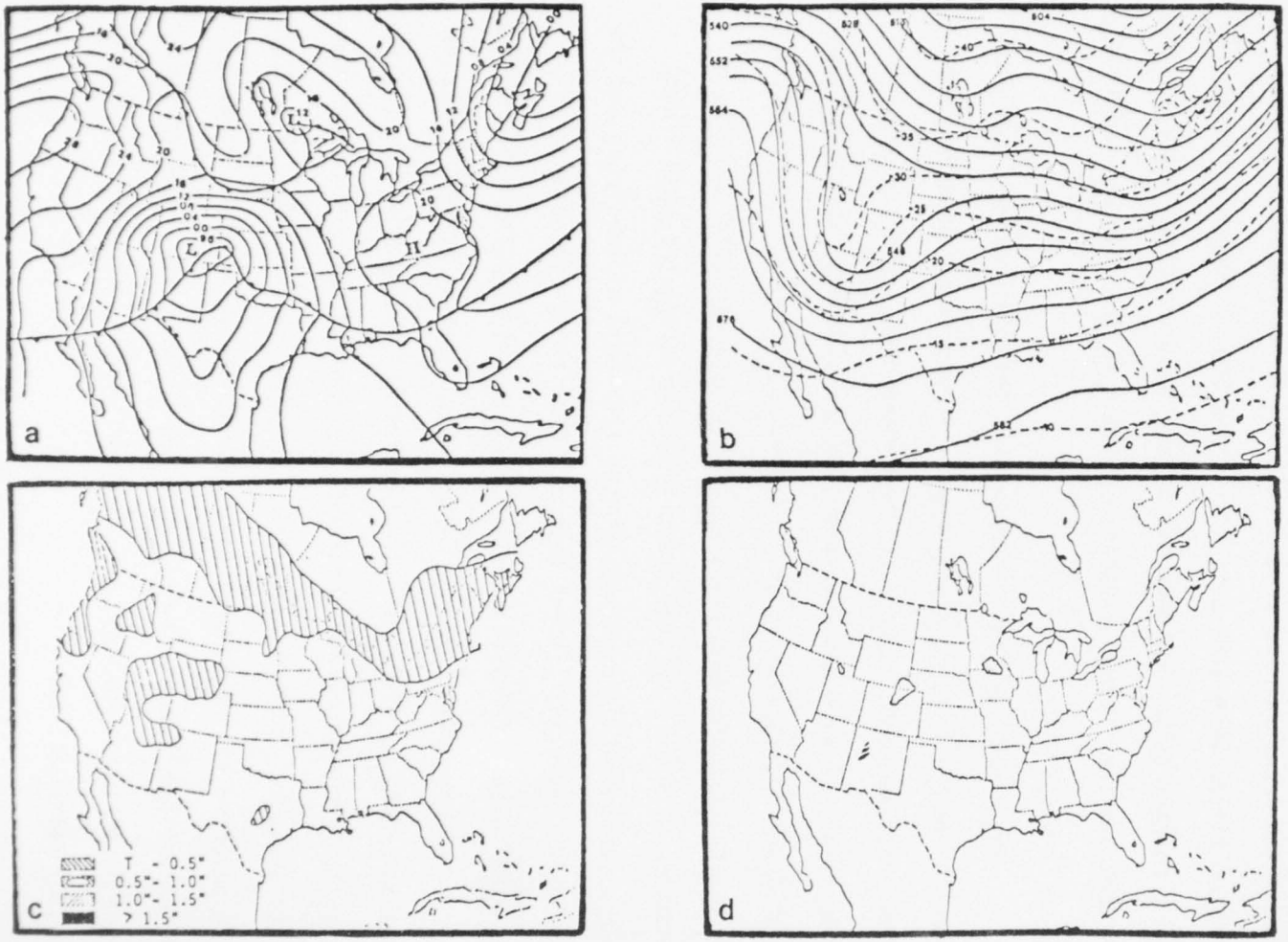

Figure 2.47. (a) Sea level pressure analysis, (b) 500 mb analysis, and (c) 6 hour precipitation amounts at 1200 GMT, and (d) radar summary at 1235 GMT on 20 February 1976.

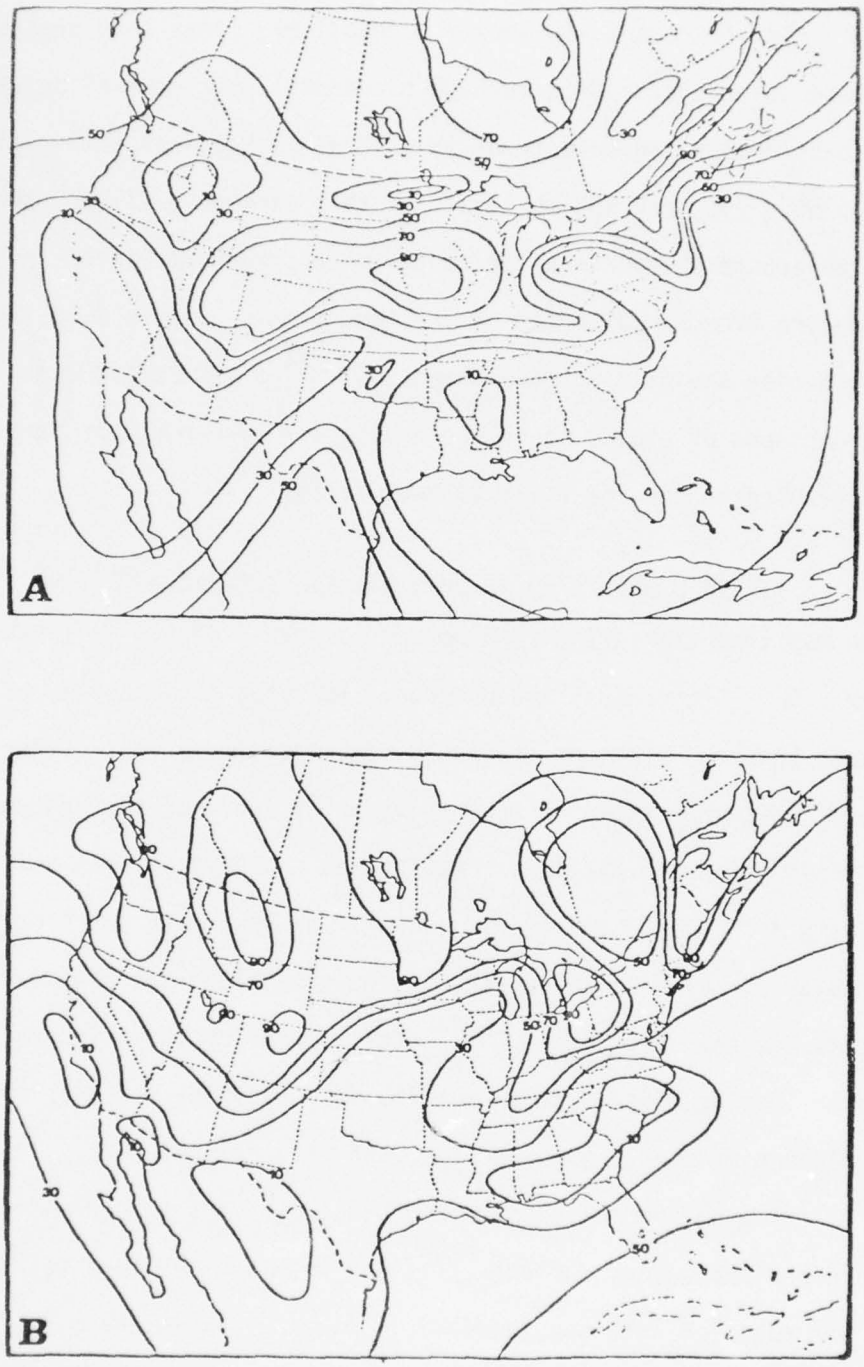

Figure 2.48. Relative humidity analysis at 1200 GMT 20 February 1976 for the (a) 500 mb level and (b) 850 mb level.

New Mexico and northern Texas. The GOES-East infrared image at this synoptic time (Figure 2.49) showed a relatively clear zone extending southwest to northeast between high cloudiness over central Texas and the clouds behind the cold front in Colorado. Vertical motion fields for the 900, 700, and 500 mb levels at this time were rising throughout the area around the surface low center with strongest ascent in the lower troposphere over Kansas ahead of the warm front. Figure 2.50 indicates rising motion amounted to more than -5 $\mu b\ s^{-1}$ at 900 and 700 mb in this area. Absence of clouds in the ascending air over northern Texas may be attributed to the low relative humidities.

2.4.2 Synoptic Situation at 0000 GMT 21 February 1976. By the second map time the surface low moved to central Kansas as shown in Figure 2.51. The central low pressure indicated no deepening at the surface; however, pressure gradients remained strong west of the low and underwent noticeable strengthening to the north of the system. A warm front stretched eastward from the low center to Kansas and southeast into Mississippi and across the Gulf of Mexico to the Florida Peninsula. A cold front reached southward through the Big Bend area of Texas and then southwest to Baja California. A third frontal zone extended into Nebraska from a weak low in the northern branch of the westerlies over Canada and was undergoing frontolysis.

The 500 mb map (Figure 2.51) indicated the trough was well defined and approached the cut-off stage over southeastern Colorado. Cold air advanced into the trough as a ridge moved inland over the Pacific Northwest. Warm air advection at 500 mb continued ahead of the surface low in Kansas and in advance of the surface warm front.

Extensive areas of precipitation were initiated at this

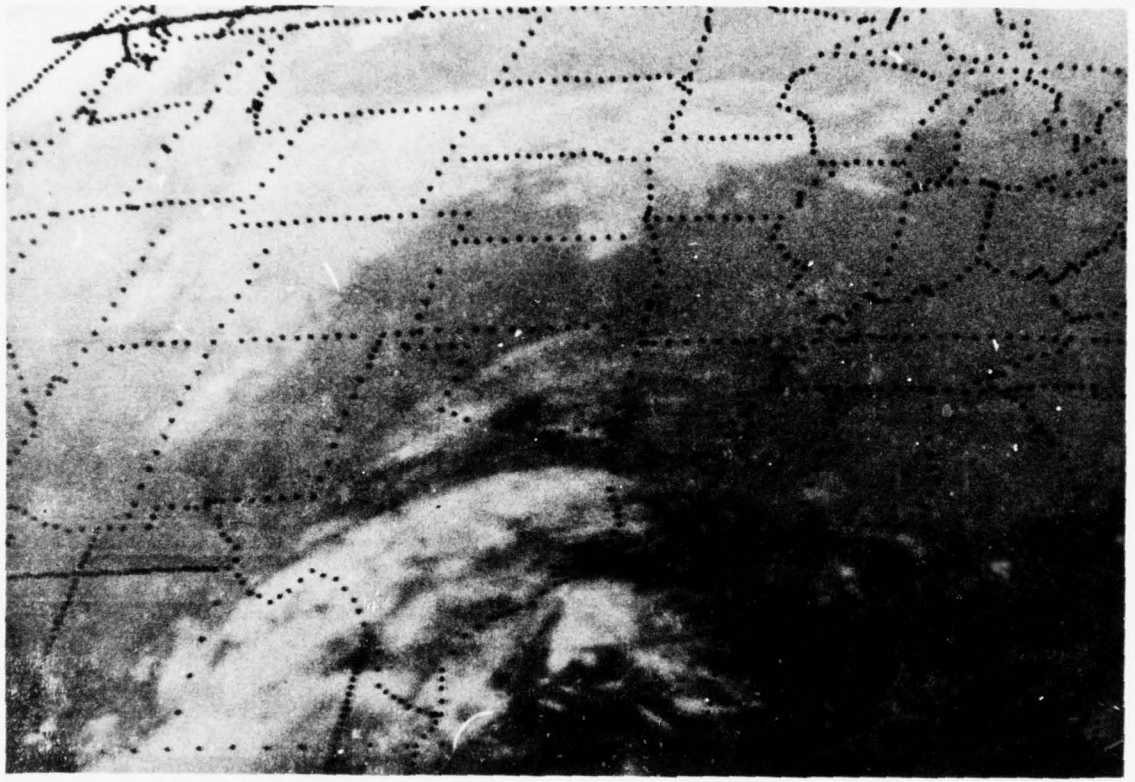

Figure 2.49. GOES-East infrared satellite image at 1200 GMT 20 February 1976.

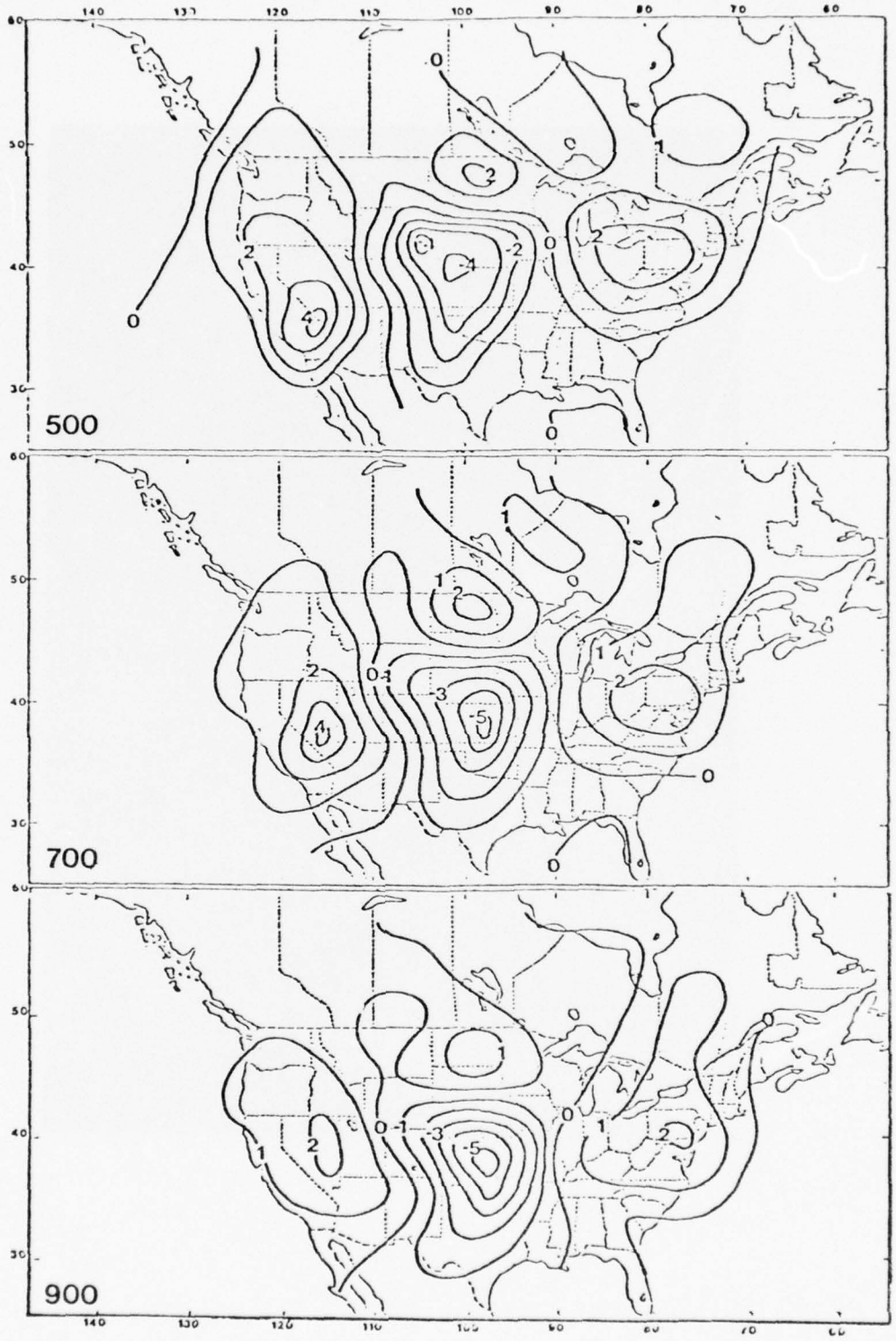

Figure 2.50. Total vertical motions for the 900, 700 and 500 mb levels at 1200 GMT 20 February 1976. Isopleth interval is 1 μb s^{-1}.

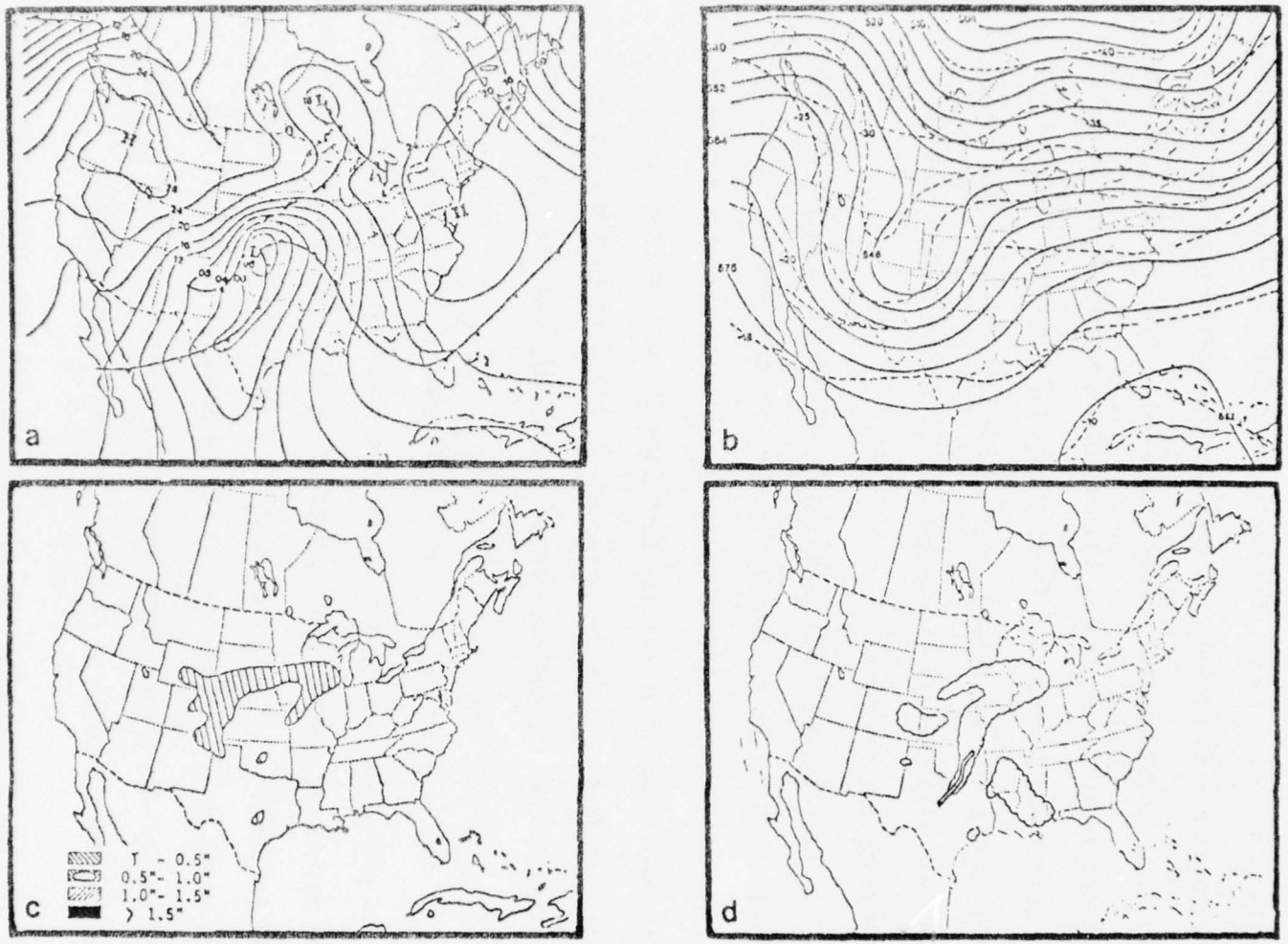

Figure 2.51. (a) Sea level pressure analysis, (b) 500 mb analysis, and (c) 6 hour precipitation amounts at 0000 GMT, and (d) radar summary at 0035 GMT on 21 February 1976.

synoptic time. Northward streaming Gulf moisture experienced substantial lifting over the warm front and resulted in an east-west oriented band of mostly snow across Iowa. The overrunning precipitation area extended into Nebraska and coincided with the strong pressure gradients and cyclonically curved isobars. Snow continued in the upslope flow along the eastern Rockies. A line of thunderstorms developed in the warm air sector just ahead of the cold front across Oklahoma and Texas in the unstable warm air where lifted index values were less than -4. This unstable air also contributed to the precipitation echoes over the lower Mississippi Valley.

The relative humidity analyses for the 850 and 500 mb levels (Figure 2.52) depicted the dry air behind the cold front. Relative humidities of less than 10% at 500 mb extended northeastward over the surface low in Kansas and values less than 30% were present at 850 mb over western Texas. This dry area and the moisture to the east spiralling around the cyclone center were nicely depicted in the GOES-East infrared image in Figure 2.53.

The vertical motion fields are shown in Figure 2.54 and indicate the system was somewhat more intense than at the previous map time. Rising motions at 900 mb strengthened to -8 $\mu b\ s^{-1}$ north of the cyclone center in the area of strong pressure gradients and cyclonic flow. Values of -6 $\mu b\ s^{-1}$ extended up to 500 mb ahead of the warm front in the area with warm air advection. Areas with high humidities and ascending motions compared favorably with the cloud fields.

2.4.3 Synoptic Situation at 1200 GMT 21 February 1976. This synoptic time was the most interesting of the sequence because of the unusual evolution into an occluded system (Figure 2.55). The surface low moved

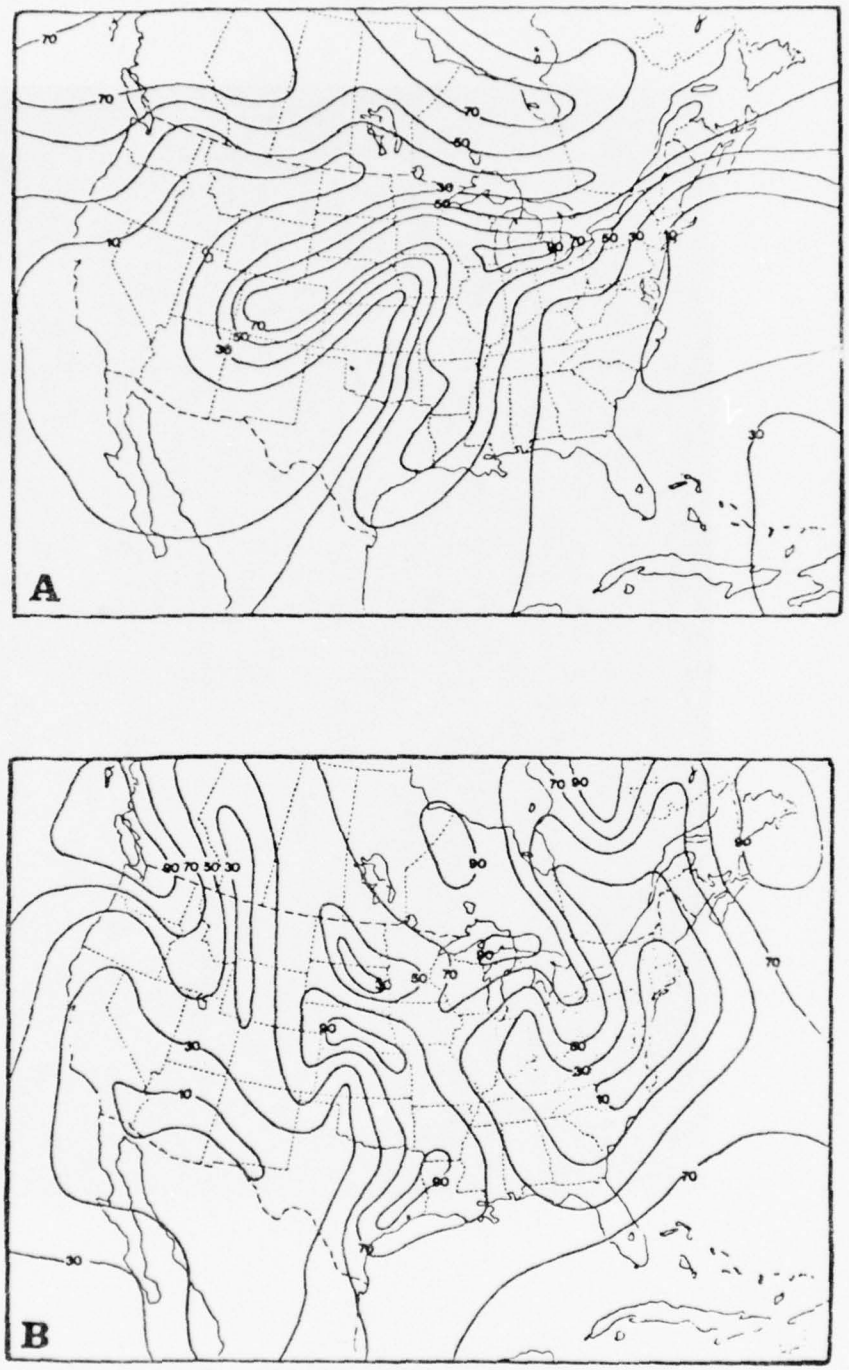

Figure 2.52. Relative humidity analysis at 0000 GMT 21 February 1976 for the (a) 500 mb level and (b) 850 mb level.

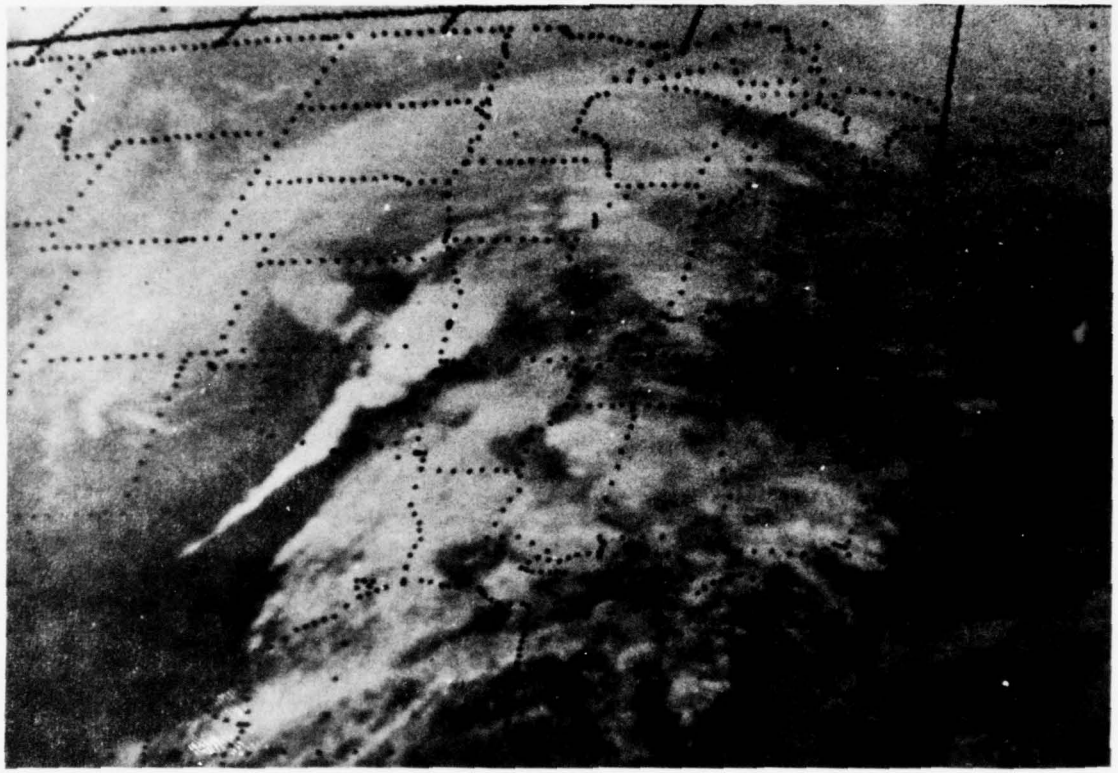

Figure 2.53. GOES-East infrared satellite image at 0000 GMT 21 February 1976.

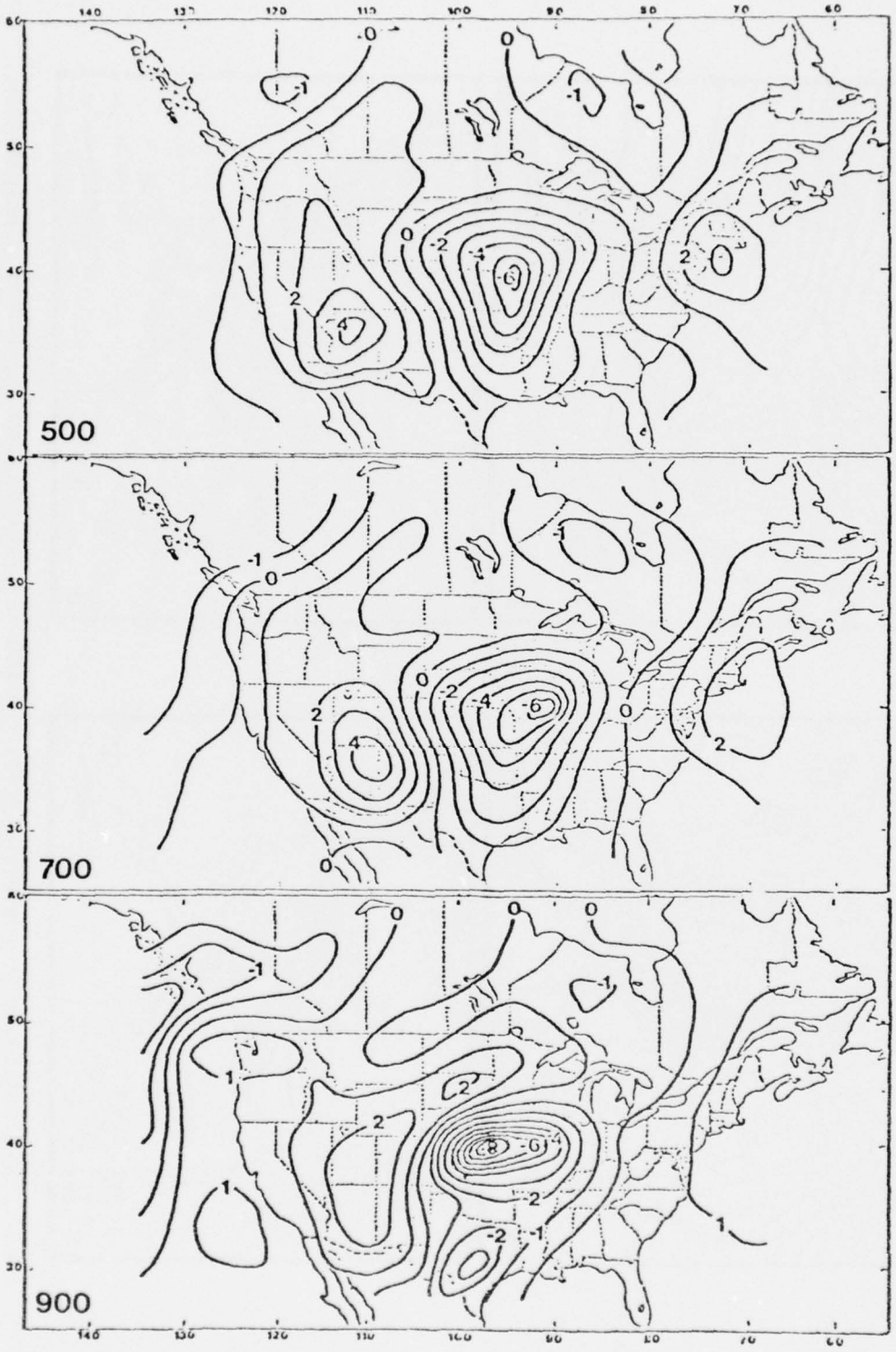

Figure 2.54. Total vertical motions for the 900, 700 and 500 mb levels at 0000 GMT 21 February 1976. Isopleth interval is 1 μb s^{-1}.

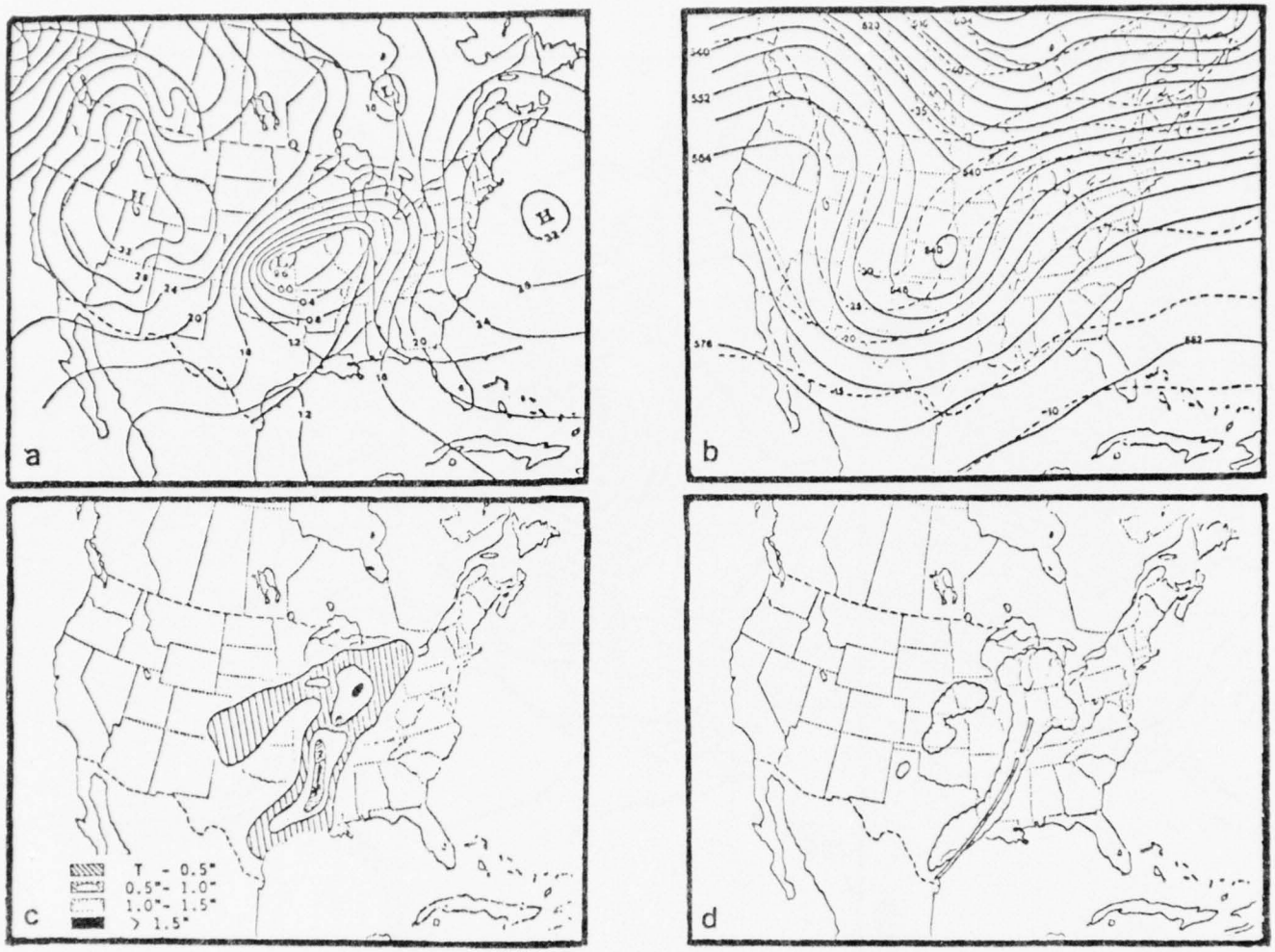

Figure 2.55. (a) Sea Level pressure analysis, (b) 500 mb analysis, and (c) 6 hour precipitation amounts at 1200 GMT, and (d) radar summary at 1235 GMT on 21 February 1976.

slowly eastward across Kansas during the previous 12 hours while the cold front moved rapidly eastward and occluded with the warm front as far east as Indiana. The warm air sector formed a narrow wedge between the cold front along the Mississippi River and the warm front to the east. Strongest pressure gradients remained on the north and west sides of the occluded cyclone.

On the 500 mb map in Figure 2.55, a deep trough was centered over Kansas with one closed isobar. Pronounced cold air advection was present in the trough, and coldest temperatures were located upstream over Colorado. Strongest 500 mb height gradients appeared ahead of the trough axis over Arkansas, Missouri, and Illinois and explained the rapid advancement of the surface frontal system in this case.

The precipitation activity was the most intense during the 12 hours ending at 1200 GMT 20 February. Six hour rainfall amounts (Figure 2.55) exceeded 1 inch at several stations along the cold front as the line of thunderstorms lengthened and maintained its strength. Snow fell along the north side of the occluded front and on the west side of the surface low center within the area of strong cyclonic flow at low levels.

The relative humidity analyses at 500 and 850 mb (Figure 2.56) continued to show the dry air behind the cold front and extending into the cyclone at 500 mb. An elongated area with relative humidities greater than 70% extended from the Texas coastal region to the eastern Great Lakes and spiralled around the dry tongue to the west side of the surface low.

The GOES-East infrared image revealed the middle and high level cloud pattern at this synoptic time (Figure 2.57). A cloud vortex center was evident over eastern Kansas and coincided with the

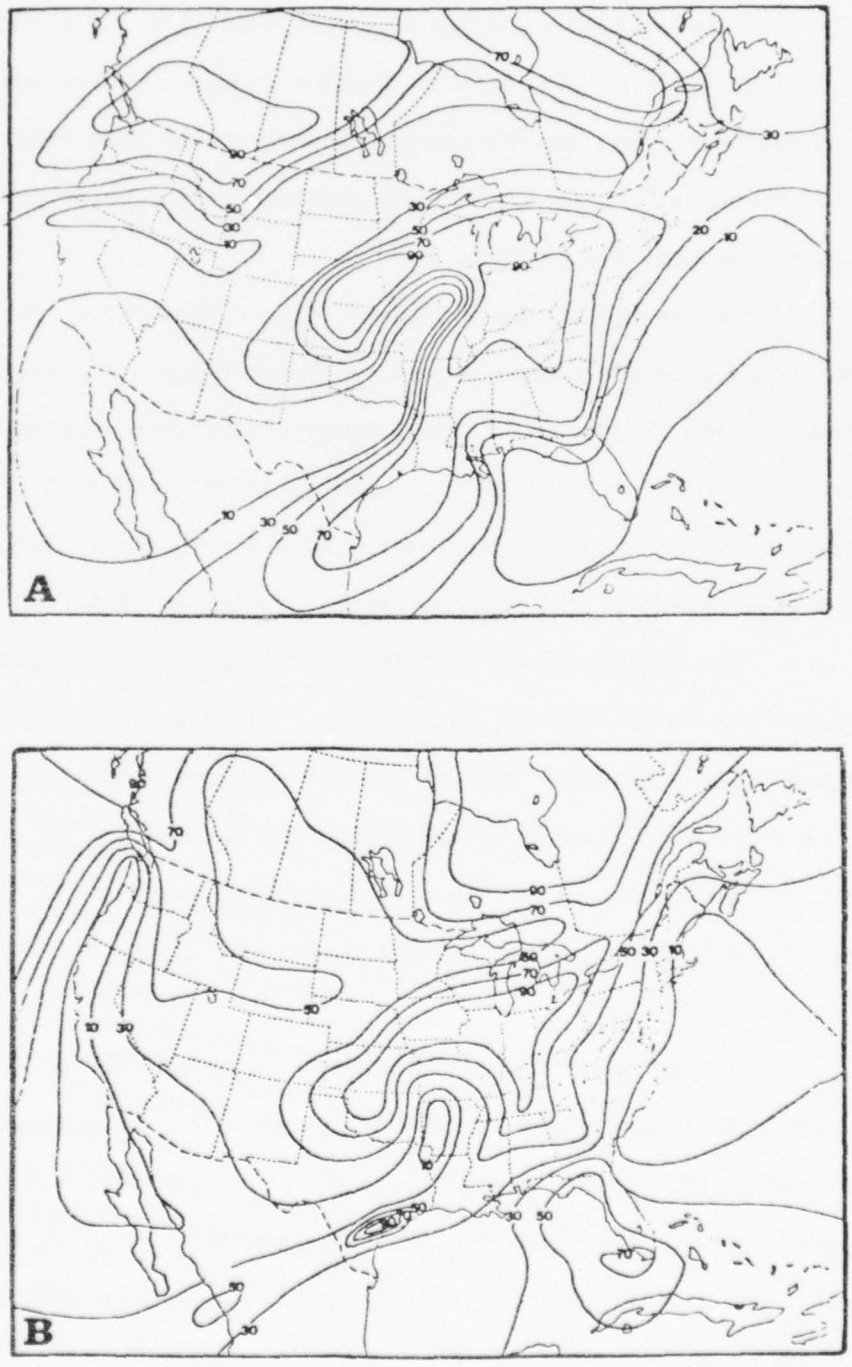

Figure 2.56. Relative humidity analysis at 1200 GMT 21 February 1976 for the (a) 500 mb level and (b) 850 mb level.

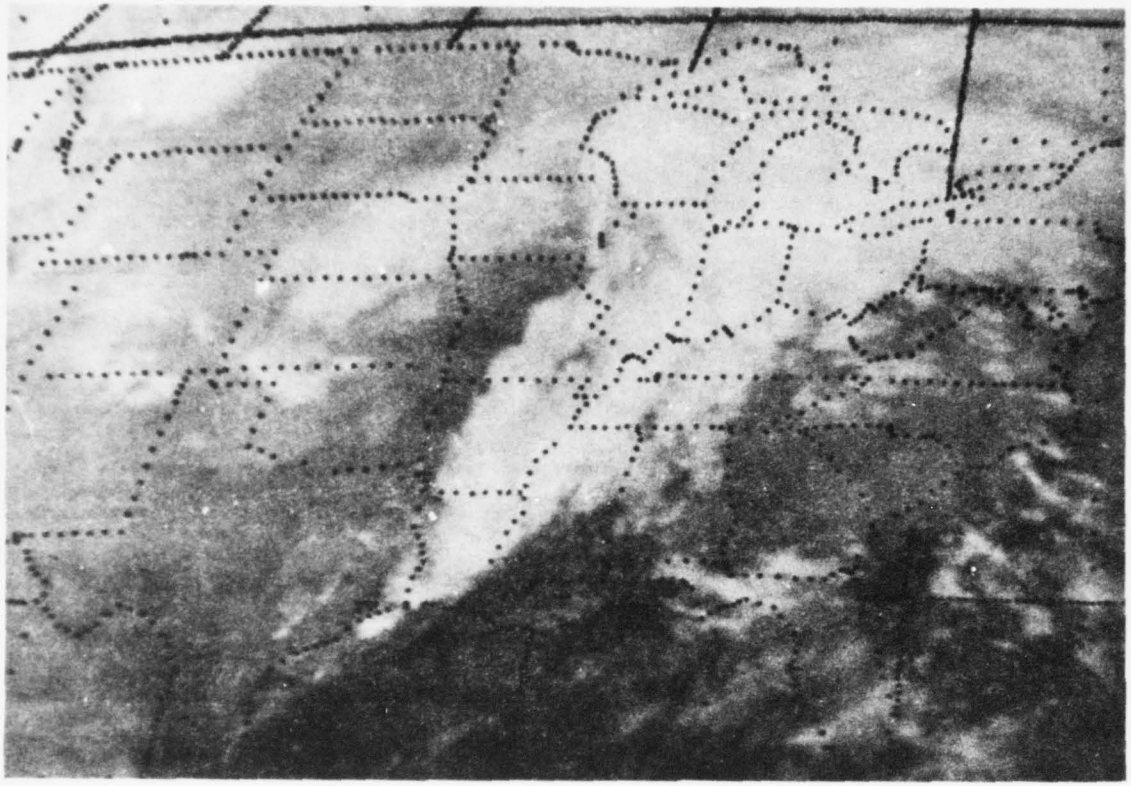

Figure 2.57. GOES East infrared satellite imagery at 1200 GMT 21 February 1976.

closed contour at 500 mb. Coldest cloud tops occurred in the line of thunderstorms along the cold front over the lower Mississippi Valley.

The vertical motion fields are illustrated in Figure 2.58. Areas of strongest ascending motions were slightly weaker than the ones for the previous 12 hours. The 900 mb omega patterns showed two centers of rising motion, one over Ohio and another along the occluded front in southern Iowa. The center of strongest ascending motions over Ohio and Indiana extended up to 500 mb but rapidly disappeared with height near the low center in Kansas. This was attributed to new development over Indiana as the Kansas cyclone dissipated. Strong subsidence was present in the dry air over Texas and in the wake of the cyclone over Colorado.

2.4.4 Synoptic Situation for 0000 GMT 22 February 1976. The Kansas low completely dissipated by the last synoptic time, and the lowest pressure was located over Indiana and amounted to 1002 mb as shown in Figure 2.59. Pressure gradients weakened around the low center, especially in the northwest quadrant of the system. There was also a weakening at 500 mb where the closed low evolved into an open wave and thermal advection decreased in the vicinity of the cyclone.

The precipitation amounts decreased from earlier map times but the overall extent of precipitation coverage remained nearly the same as indicated in the distribution of radar precipitation echoes in

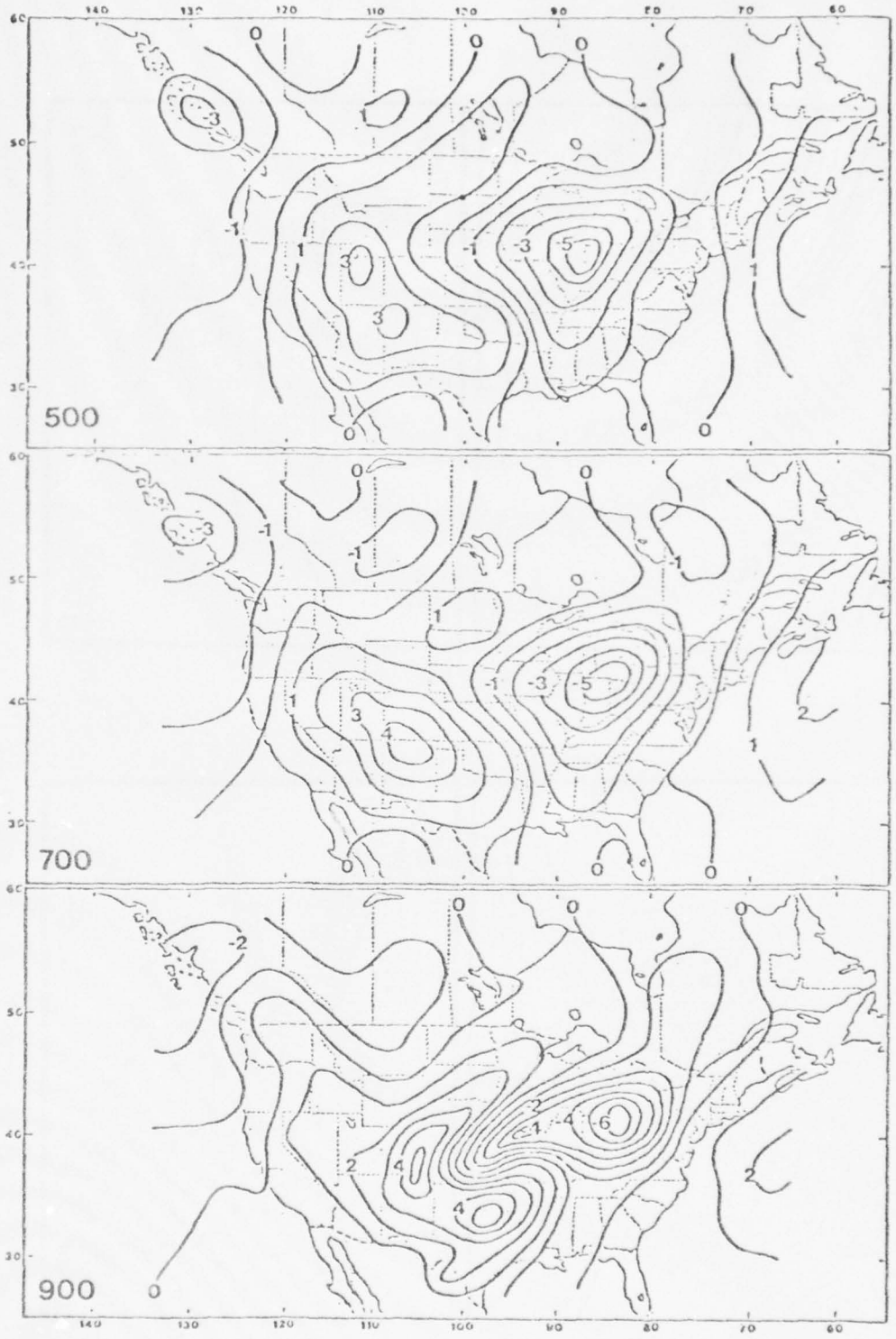

Figure 2.58. Total vertical motions for the 900, 700 and 500 mb level at 1200 GMT 21 February 1976. Isopleth interval is 1 μb

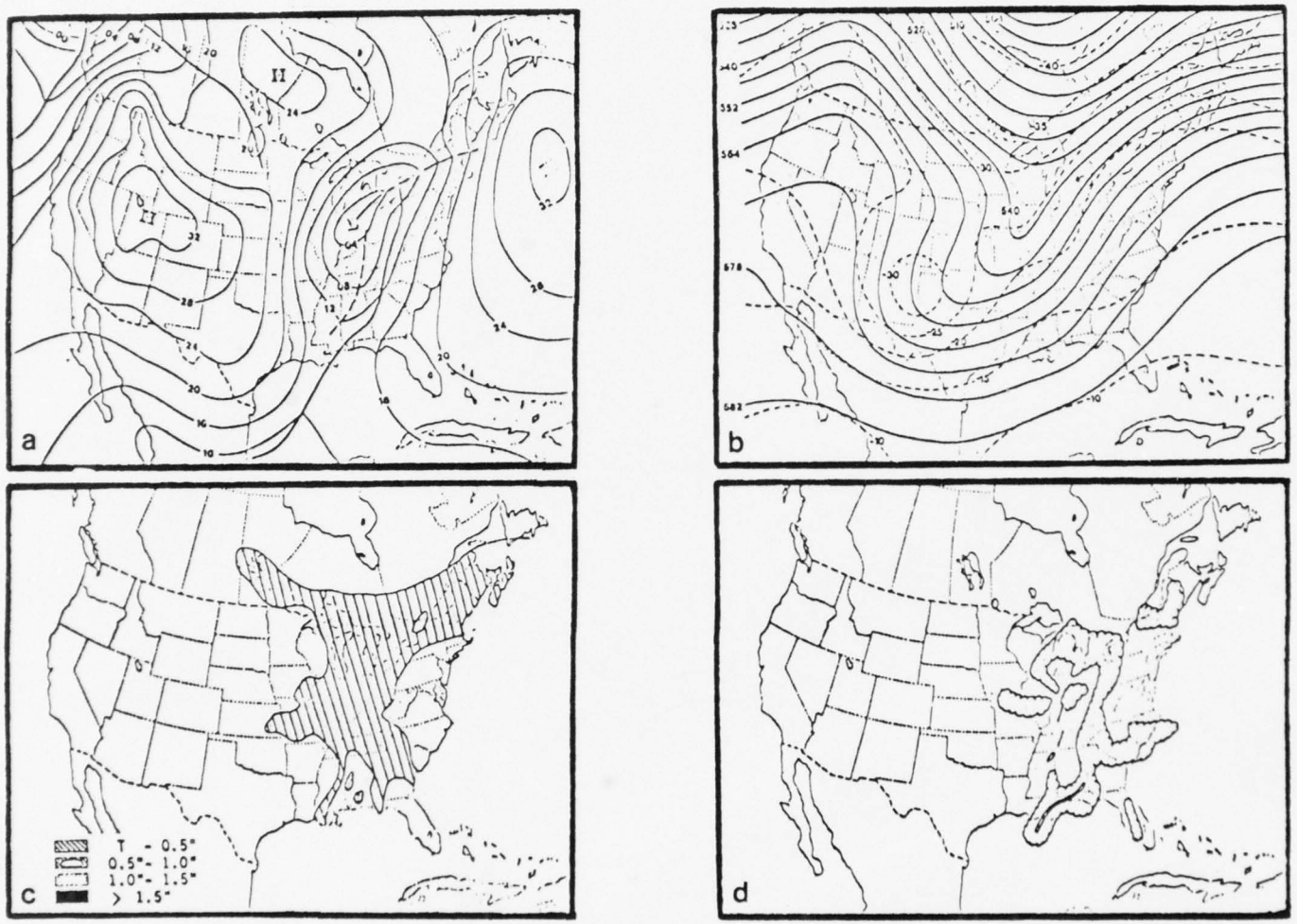

Figure 2.59. (a) Sea level pressure analysis, (b) 500 mb analysis, and (c) 6 hour precipitation amounts at 0000 GMT, and (d) radar summary at 0035 GMT 22 February 1976.

pronounced decrease in the area of values with more than 70% at the 500 mb level (Figure 2.60). The dry tongue with relative humidity values less than 10% continued to extend over the surface low at 500 mb and separate moist air to the east of the system from moisture to the west. However, values greater than 70% were present at 850 mb around the entire low center. Cloud tops in the GOES East infrared image in Figure 2.61 did not appear to be as cold as in Figure 2.57; however, the spiral cloud pattern continued to persist around the cyclone system.

The vertical motion fields (Figure 2.62) also indicated a decrease at this synoptic time. Strongest ascending motions were present near the cyclone center and were weaker than 12 hours earlier. Omega values in the subsiding dry air southwest of the cyclone center were also weaker. These four sequences of synoptic events covered a period when this mid-latitude cyclone evolved through a complete life cycle. Data from the Nimbus VI orbital passes will help supplement the conventional observations and provide opportunities to improve the analyses of various meteorological parameters.

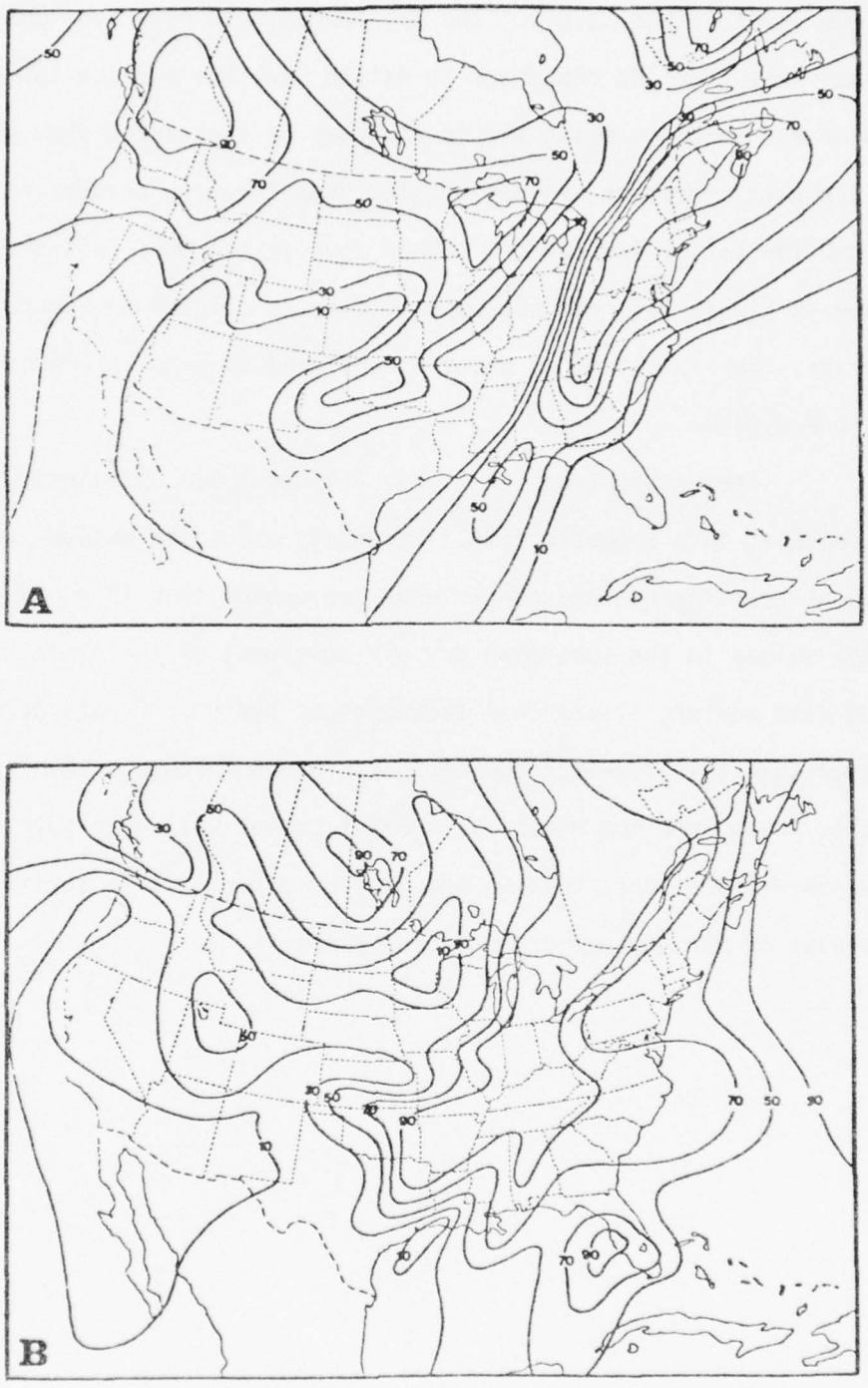

Figure 2.60. Relative humidity analysis at 0000 GMT 22 February 1976 for the (a) 500 mb level and (b) 850 mb level.

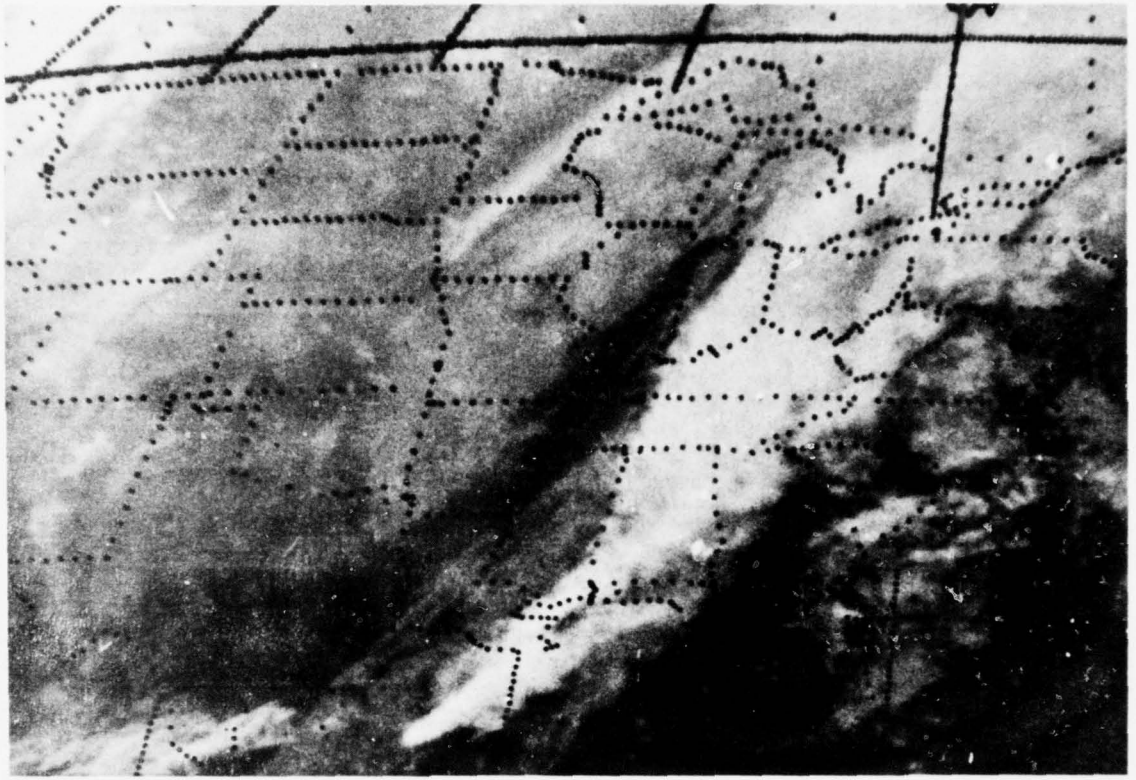

Figure 2.61. GOES East infrared satellite imagery at 0000 GMT 22 February 1976.

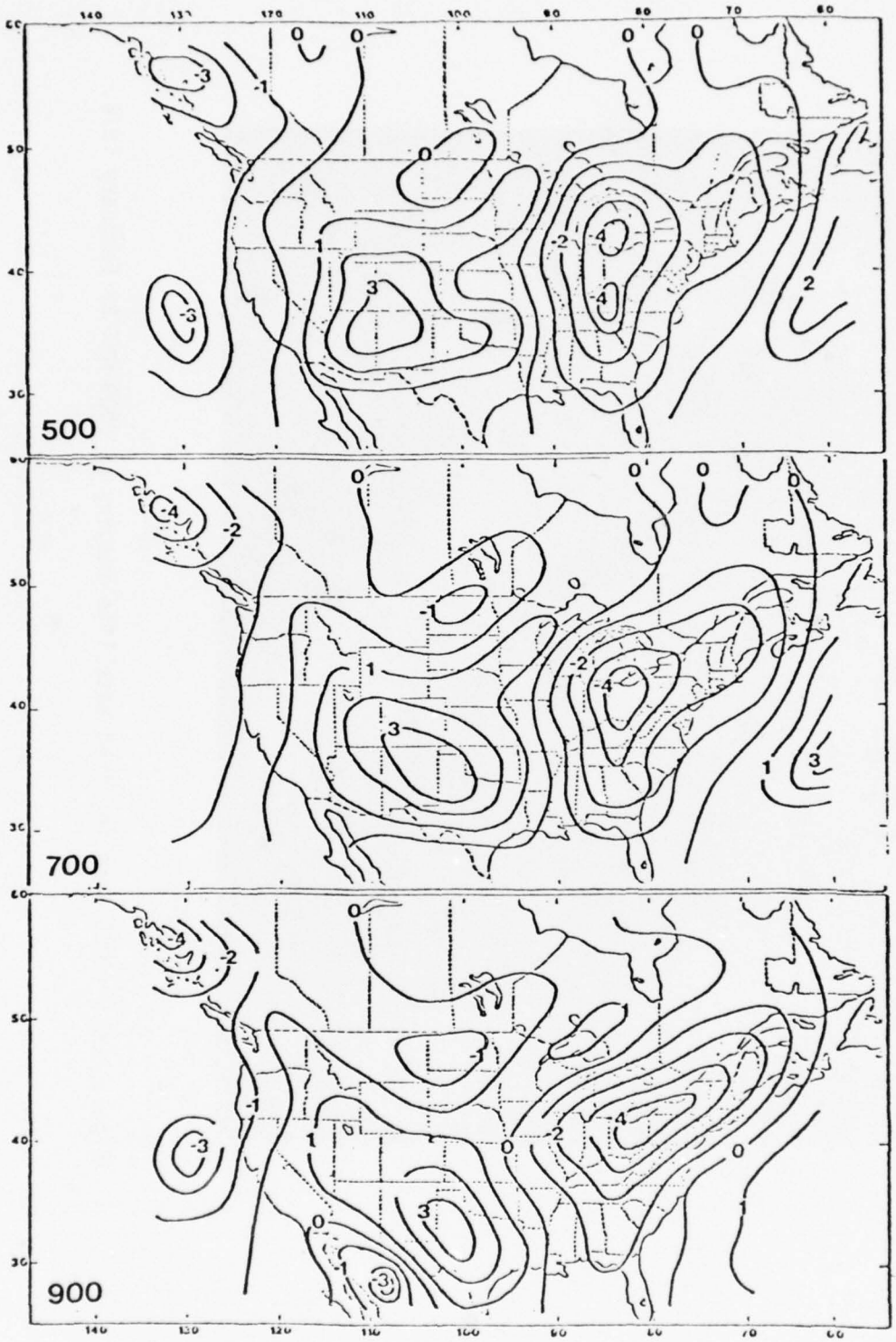

Figure 2.62. Total vertical motions for the 900, 700 and 500 mb levels at 0000 GMT 22 February 1976. Isopleth interval is 1 μb s^{-1}.

SECTION 3

ANALYSIS OF NIMBUS VI DATA

This section presents analysis of ESMR, SCAMS and THIR data from Nimbus VI. A similar objective analysis procedure was applied to all of the satellite data in order to merge the data from successive orbital passes and to compare with analysis of conventional meteorological data.

The objective analysis procedure transferred Nimbus VI data from scan points along the orbital path to a latitude-longitude grid array on one map. The basic analysis technique was similar to a scheme used by Cressman (1959) except the preliminary analysis was omitted in order to avoid contamination from other data sources. Data at each grid point were computer analyzed from the following relationship where a weighting factor, W_s, was used to interpolate scan point data to the nearest grid point

$$T_{ij} = \frac{\sum_{s}^{n} W_s T_s}{\sum_{s}^{h} W_s} \quad , \qquad \text{where } W_s = \frac{D^2 - d_s^2}{D^2 + d_s^2} \quad ,$$

and T_s is the satellite observation for a given scan point near the grid point (i,j), d_s is the distance of the s-th satellite scan point from the grid point location and D is the analysis scale size. Whenever $d_s \geq D$ at a given grid point, $W_s = 0$. After a number of experimental analyses were carried out, values chosen for D were 2.5° latitude (227 km) for the SCAMS data and 1° latitude (111 km) for the THIR and ESMR data. It should be noted that whenever data voids occurred along the subsatellite path or between successive orbital passes, anomalous

gradients formed because no first guess field was used. To minimize this effect, averaged data for the entire map were interpolated to the grid points with no satellite data. The analyzed maps were then printed on a CalComp plotter.

3.1 SCAMS Data

Nimbus VI SCAMS radiometer scans to each side of the subpoint track and provides nearly full earth coverage every 12 h. The SCAMS consist of five channels. The first is centered at 22.235 GHz, located on a weak water vapor resonance. Channel 2, centered at 31.65 GHz, is located in a spectral window, where the atmosphere is essentially transparent. Channels 3 (52.85 GHz), 4 (53.85 GHz) and 5 (55.45 GHz) are on the edge of the 60 GHz oxygen band having the peak weighting functions approximately at the surface, 4.9 km and 14 km, respectively. The ground resolution of SCAMS is about 145 km at nadir and 330 km at 43° from nadir.

Brightness temperatures from all 5 channels on this instrument were analyzed over the United States for 10 orbital passes by Nimbus VI on 22 and 25 August 1975 and 20 to 21 February 1976. These analyses are shown in Figures 3.1.1 to 3.1.20. In addition, surface reflectivities were analyzed for the February case.

In general, the water vapor channel (1) at 22.235 GHz and the atmospheric window channel (2) at 31.65 GHz indicated the largest gradients of brightness temperatures along coast lines while the other three channels in the oxygen band exhibited considerably smaller gradients. Figures 3.1.1 and 3.1.2 show the contrast between land and ocean in the channel 1 and 2 data for the 22 August 1975 case. Brightness temperatures were generally less than 200°K over oceans and greater

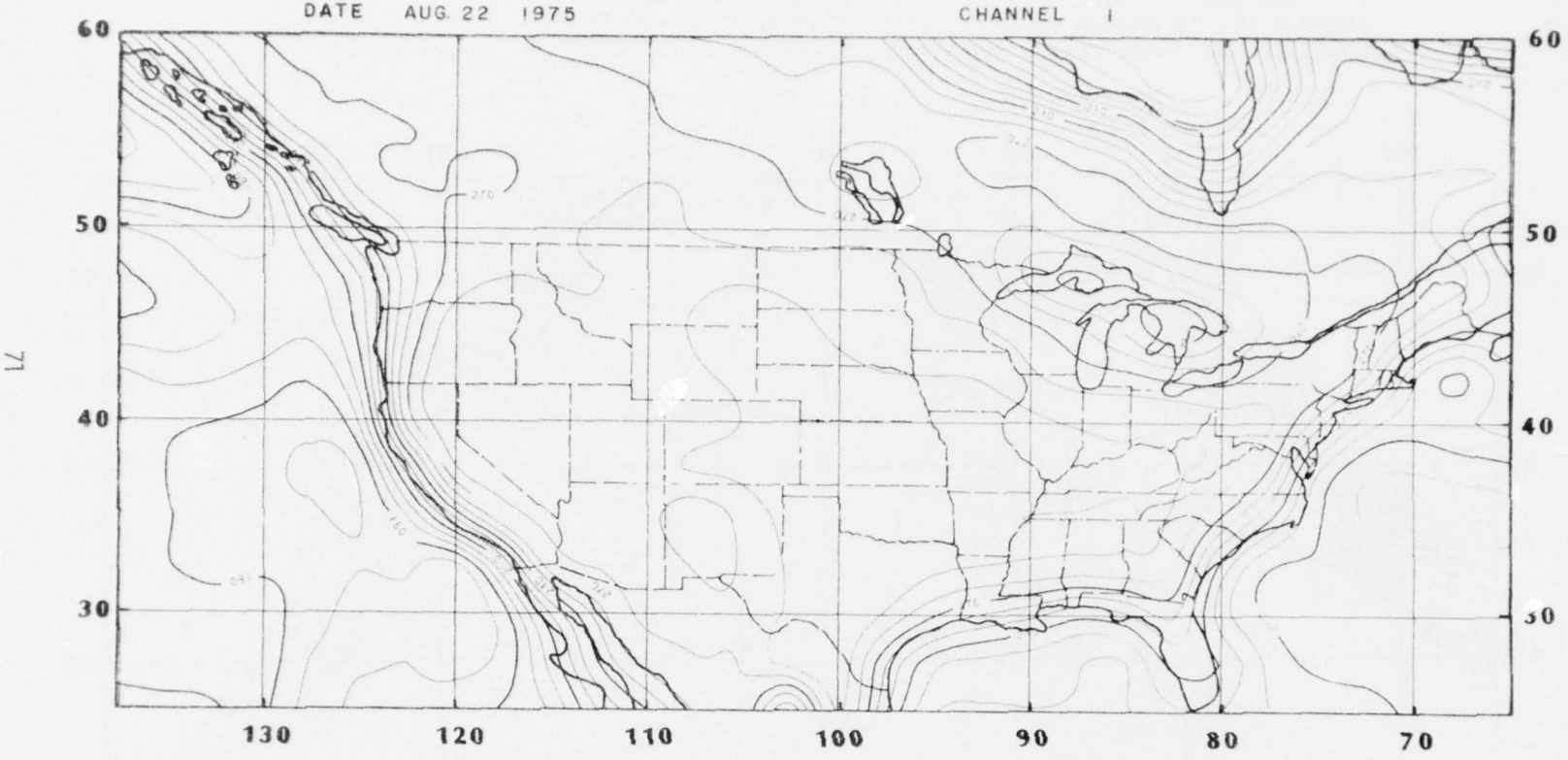

Figure 3.1.1. Brightness temperatures in degrees Kelvin from the water vapor channel (22,235 GHz) of SCAMS on Nimbus VI for orbital passes 957, 958 and 959 from 1605 to 1935 GMT.

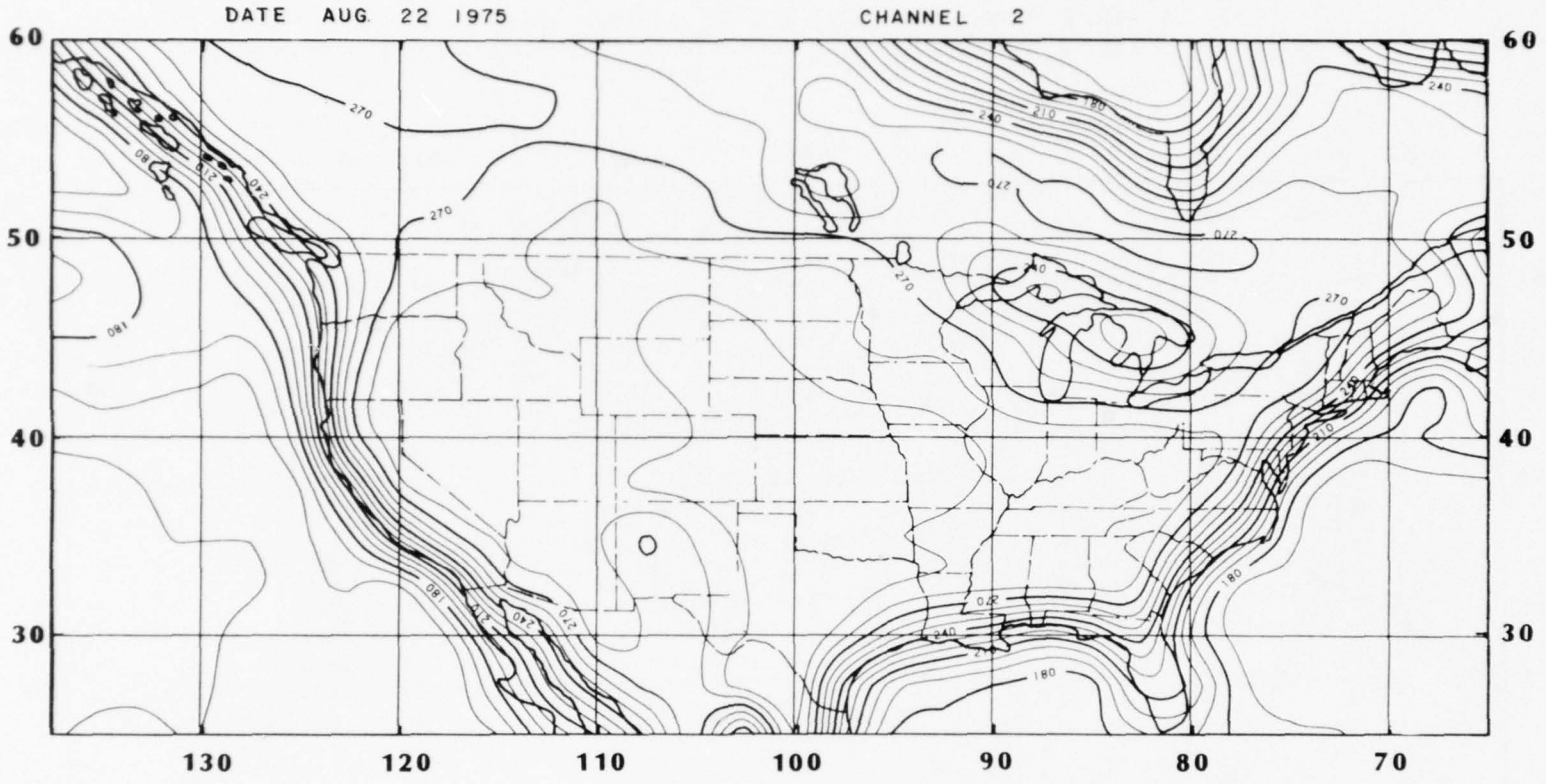

Figure 3.1.2. Brightness temperatures in degrees Kelvin from the atmospheric window channel (31.65 GHz) of SCAMS on Nimbus VI for orbital passes 957, 958 and 959. Time is from 1605 to 1935 GMT.

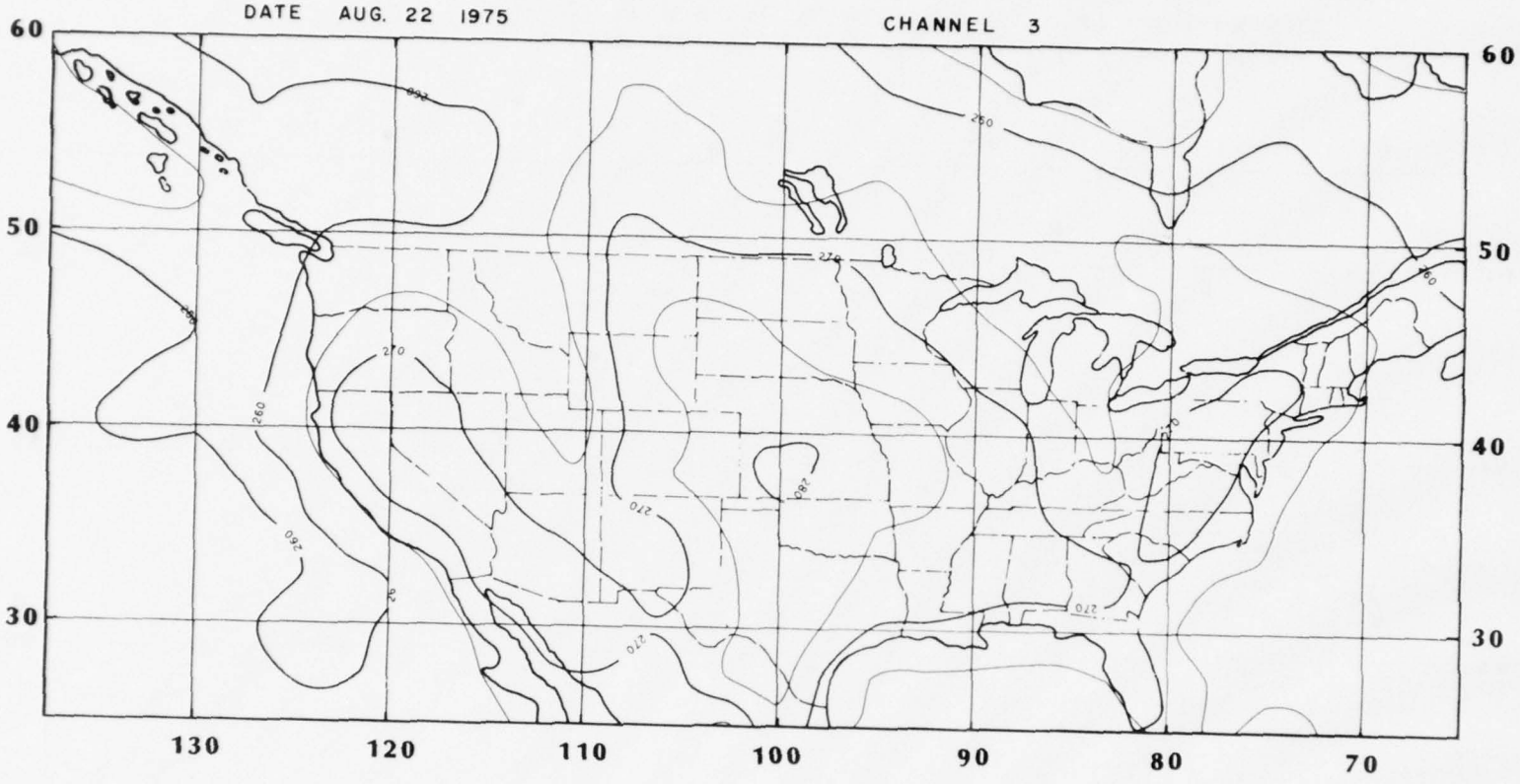

Figure 3.1.3. Brightness temperatures in degrees Kelvin from the oxygen band at 52.85 GHz of SCAMS on Nimbus VI for orbital passes 957, 958 and 959. Time is from 1605 to 1935 GMT.

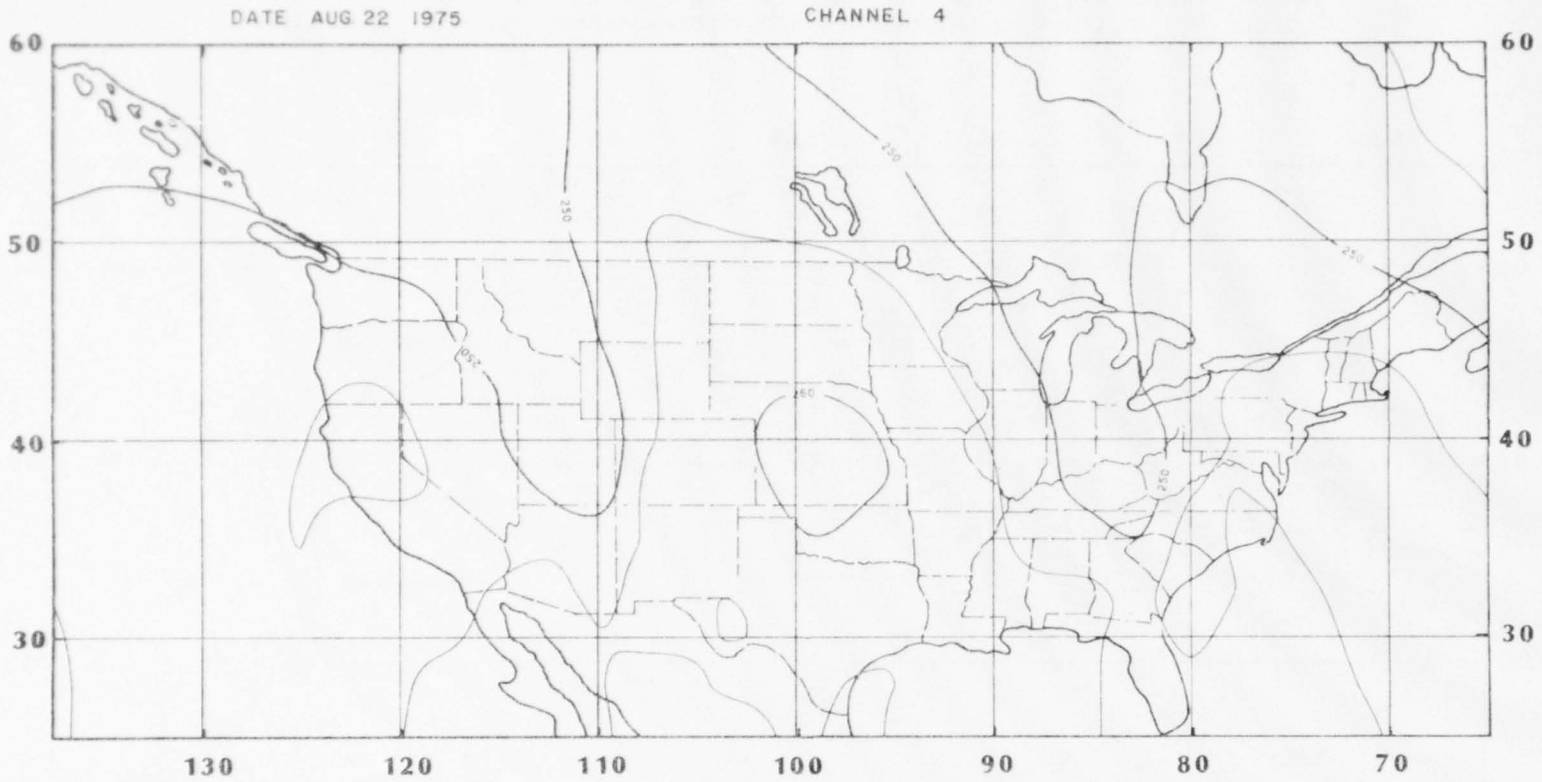

Figure 3.1.4. Brightness temperatures in degrees Kelvin from the oxygen band at 53.85 GHz of SCAMS on Nimbus VI for orbital passes 957, 958 and 959. Time is from 1605 to 1935 GMT.

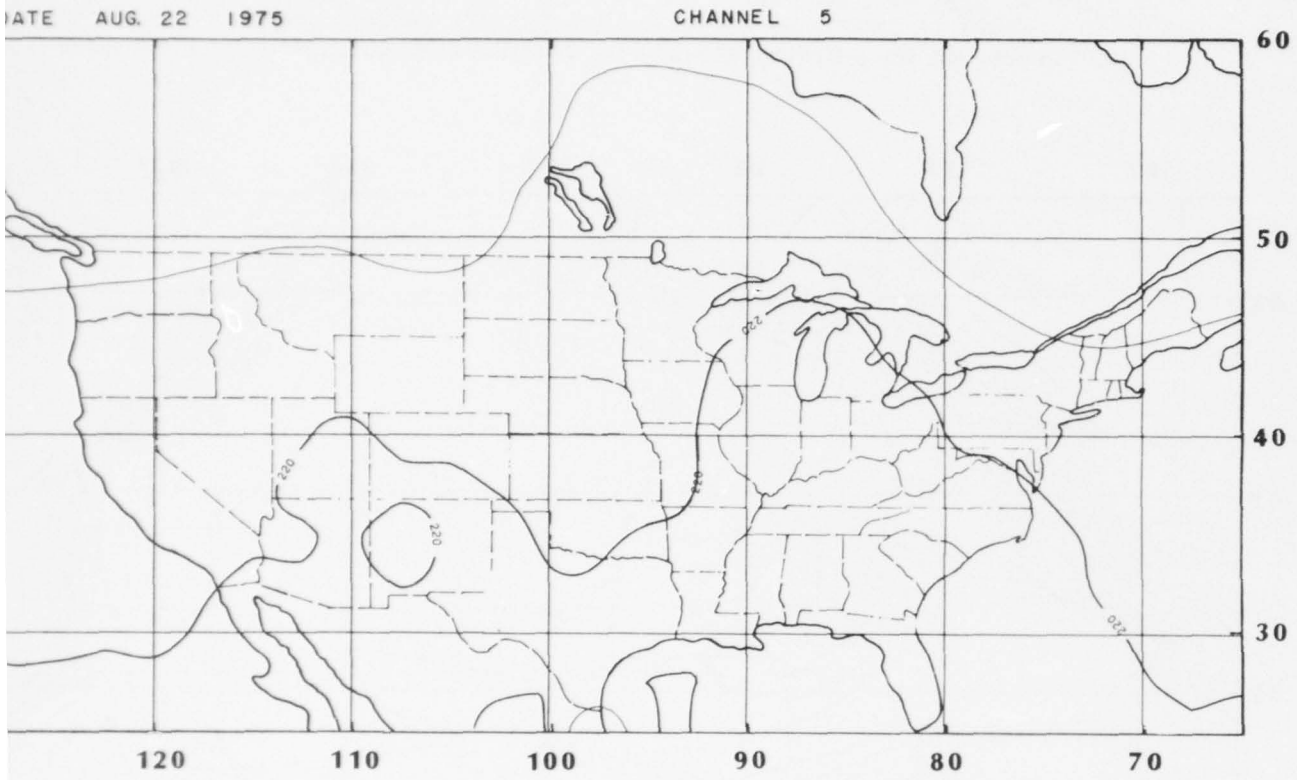

Figure 3.1.5. Brightness temperatures in degrees Kelvin from the oxygen band at 55.45 GHz of SCAMS on Nimbus VI for orbital passes 957, 958 and 959. Time is from 1605 to 1935 GMT.

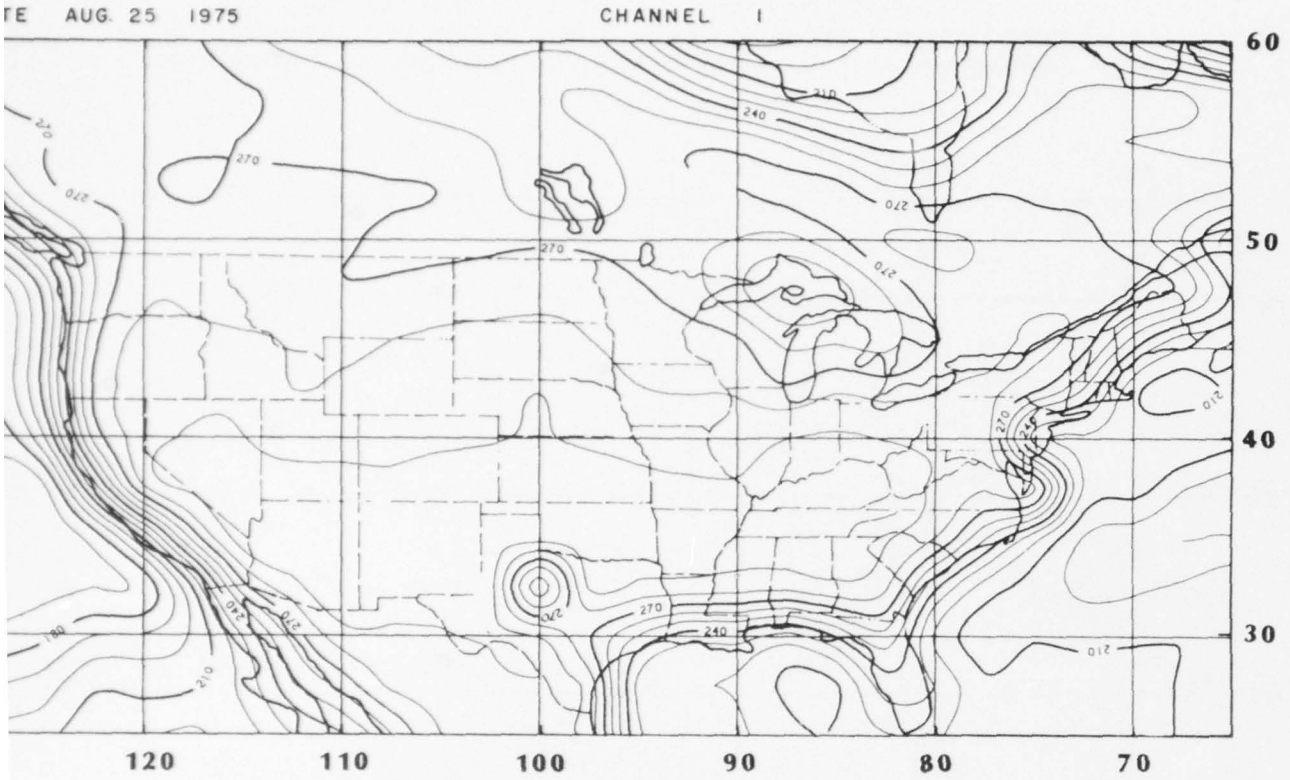

Figure 3.1.6. Brightness temperatures in degrees Kelvin from the water vapor channel (22.235 GHz) of SCAMS on Nimbus VI for orbital passes 997, 998 and 999. Time is from 1525 to 1900 GMT.

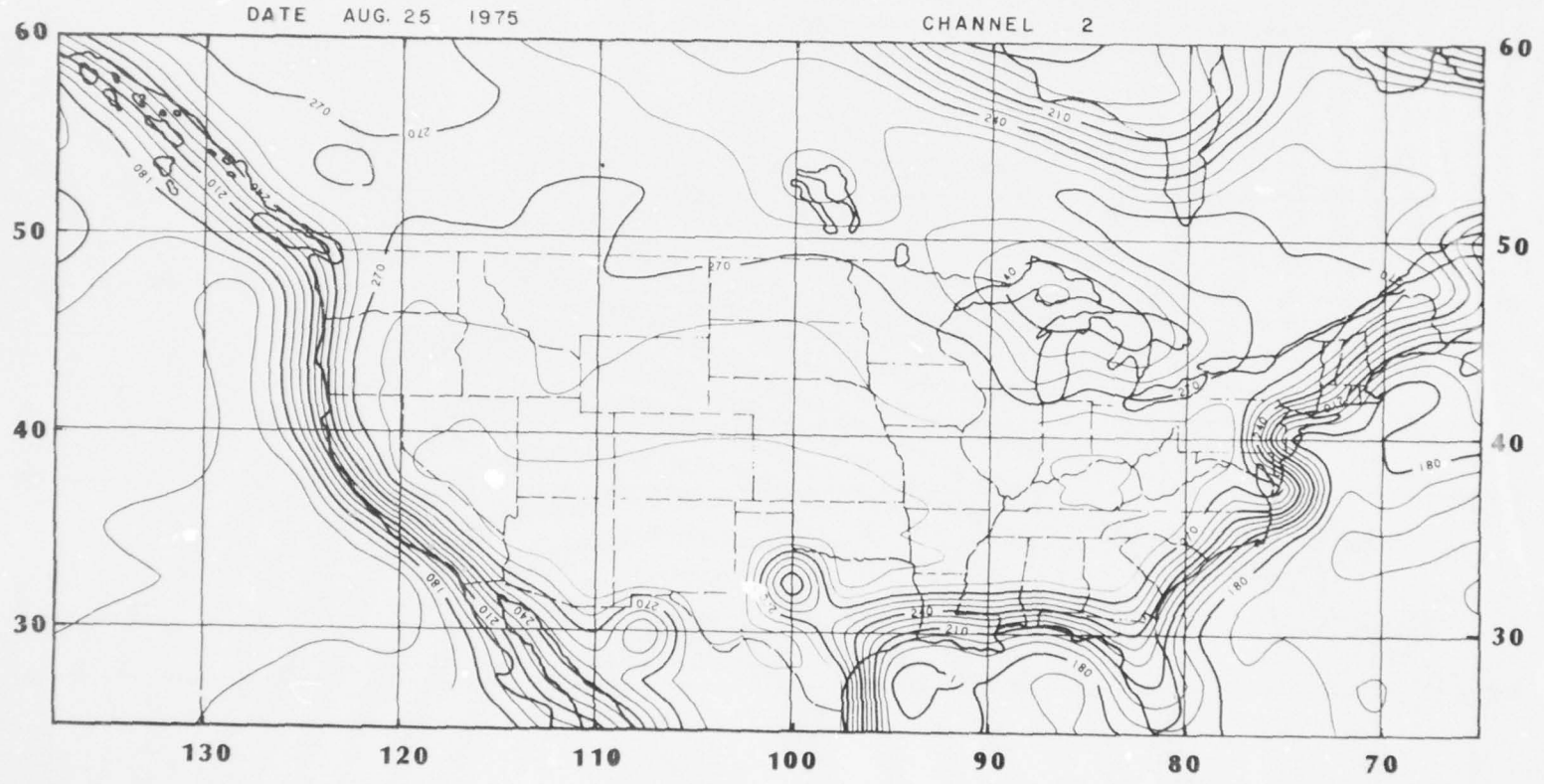

Figure 3.1.7. Brightness temperatures in degrees Kelvin from the atmospheric window channel (31.65 GHz) of SCAMS on Nimbus VI for orbital passes 997, 998 and 999. Time is from 1525 to 1900 GMT.

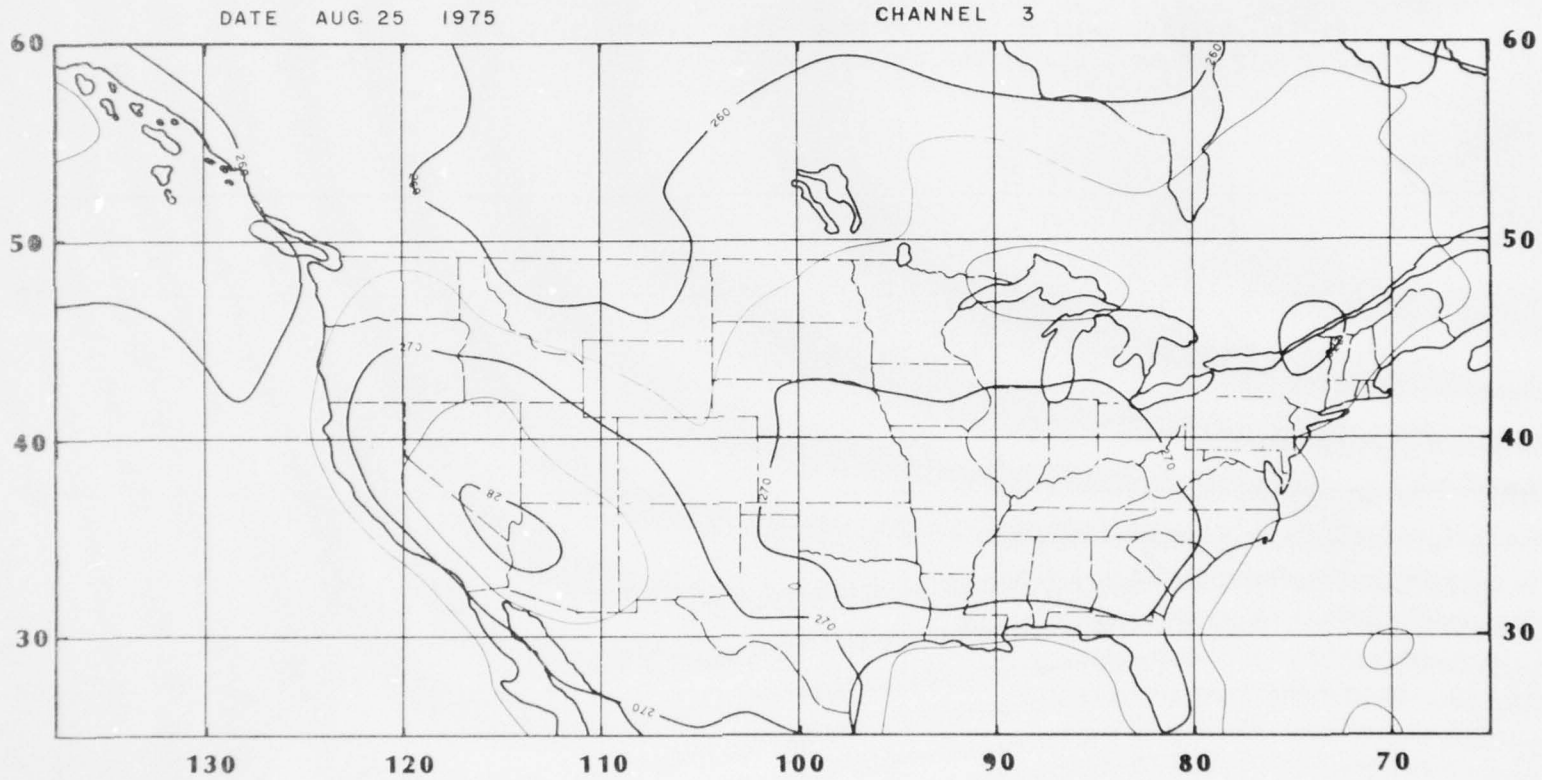

Figure 3.1.8. Brightness temperatures in degrees Kelvin from the oxygen band at 52.85 GHz of SCAMS on Nimbus VI for orbital passes

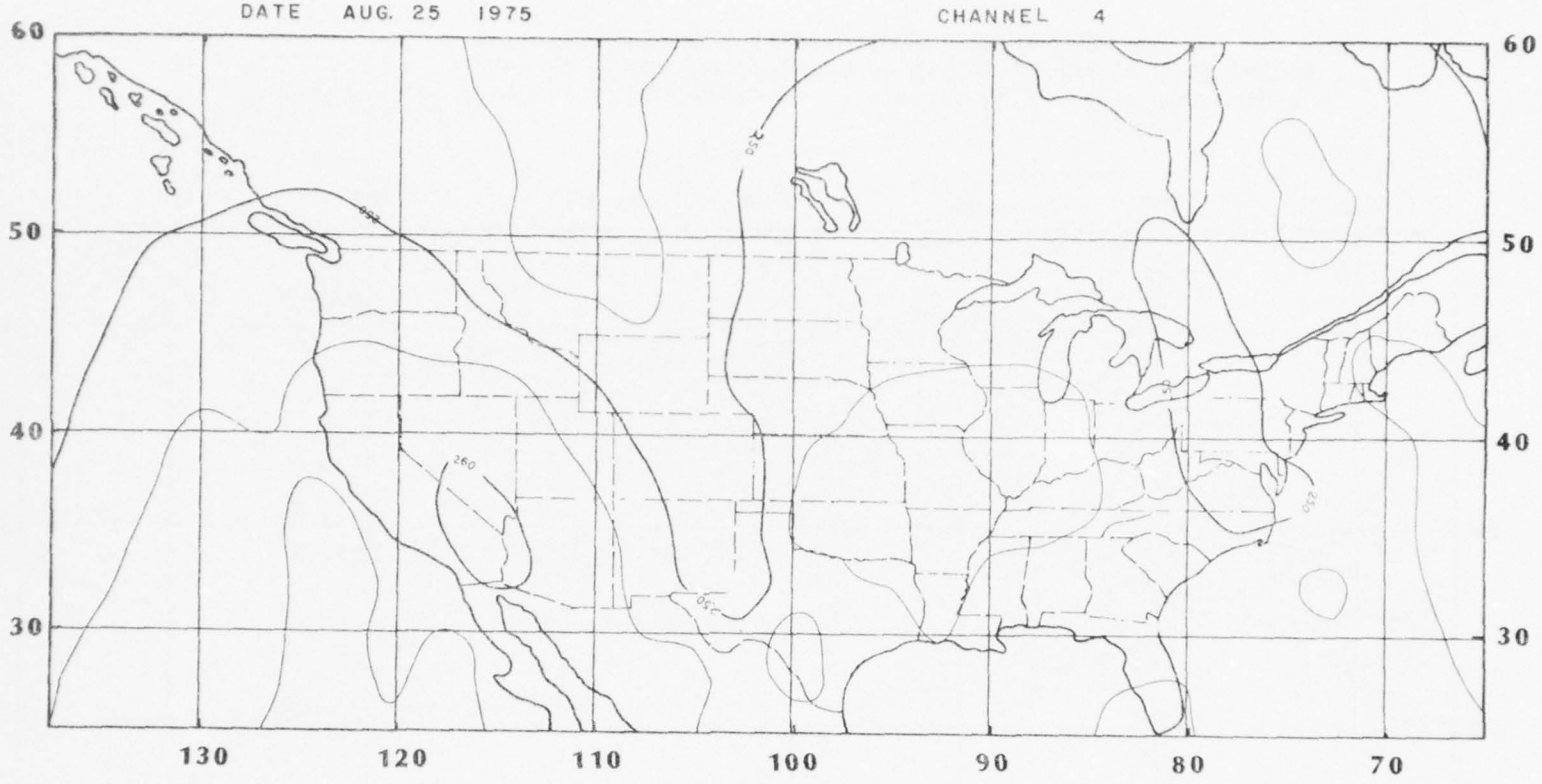

Figure 3.1.9. Brightness temperatures in degrees Kelvin from the oxygen band at 53.85 GHz of SCAMS on Nimbus VI for orbital passes 997, 998 and 999. Time is from 1525 to 1900 GMT.

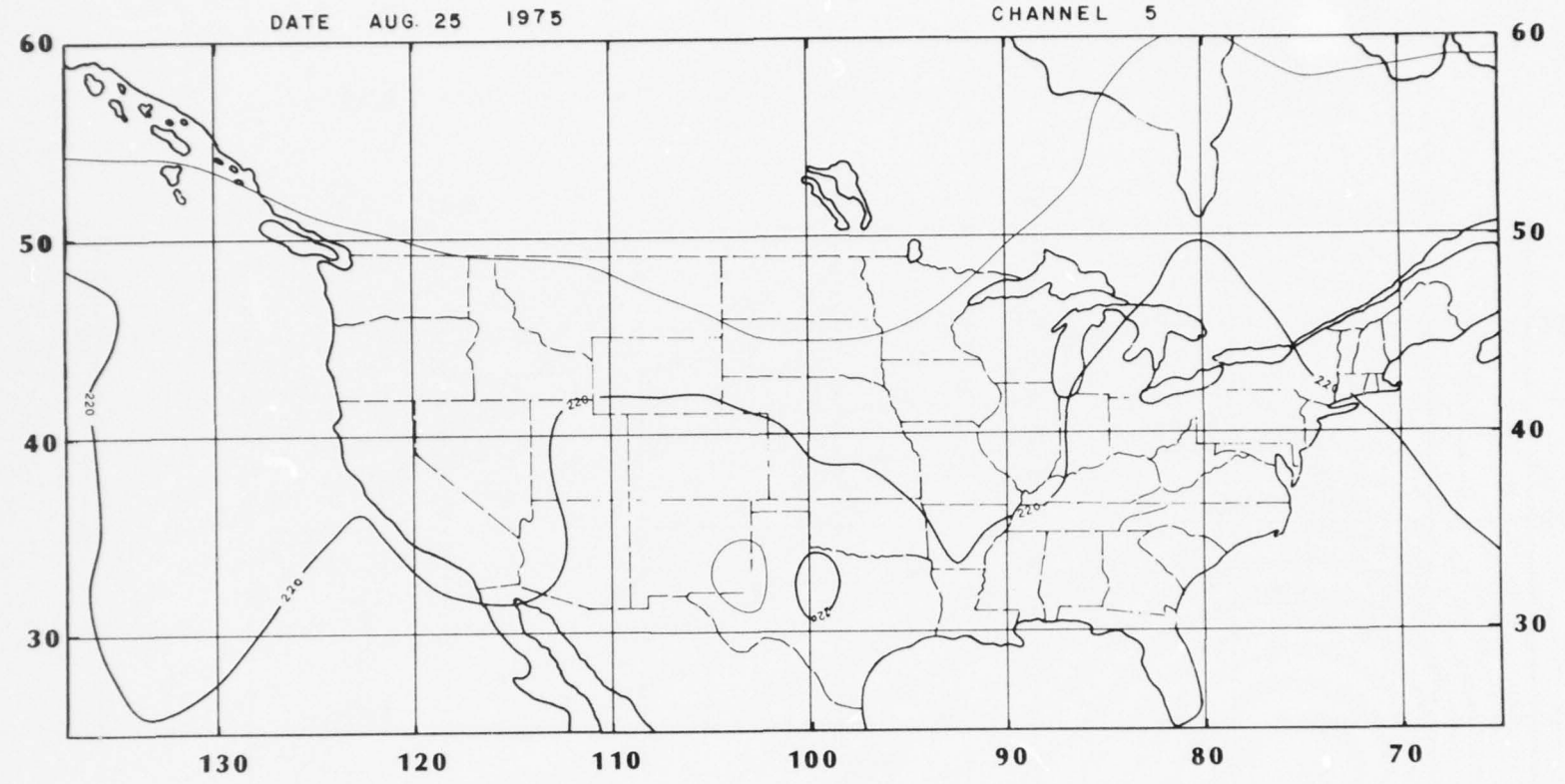

Figure 3.1.10. Brightness temperatures in degrees Kelvin from the oxygen band at 55.45 GHz of SCAMS on Nimbus VI for orbital passes 997, 998 and 999. Time is from 1525 to 1900 GMT.

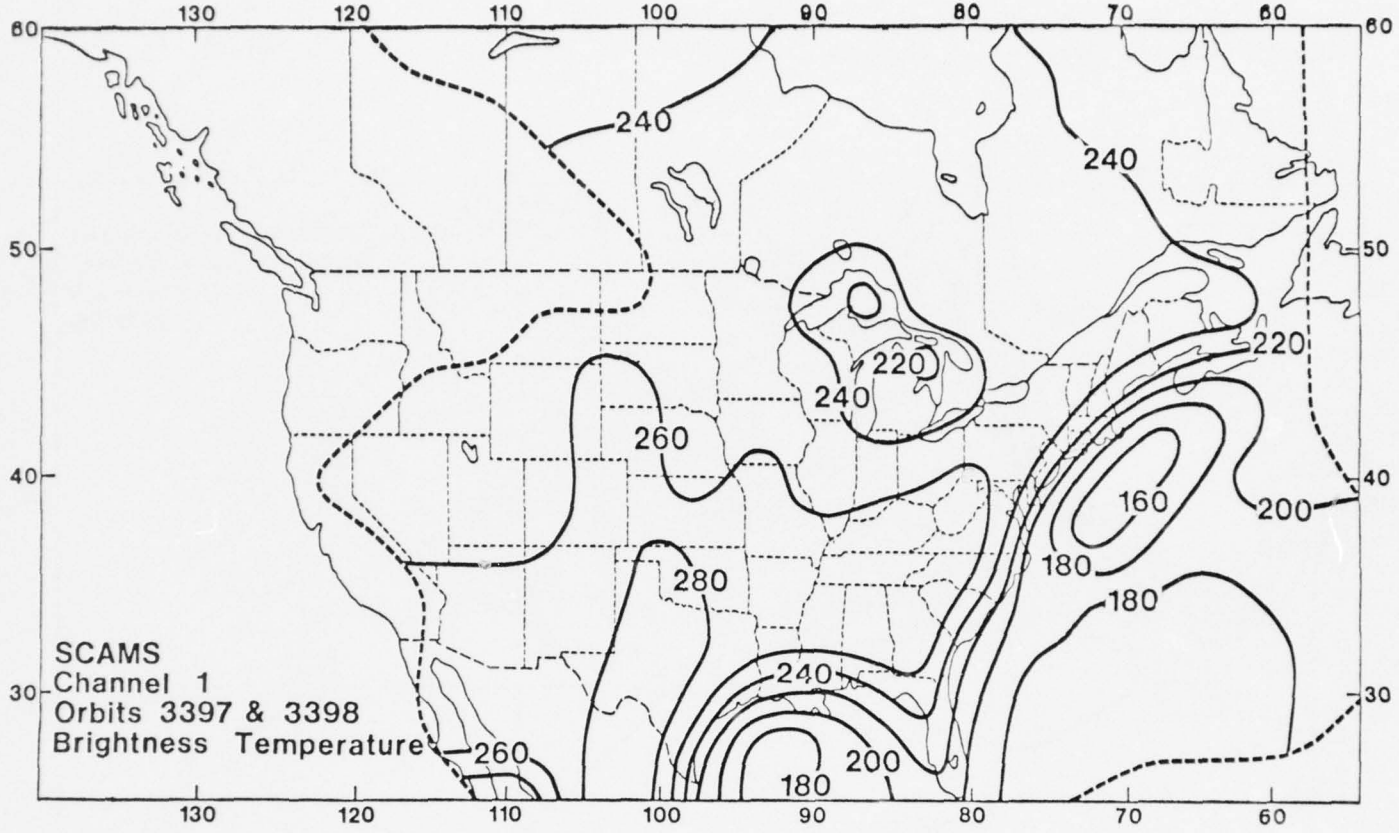

Figure 3.1.11. Brightness temperatures in degrees Kelvin from the water vapor channel (22.235 GHz) of SCAMS on Nimbus VI between 1720 and 1910 GMT on 20 February 1976.

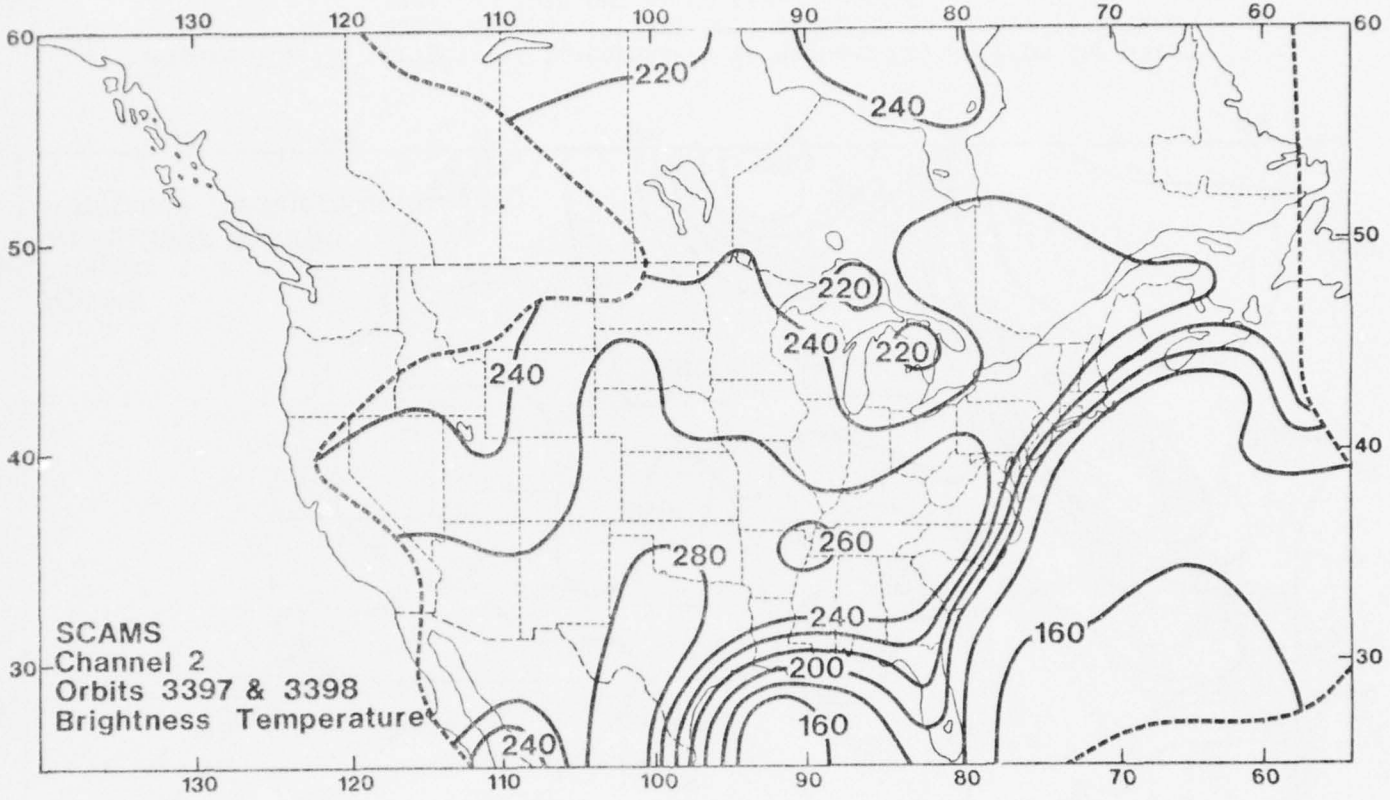

Figure 3.1.12. Brightness temperatures in degrees Kelvin from the atmospheric window channel (31.65 GHz) of SCAMS on Nimbus VI between 1720 and 1910 GMT on 20 February 1976.

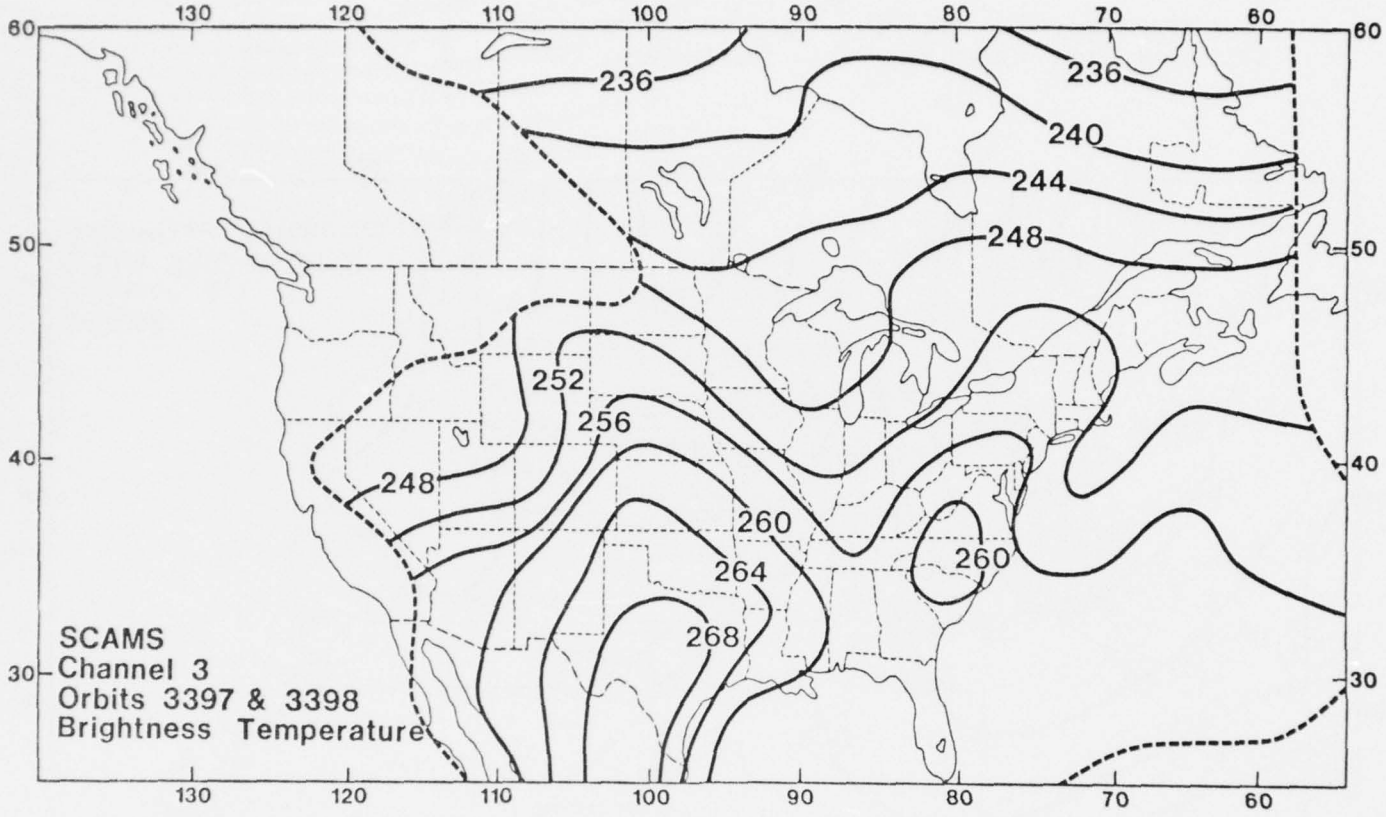

Figure 3.1.13. Brightness temperatures in degrees Kelvin from the oxygen band at 52.85 GHz of SCAMS on Nimbus VI between 1720 and 1910 GMT on 20 February 1976.

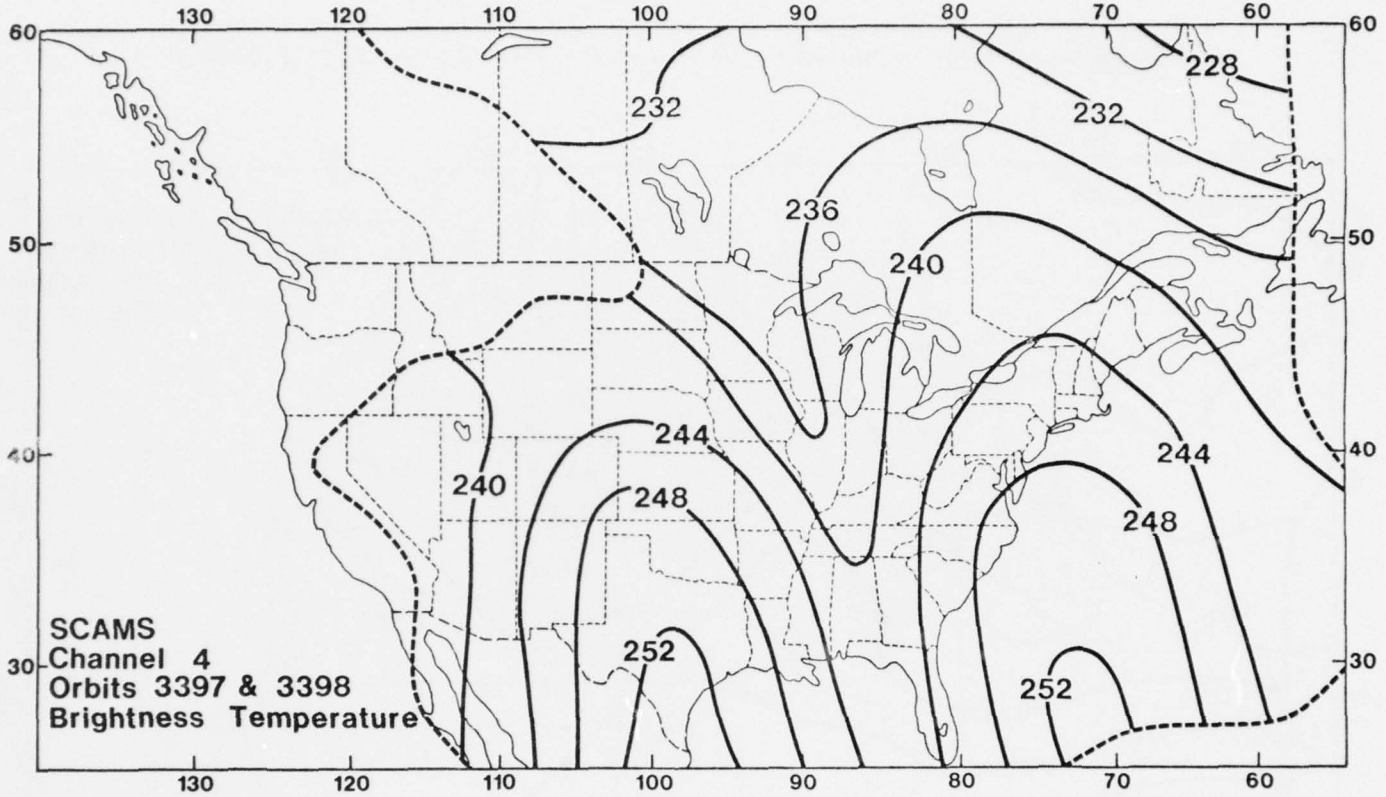

Figure 3.1.14. Brightness temperatures in degrees Kelvin from the oxygen band at 53.85 GHz of SCAMS on Nimbus VI between 1720 and 1910 GMT on 20 February 1976.

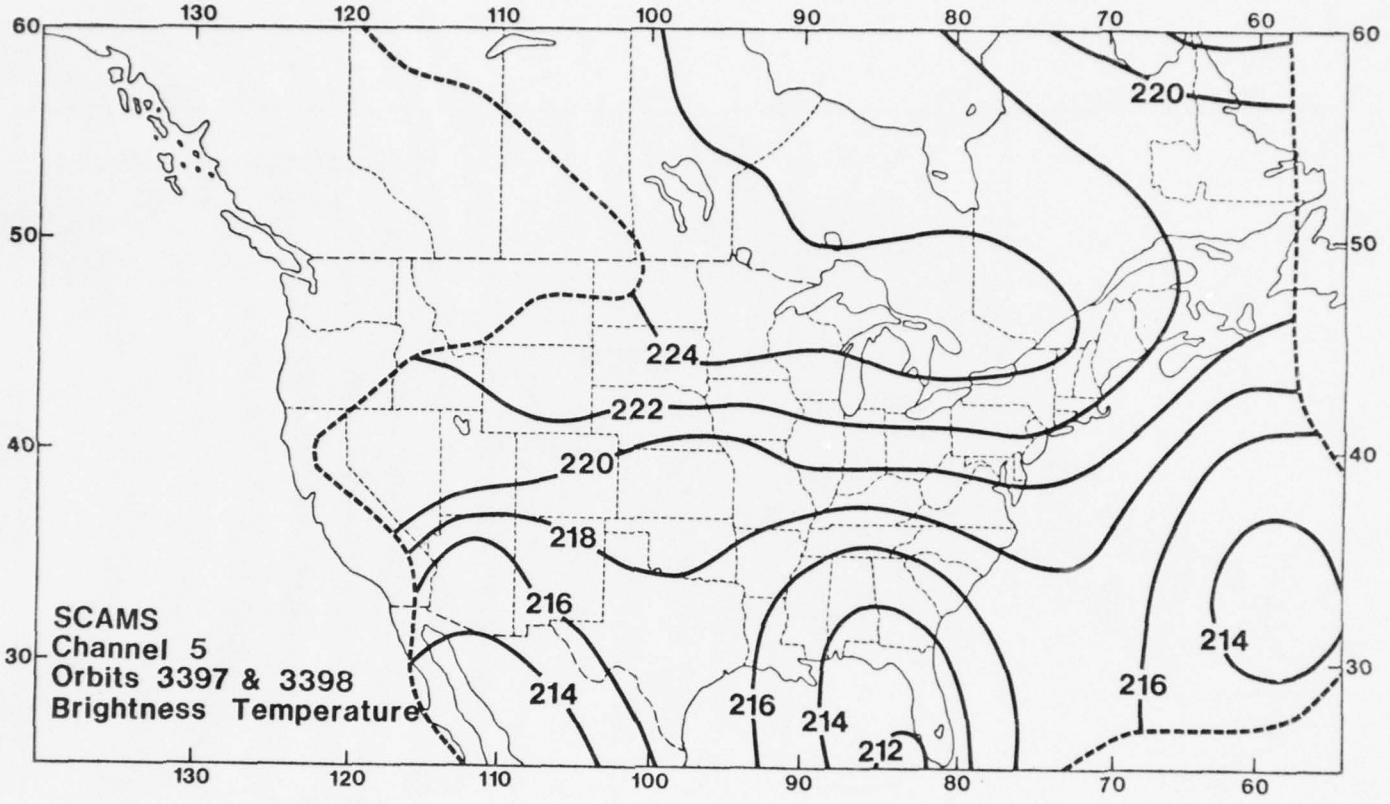

Figure 3.1.15. Brightness temperatures in degrees Kelvin from the oxygen band at 55.48 GHz of SCAMS on Nimbus VI between 1720 and 1910 GMT on 20 February 1976.

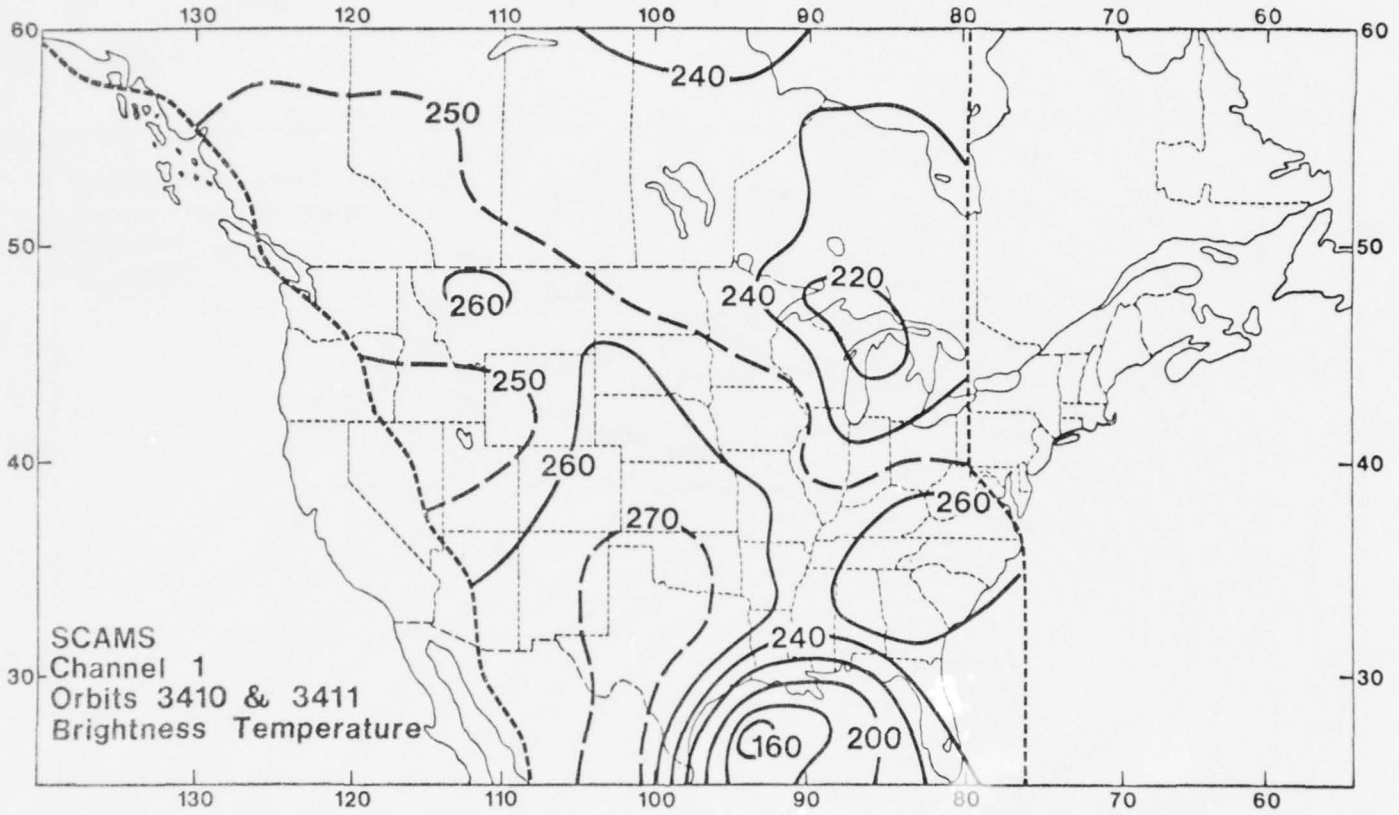

Figure 3.1.16. Brightness temperatures in degrees Kelvin from the water vapor channel (22.235 GHz) of SCAMS on Nimbus VI between 1625 and 1845 GMT on 21 February 1976.

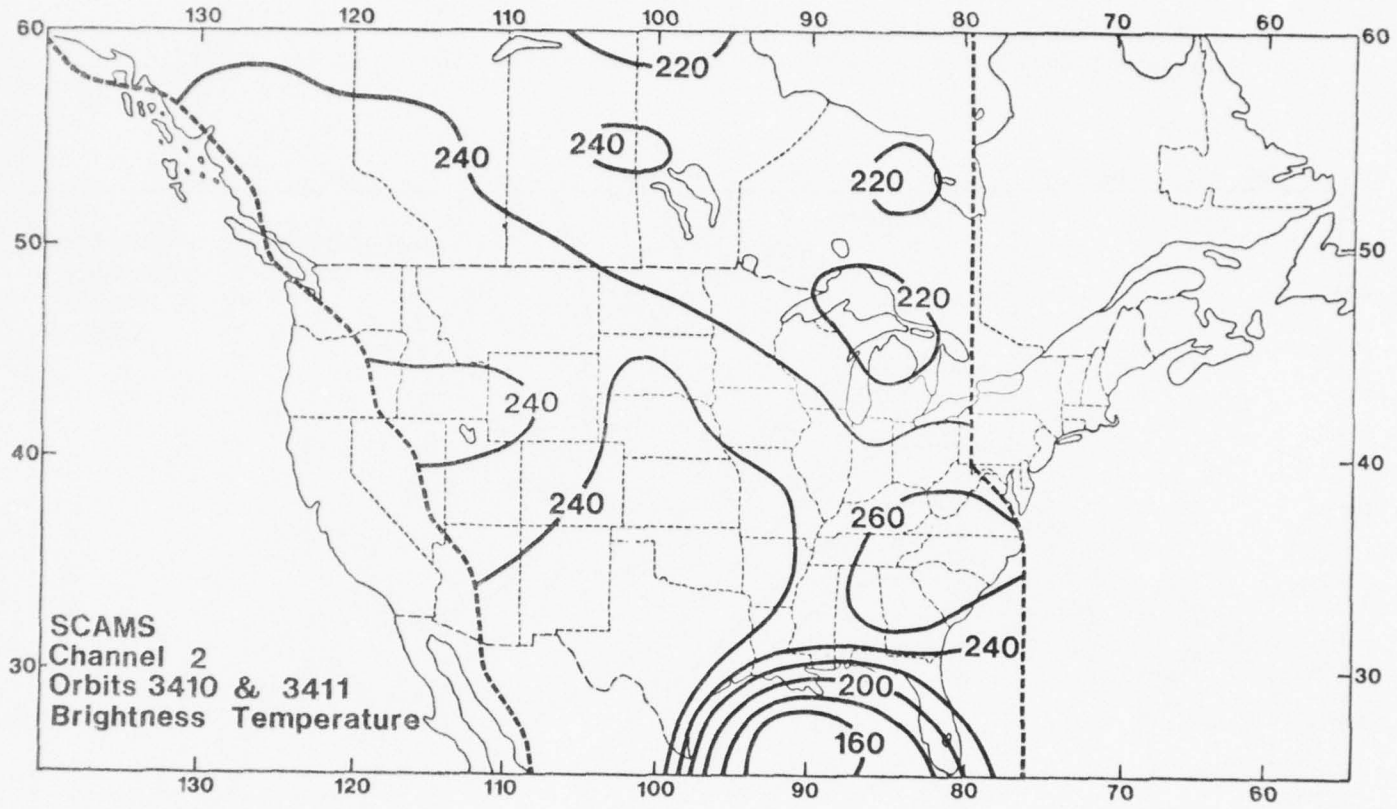

Figure 3.1.17. Brightness temperatures in degrees Kelvin from the atmospheric window channel (31.65 GHz) of SCAMS on Nimbus VI between 1625 and 1845 GMT on 21 February 1976.

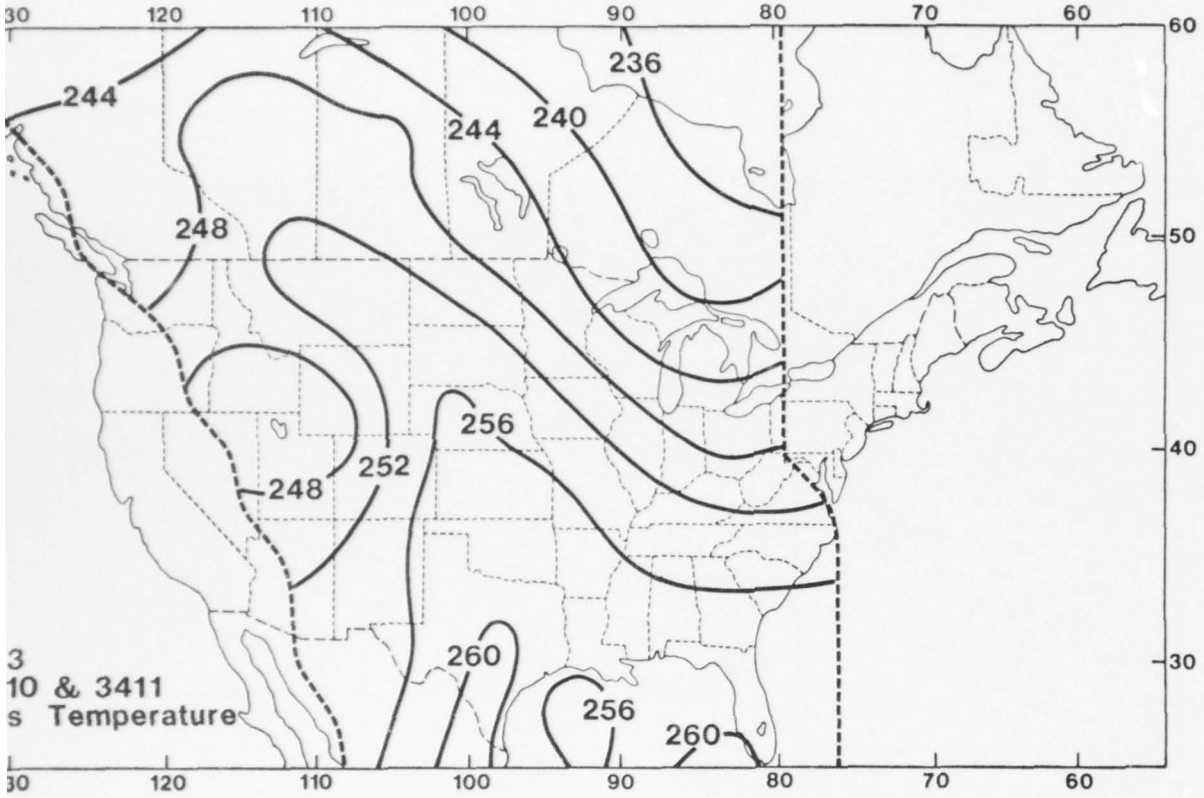

Figure 3.1.18. Brightness temperatures in degrees Kelvin from the oxygen band at 52.85 GHz of SCAMS on Nimbus VI between 1625 and 1845 GMT on 21 February 1976.

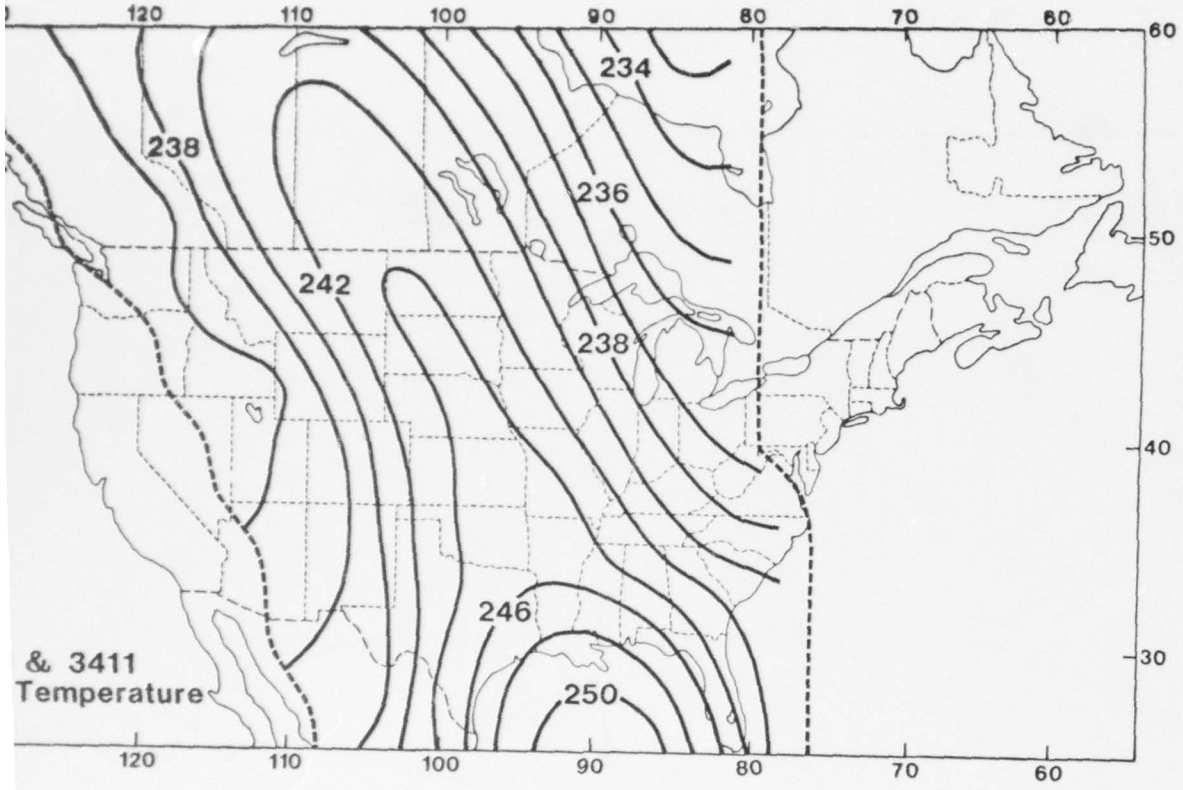

ure 3.1.19. Brightness temperatures in degrees Kelvin from the oxygen band at 53.85 GHz of SCAMS on Nimbus VI between 1625 and 1845 GMT on 21 February 1976.

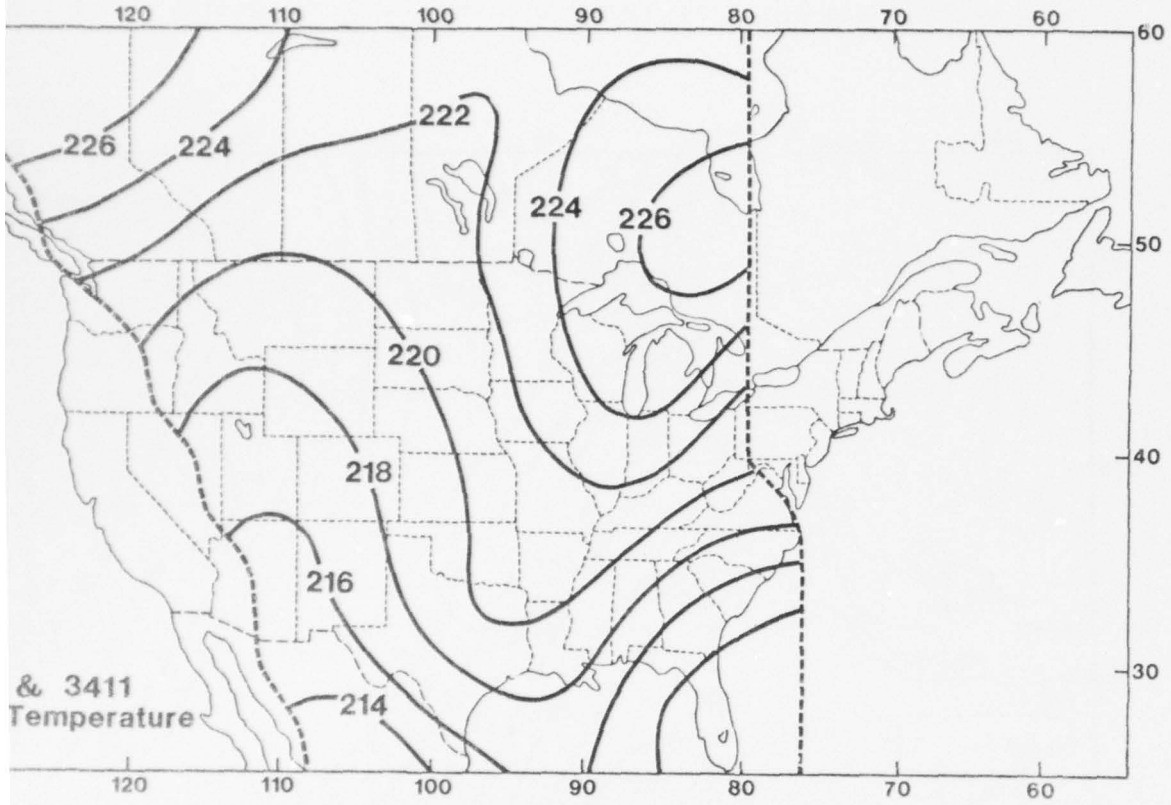

re 3.1.20. Brightness temperatures in degrees Kelvin from the oxygen band at 55.45 GHz of SCAMS on Nimbus VI between 1625 and 1845 GMT on 21 February 1976.

AD-A077 292 UTAH UNIV SALT LAKE CITY DEPT OF METEOROLOGY F/G 4/2
ANALYZE, CALCULATE, AND DEVELOP TECHNIQUES FOR WEATHER SATELLIT--ETC(U)
JUN 79 E G ASTLING , K LIOU F19628-78-C-0130

UNCLASSIFIED AFGL-TR-79-0140 NL

2 OF 2
AD
A077292

END
DATE
FILMED
12-79
DDC

than 270°K over land. Relatively low brightness temperatures were present over inland water bodies such as Lake Winnipeg and the Great Lakes.

Similar brightness temperature fields appeared in the data from these two channels on 25 August 1975 except for a cold spot over Texas where the temperature was less than 250°K. This low temperature was attributed to instrument noise or a data error. Comparisons with radar echoes at this time (Figure 2.43) and 6 hour precipitation accumulations (Figure 2.45) indicated soil moisture could not be an explanation.

Analyses of brightness temperatures from the three oxygen bands on 22 August 1975 are shown in Figures 3.1.8 to 3.1.10. Temperature differences amounted to less than 25°K between the warmest and coldest values for channels 3 and 4 and less than 10°K for channel 5. The dependency on viewing angle was most pronounced in the channel 4 temperature analysis over land areas where highest temperatures occurred along the subsatellite track. Temperatures decreased toward the north in channels 3 and 4 data, while temperature gradients were reversed in the channel 5 data. This can be explained by the level of largest energy contribution being located in the stratosphere for channel 5 and in the troposphere for channels 3 and 4.

The brightness temperatures for the wintertime mid-latitude cyclone are depicted in Figures 3.1.11 to 3.1.22 and show features similar to the summertime case. Temperature contrasts were evident along coast lines and reflected emissivity differences between land and ocean for data from channels 1 and 2. However, more meteorological information was apparent in the brightness temperatures derived from channel 3. For example, a comparison of Figure 3.1.13 with GOES-East infrared image in Figure 2.49 indicated brightness temperatures greater

than 268°K coincided with the band of dense clouds over Texas and Mexico. Lower temperatures over the Great Basin (<248°K) were associated with the cold trough at 500 mb in Figure 2.47.

Reflectivities were available on the Nimbus VI data tapes and were analyzed in addition to the brightness temperatures. Figures 3.1.21 and 3.1.22 show the reflectivity analyses for 20 and 21 February. Values greater than 50% occurred over the oceanic regions while values less than 10% were located over land. Some notable variations were found in Figure 3.1.21 where reflectivities exceeded 20% over the United States. One area was located north of the cyclone center over Nebraska where clouds and precipitation were produced in the core of strongest ascending motions. The synoptic maps and vertical motion fields closest to the satellite observations were discussed in Section 2 and were shown in Figures 2.51 and 2.53. A second area was centered over Utah and was possibly related to clouds and precipitation behind the cold front and within the area of cold air advection at the 500 mb level.

3.2 ESMR Data

The Nimbus VI ESMR receives the thermal infrared radiation from the earth-atmosphere at 37 GHz. The ESMR measures both horizontal and vertical components by using two separate radiometer channels. The resolution of the ESMR is between 25 km near nadir to 125 km at the end of the scan sweep.

The emissivity of water surface at 37 GHz is generally less than about 0.5 depending on such parameters as roughness and foam cover and therefore on the wind at the surface. On the other hand, the emissivity of a land surface is typically greater than 0.9 depending on the soil characteristics. Thus, the brightness temperature contrast

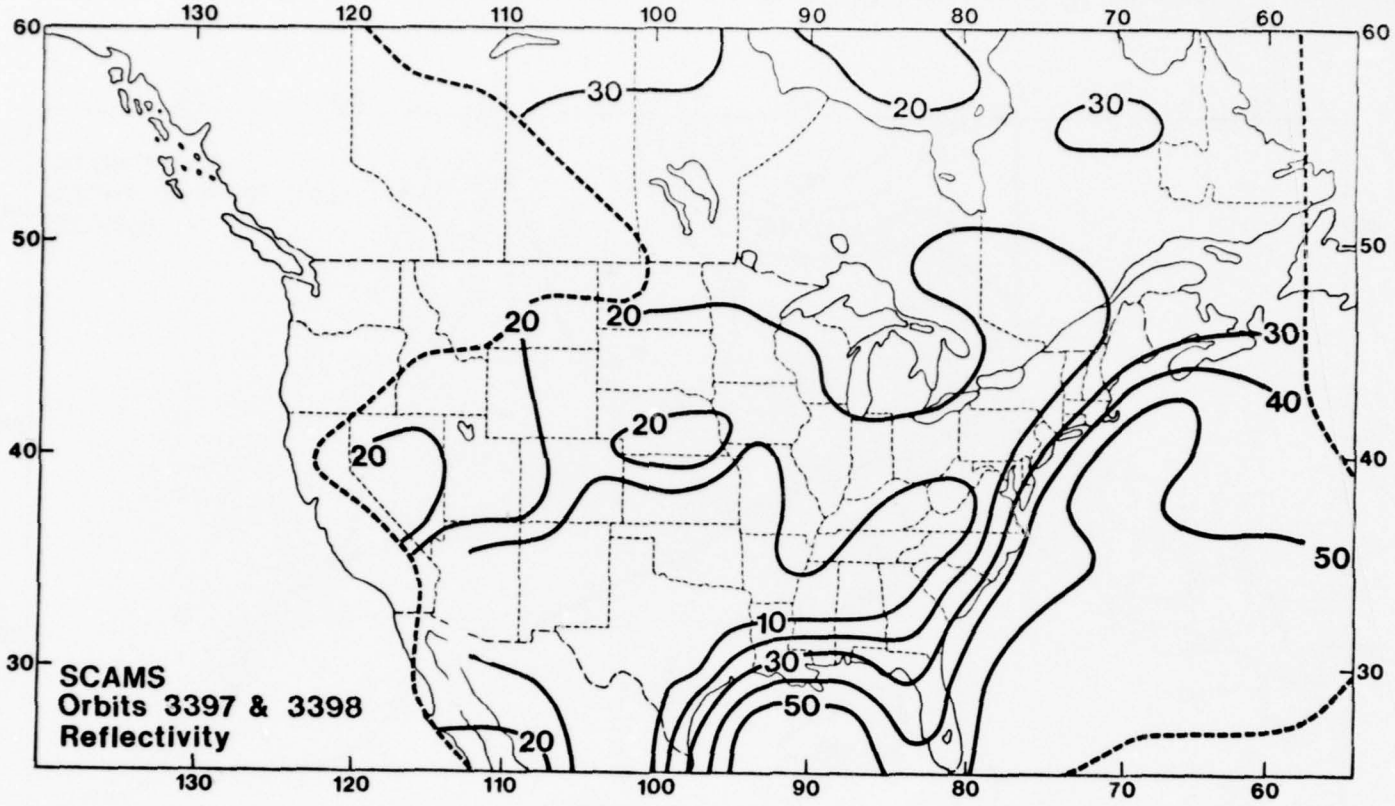

Figure 3.1.21. Reflectivity in percent from SCAMS on Nimbus VI between 1720 and 1910 GMT on 20 February 1976.

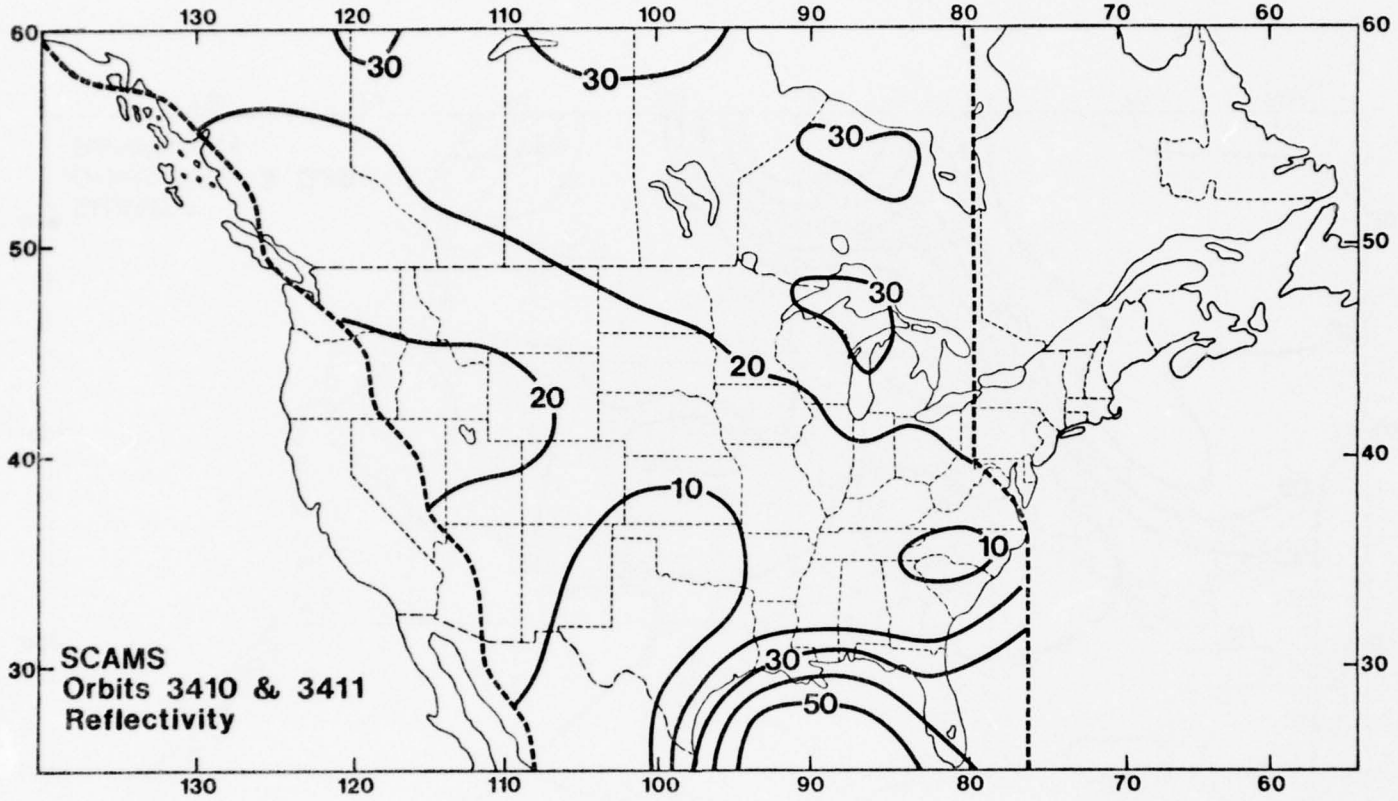

Figure 3.1.22. Reflectivity in percent from SCAMS on Nimbus VI between 1625 and 1845 GMT on 21 February 1976.

between land and water is generally greater than 100°K and so the outlines of the land and water is quite visible in the ESMR images. The emissivities of ice and snow cover have been observed to be a function of water content within and they are subject areas requiring further investigation. Moreover, we also note that brightness temperatures of rain clouds and flooded areas are lower than those of surrounding dry land surfaces. However, radiation emitted by calm water surfaces is strongly polarized compared to that emitted by clouds. This polarization distinction leads to the possiblility of discriminating between cloudy areas and land surfaces covered by water both of which give colder brightness temperatures. In view of these factors, the data received by ESMR will be affected by clouds, rain and surface characteristics and so information on all these variables requires physical interpretation and proper radiometric analysis. It is quite apparent that a comprehensive synoptic, radiosonde and cloud data base associated with ESMR data is essential to the extraction of the information content of clouds, rain and surface properties.

All the available ESMR data including the brightness temperatures corresponding to the vertical and horizontal polarization for eight orbits covering the summertime (22 and 25 August 1975) and wintertime (20 and 21 February 1976) cloud cases are contoured on the appropriate geographic maps. Let the vertical and horizontal brightness temperatures be T_B^v and T_B^h, respectively. We define the average brightness temperature and degree of linear polarization, respectively, as follows:

$$T_B = (T_B^v + T_B^h) /2$$

$$P\ (\%) = \frac{T_B^v - T_B^h}{T_B^h + T_B^v} \times 100\%$$

These two parameters are also mapped along with the vertical and horizontal brightness temperatures.

Figures 3.2.1 - 3.2.4 show the contours of the brightness temperatures for the horizontal, vertical and average components, and the percentage of polarization, respectively, for 22 August 1975.

The maps for 25 August 1975 consist of two orbits; one covers the western region and the other corresponds to the central part of the United States. Figures 3.2.5 - 3.2.8 are for the western orbit and Figures 3.2.9 - 3.2.12 are for the central orbit.

Mapping of the meso-scale ice/water content covering the area from 40 to 55°N and from 90 to 110°W utilizing the HIRS and SCAMS data based on empirical parameterization for 22 and 25 August has been comprehensively reported by Feddes and Liou (1978) and Liou and Duff (1979). In conjunction with these investigations, we examine the ESMR patterns of the average brightness temperature and percentage of polarization (Figures 3.2.11 and 3.2.12). There appears to be no direct correlation between the amount of ice/water content and the contour lines of these two parameters because of the larger scale employed in performing the mapping. However, it is believed that a more detailed analysis for the ESMR data for scales comparable to those used by Feddes and Liou, and Liou and Duff would provide valuable information regarding cloud, rain and surface characteristics. Microwave radiative transfer calculations using the available synoptic, radiosonde and cloud data will also be needed to physically understand the quantitative effects of

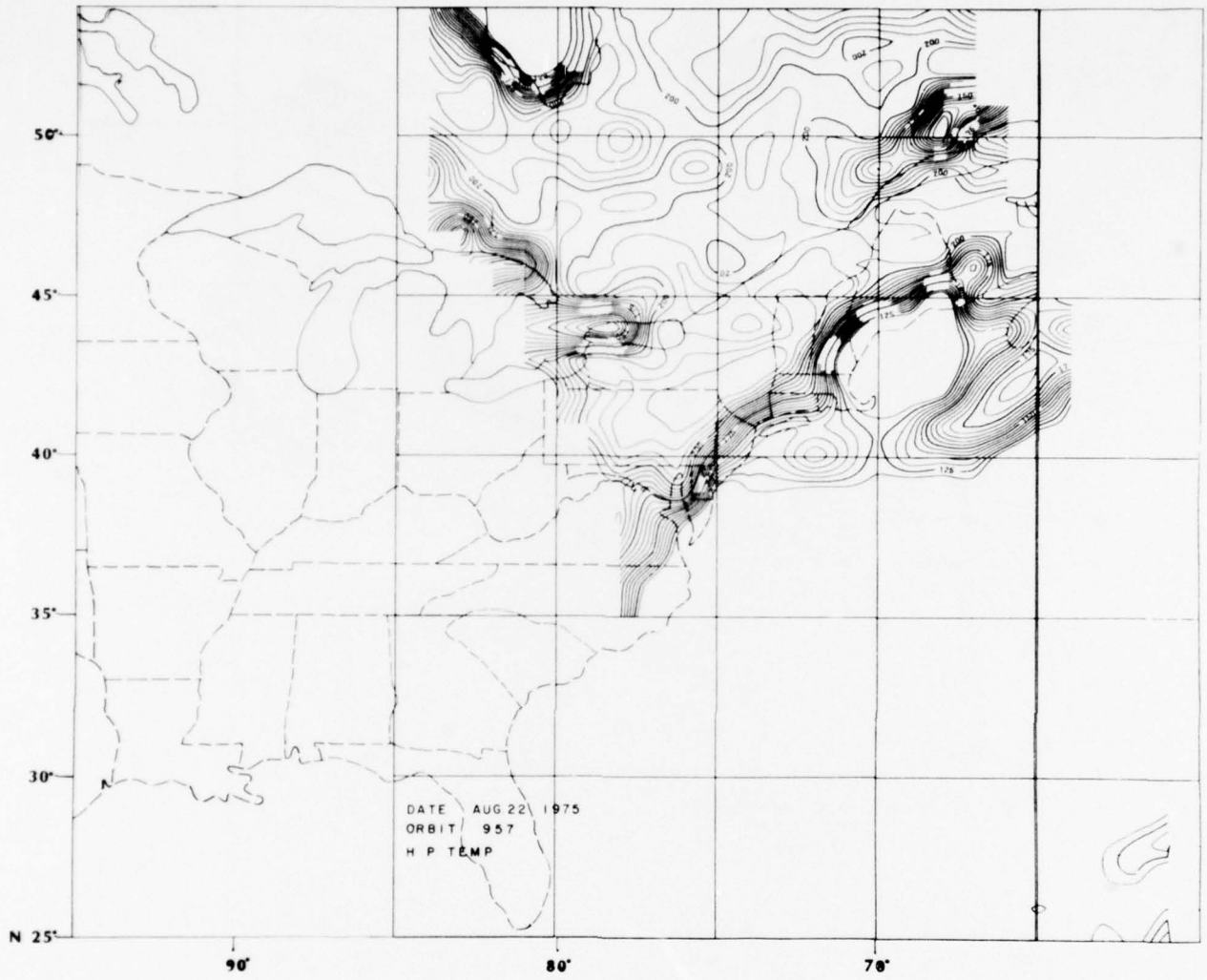

Figure 3.2.1. Brightness temperatures of the horizontally polarized component in the 37GHz band from the ESMR experiment on Nimbus VI. Note: There is a small displacement in the data along the orbital path as evident in the temperature fields near coastal areas. This may be attributed to errors in earth location using standard satellite ephemeris information. Also, values of isotherms in the ESMR data should be increased by 50°K.

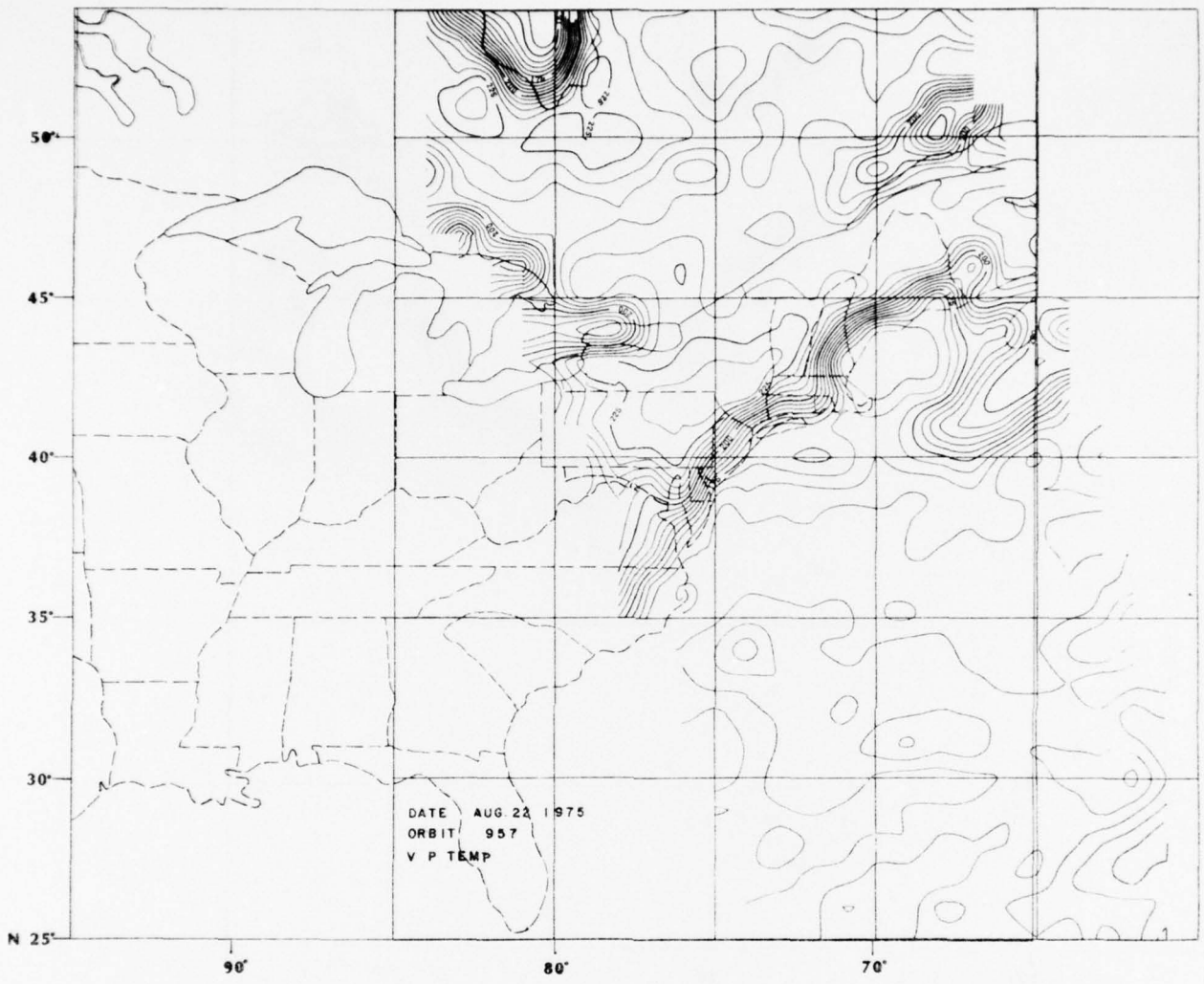

Figure 3.2.2. Brightness temperatures of the vertically polarized component in the 37 GHz band from the ESMR experiment on Nimbus VI.

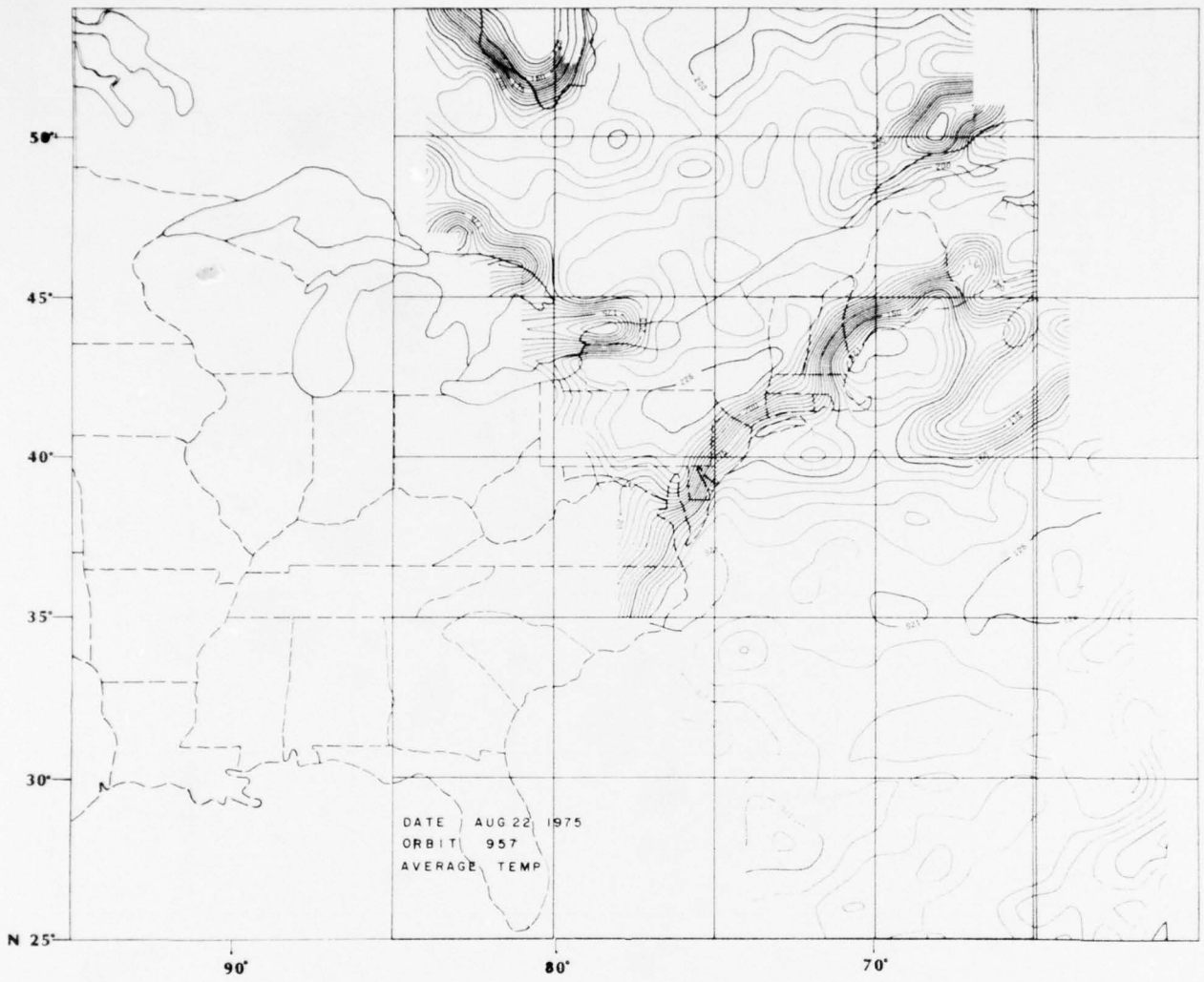

Figure 3.2.3. Average Brightness temperature of the horizontal and vertical components in the 37 GHz band from the ESMR experiment on Nimbus VI.

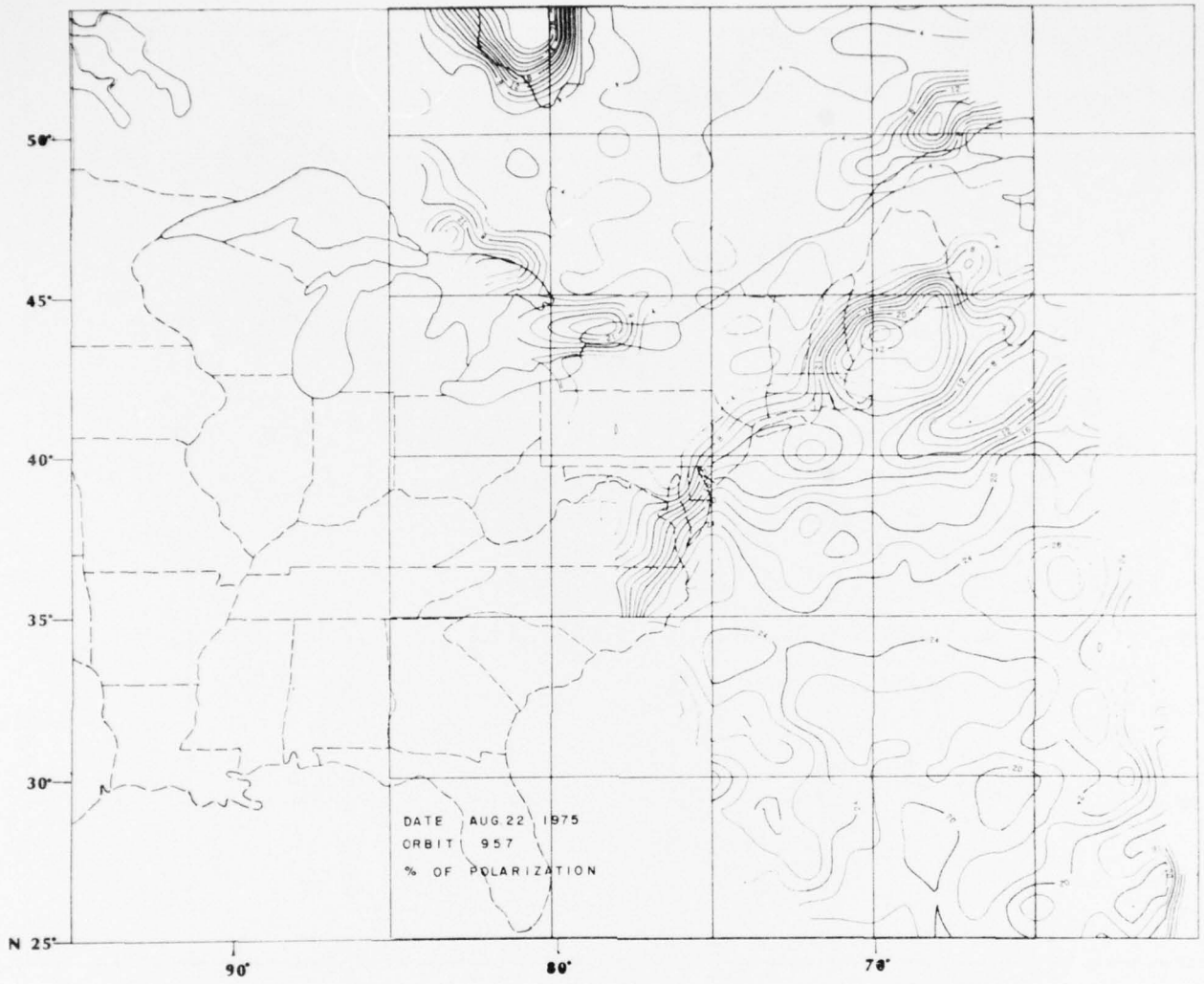

Figure 3.2.4. Percentage of polarization in the 37 GHz band from the ESMR experiment on Nimbus VI.

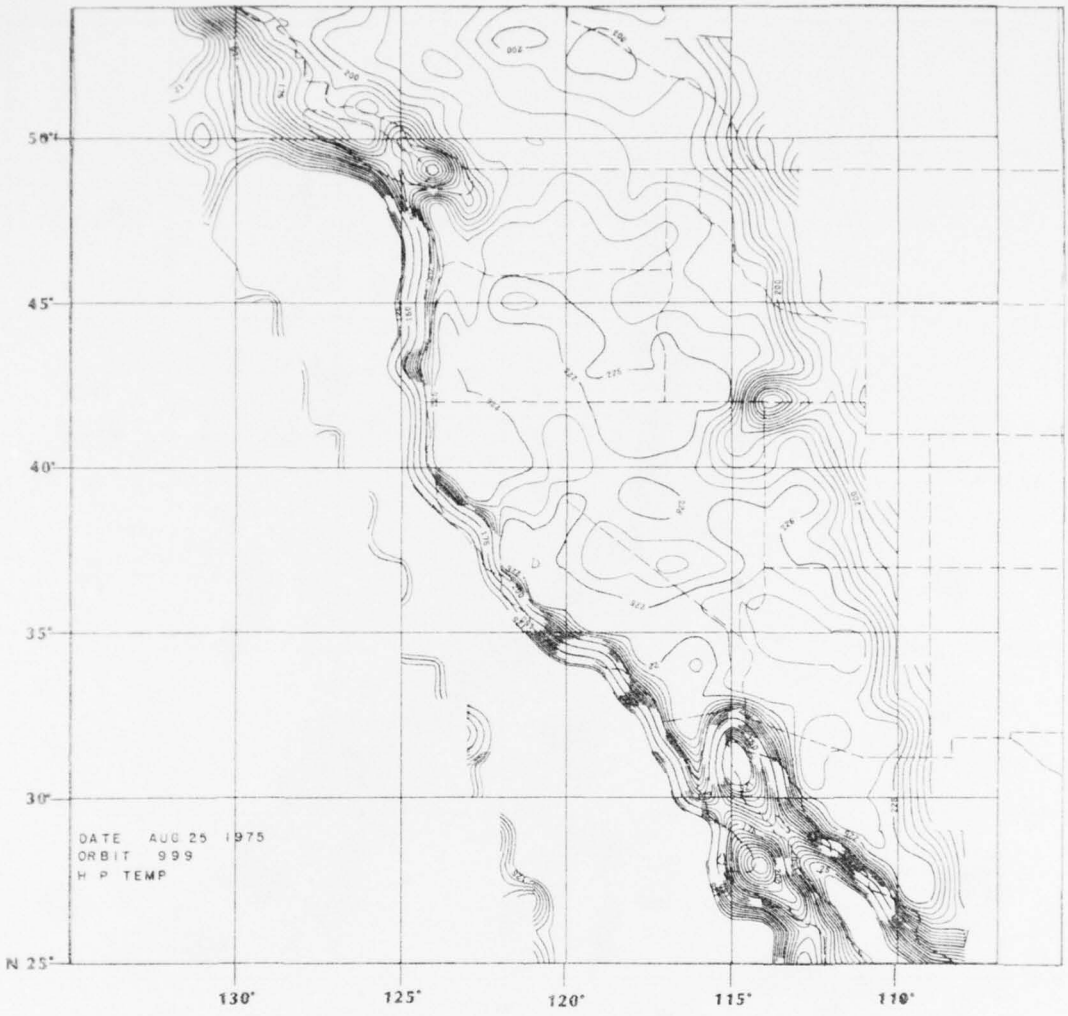

Figure 3.2.5. Brightness temperatures of the horizontally polarized component in the 37GHz band from the ESMR experiment on Nimbus VI.

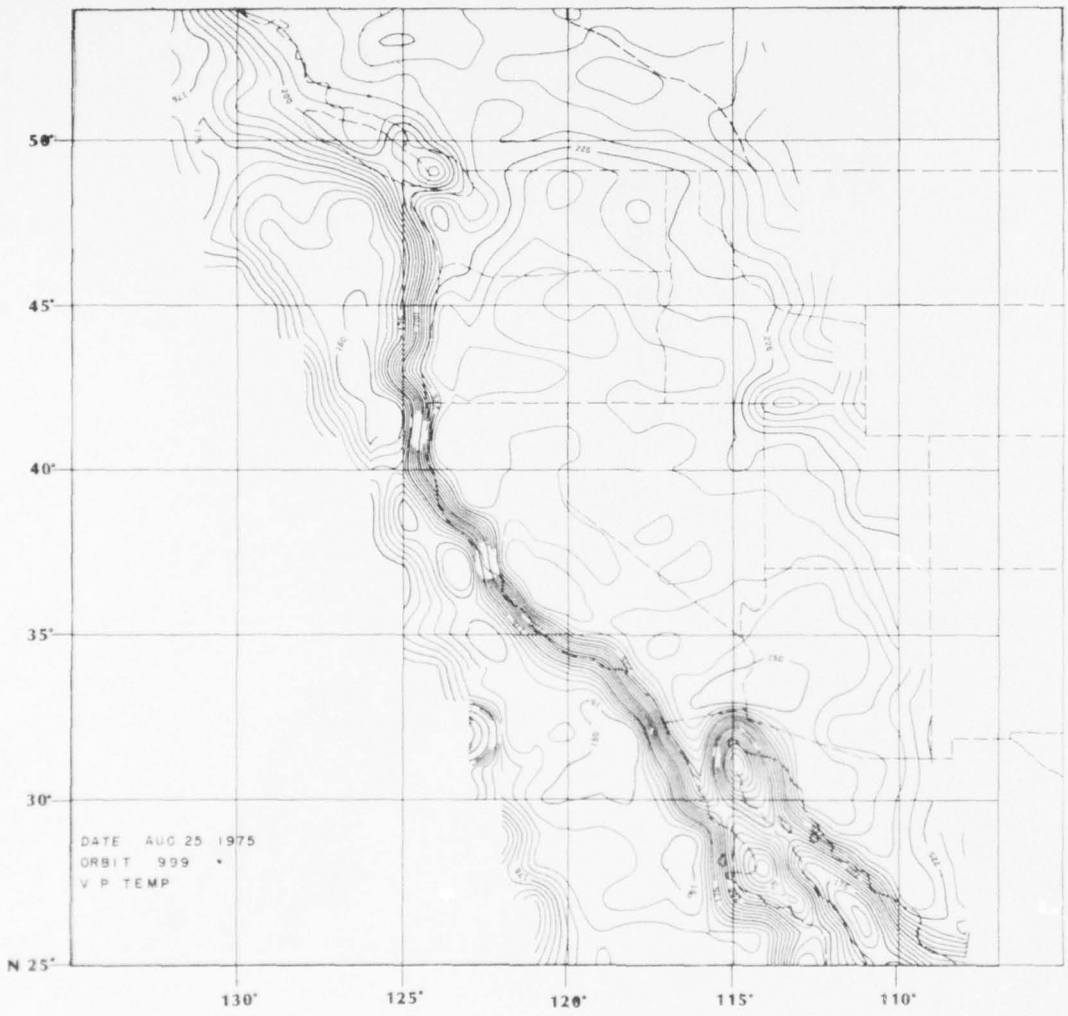

Figure 3.2.6. Brightness temperatures of the vertically polarized component in the 37 GHz band from the ESMR experiment on Nimbus VI.

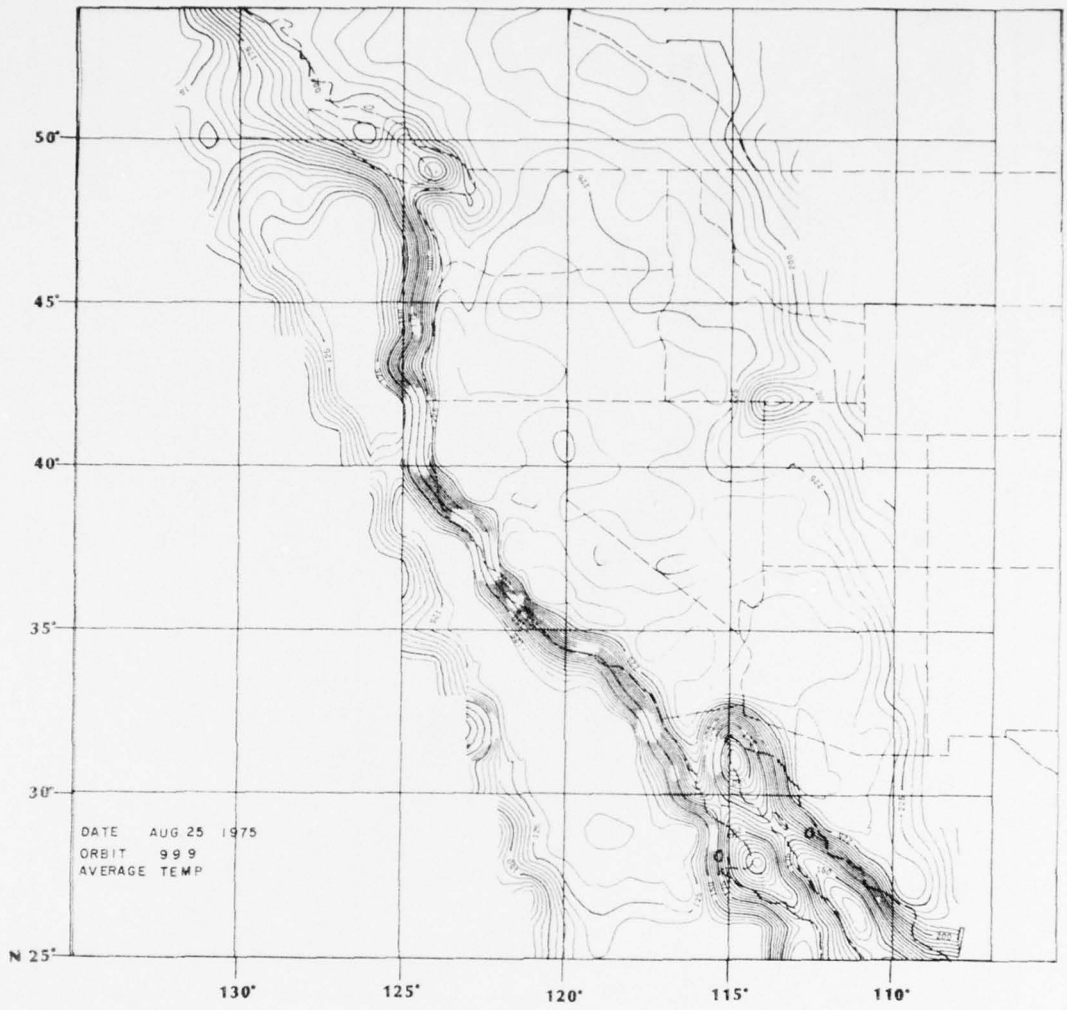

Figure 3.2.7. Average Brightness temperature of the horizontal and vertical components in the 37 GHz band from the ESMR experiment on Nimbus VI.

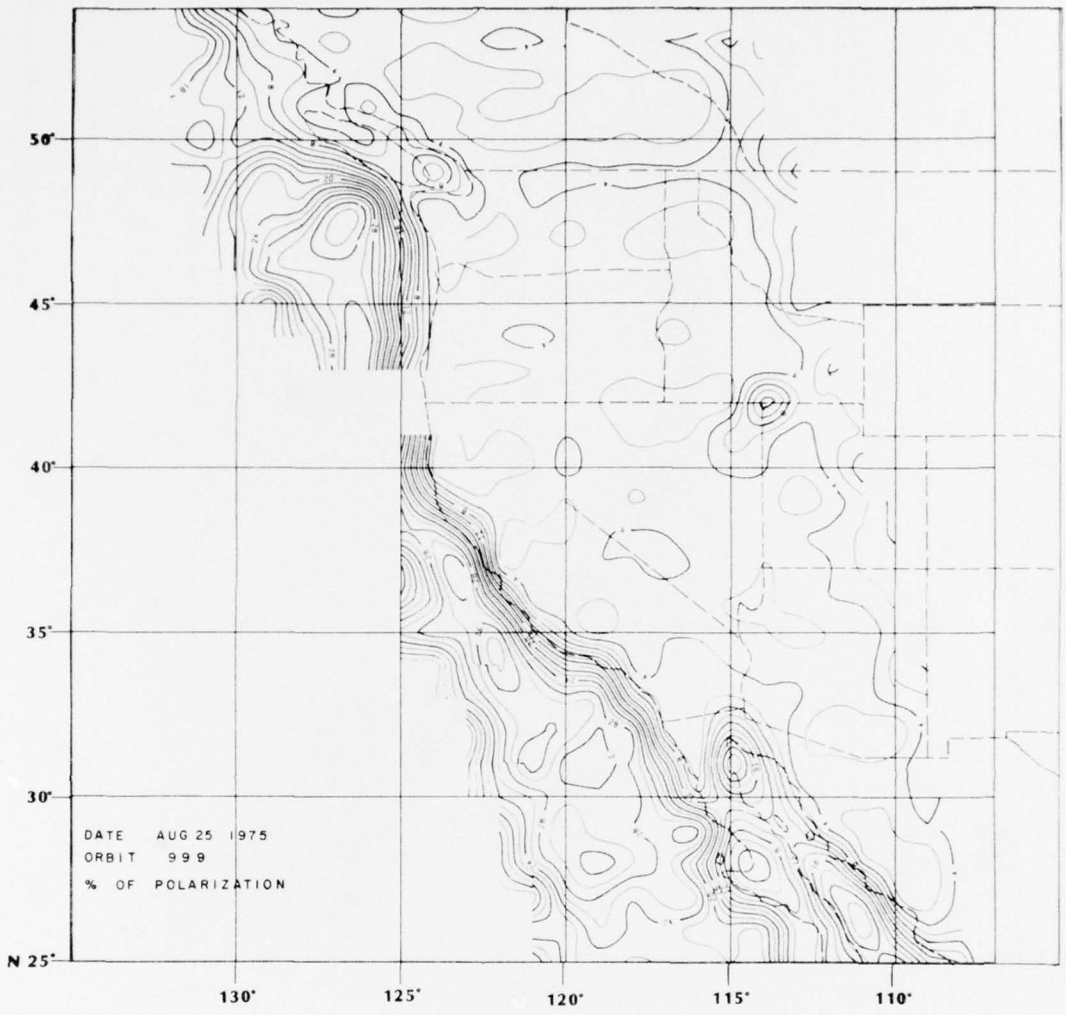

Figure 3.2.8. Percentage of polarization in the 37 GHz band from the ESMR experiment on Nimbus VI.

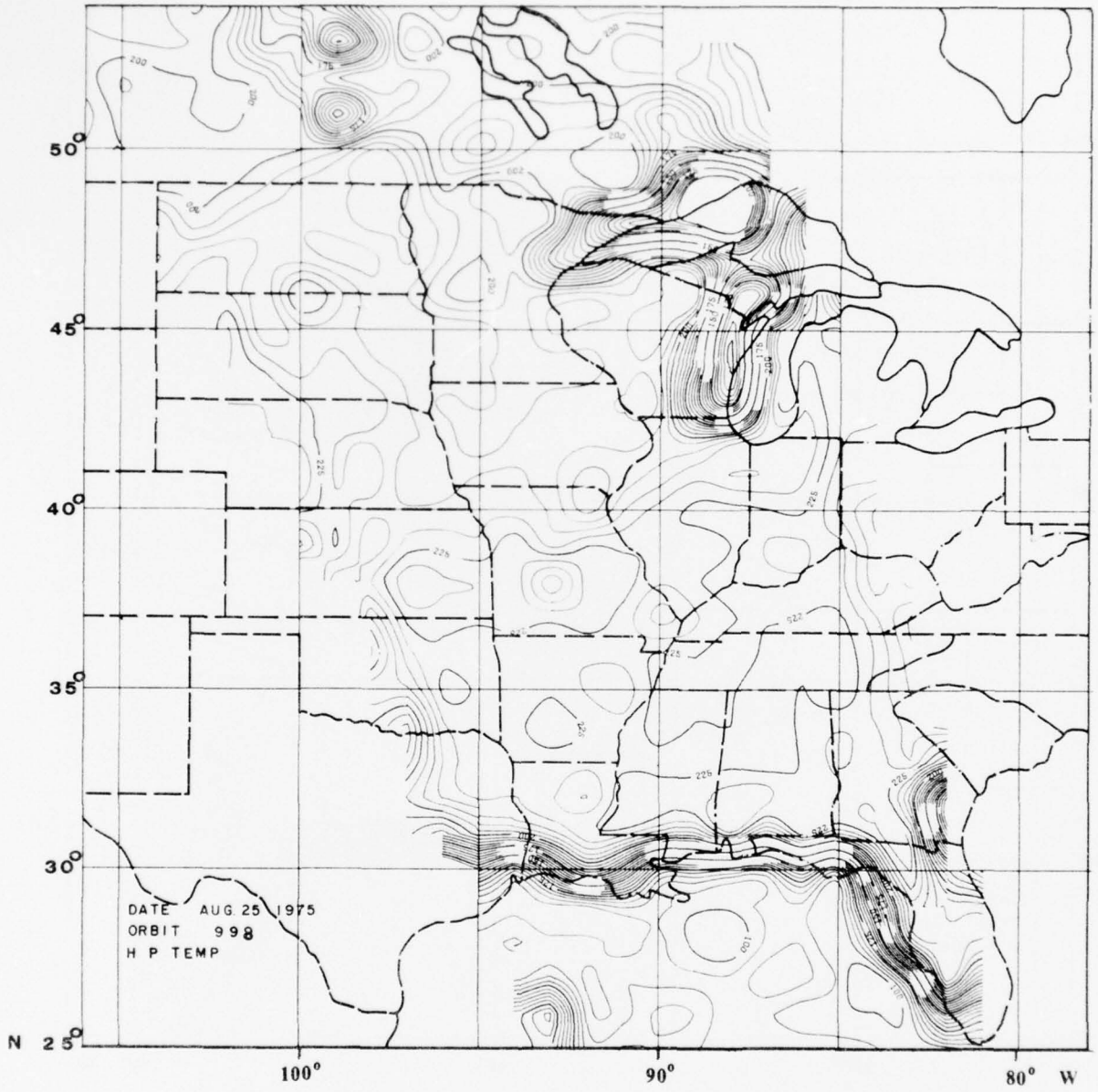

Figure 3.2.9. Brightness temperatures of the horizontally polarized component in the 37GHz band from the ESMR experiment on Nimbus VI.

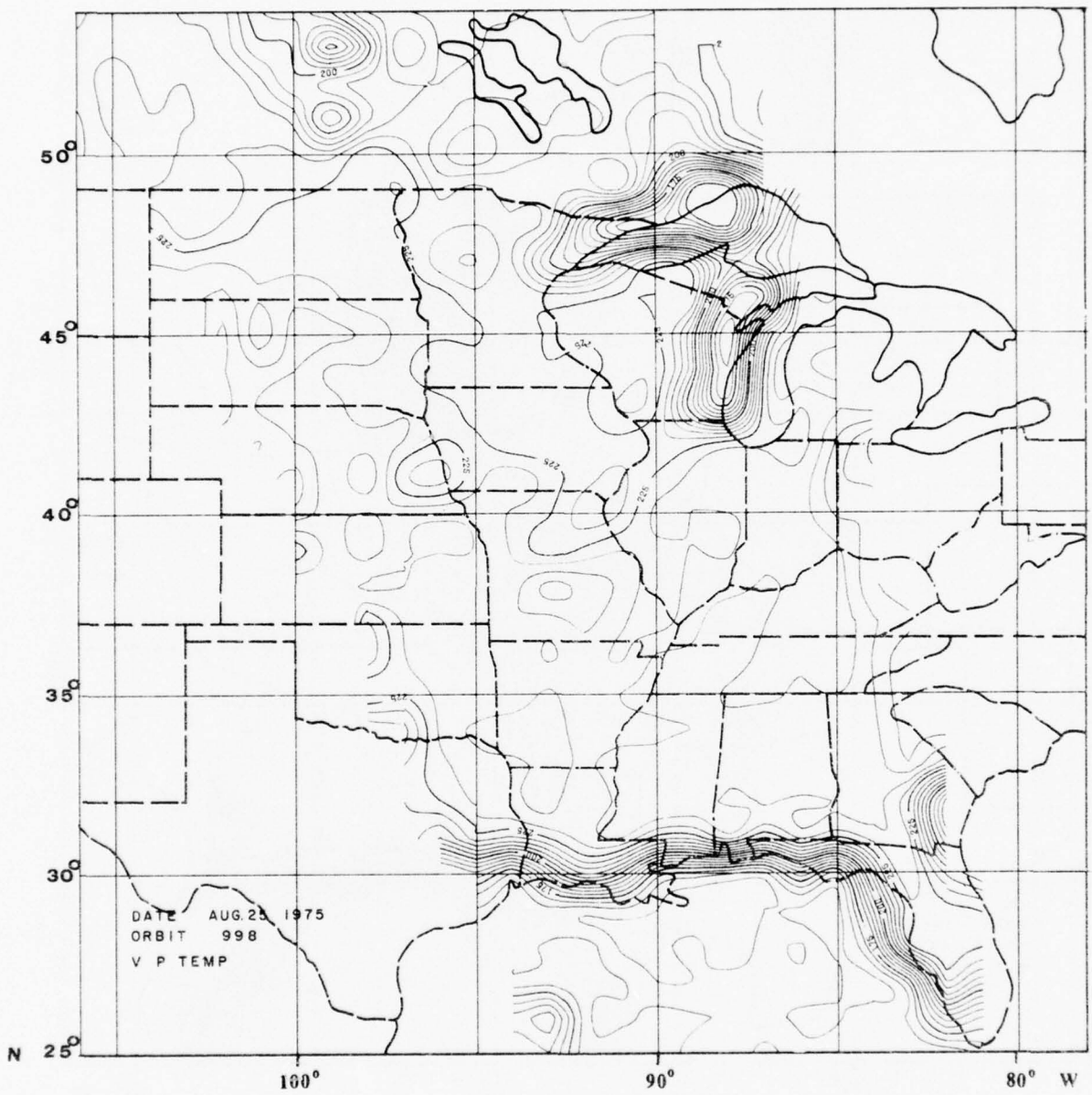

Figure 3.2.10. Brightness temperatures of the vertically polarized component in the 37 GHz band from the ESMR experiment on Nimbus VI.

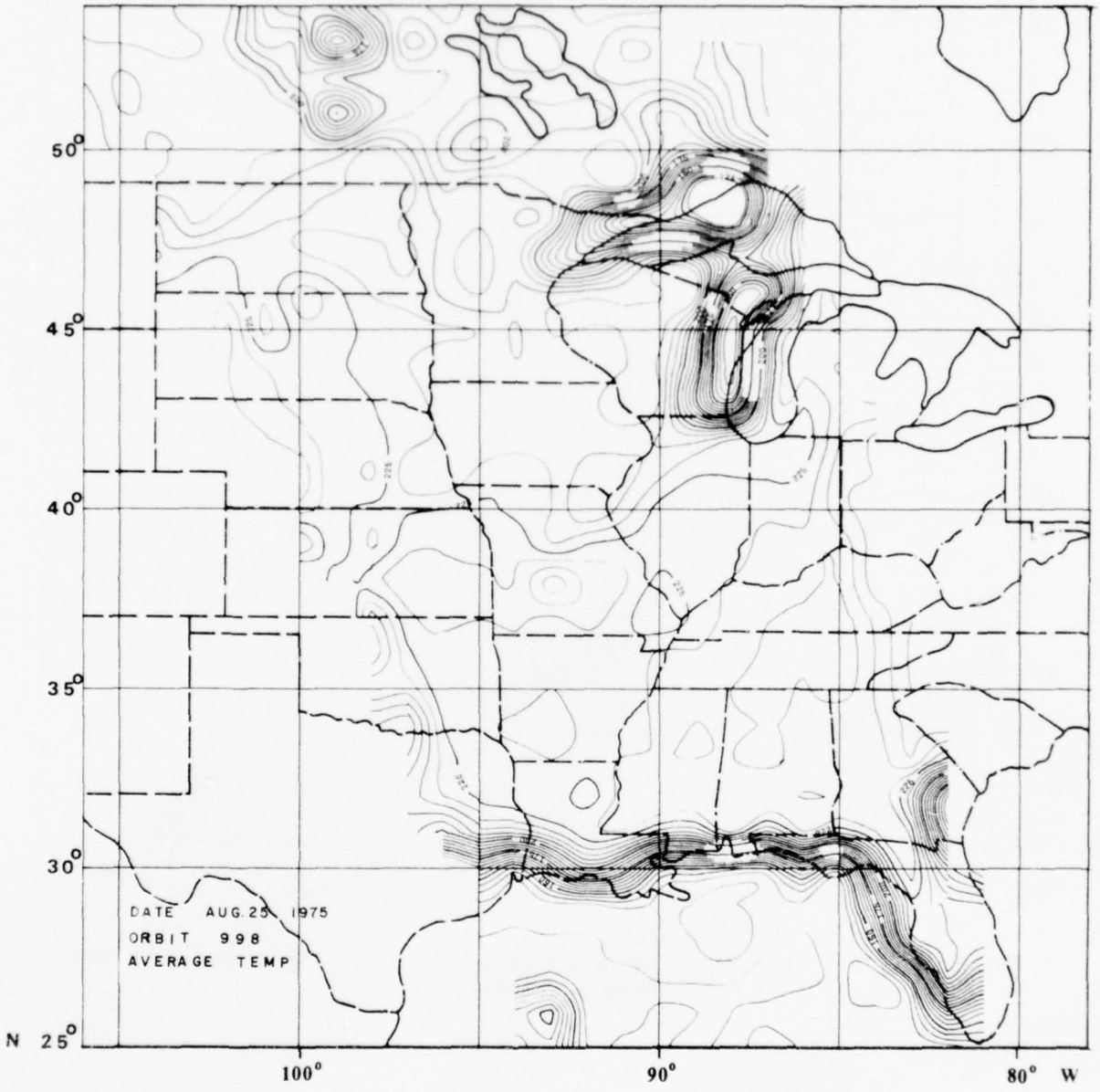

Figure 3.2.11. Average Brightness temperature of the horizontal and vertical components in the 37 GHz band from the ESMR experiment on Nimbus VI.

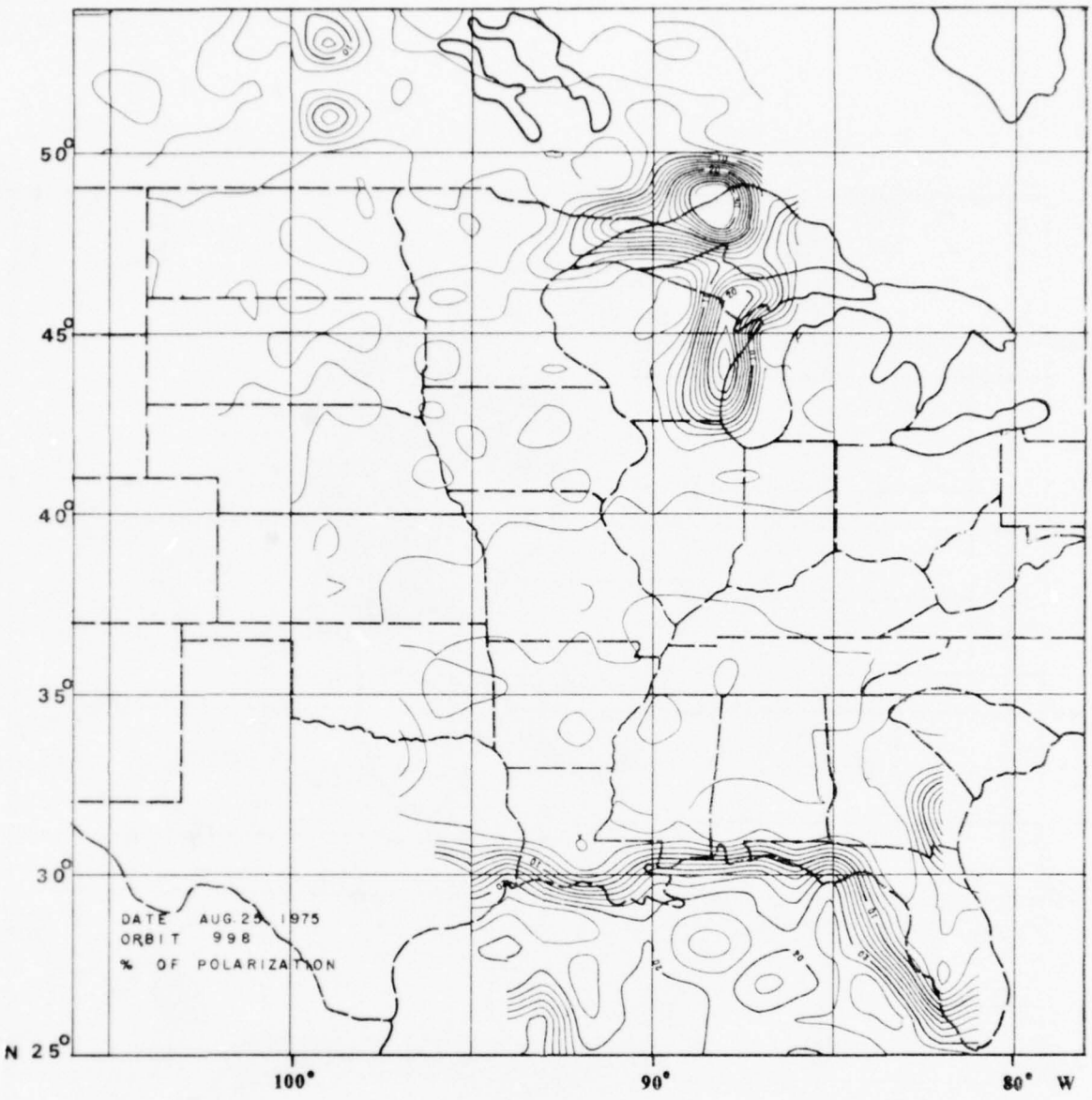

Figure 3.2.12. Percentage of polarization in the 37 GHz band from the ESMR experiment on Nimbus VI.

these variables on the brightness temperature and polarization observed by ESMR.

The ESMR data corresponding to the wintertime cloud case are available for 20 and 21 February 1976. Figures 3.2.13 - 3.2.16 are for 20 February 1976 covering the central part of the United States. Two orbits are available on 21 February 1976. The data for the eastern and central orbits are depicted in Figures 3.2.17 - 3.2.20 and Figures 3.2.21 - 3.2.24, respectively. Inspection of the average brightness temperature contours in this case reveals greater variations compared to the summertime cloud case. This is due to the large cloud cover (see Figure 2.53) and the variable surface condition during the wintertime. To understand the detailed average brightness temperature and percentage of polarization signatures in relation to cloud compositions and structure again requires physical interpretation by means of microwave radiative transfer calculation.

3.3 THIR Data Analysis

A detailed analysis of equivalent blackbody temperatures were carried out for the 11.5 and 6.7 μm channels of the THIR instrument on Nimbus VI. Data were available for a portion of orbital pass 4134 over the United States on 15 April 1976 when intense convection was present. Analyzed maps of equivalent blackbody temperatures are shown in Figures 3.3.1 and 3.3.2 for the atmospheric window and water vapor channels. Temperatures less than 220°K were observed in both channels and were associated with convective clouds. Low temperatures are denoted by shaded areas in Figures 3.3.1 and 3.3.2. Highest temperatures exceeded 300°K in the 11.5 μm channel and appeared in cloud free areas over Mexico and South Dakota.

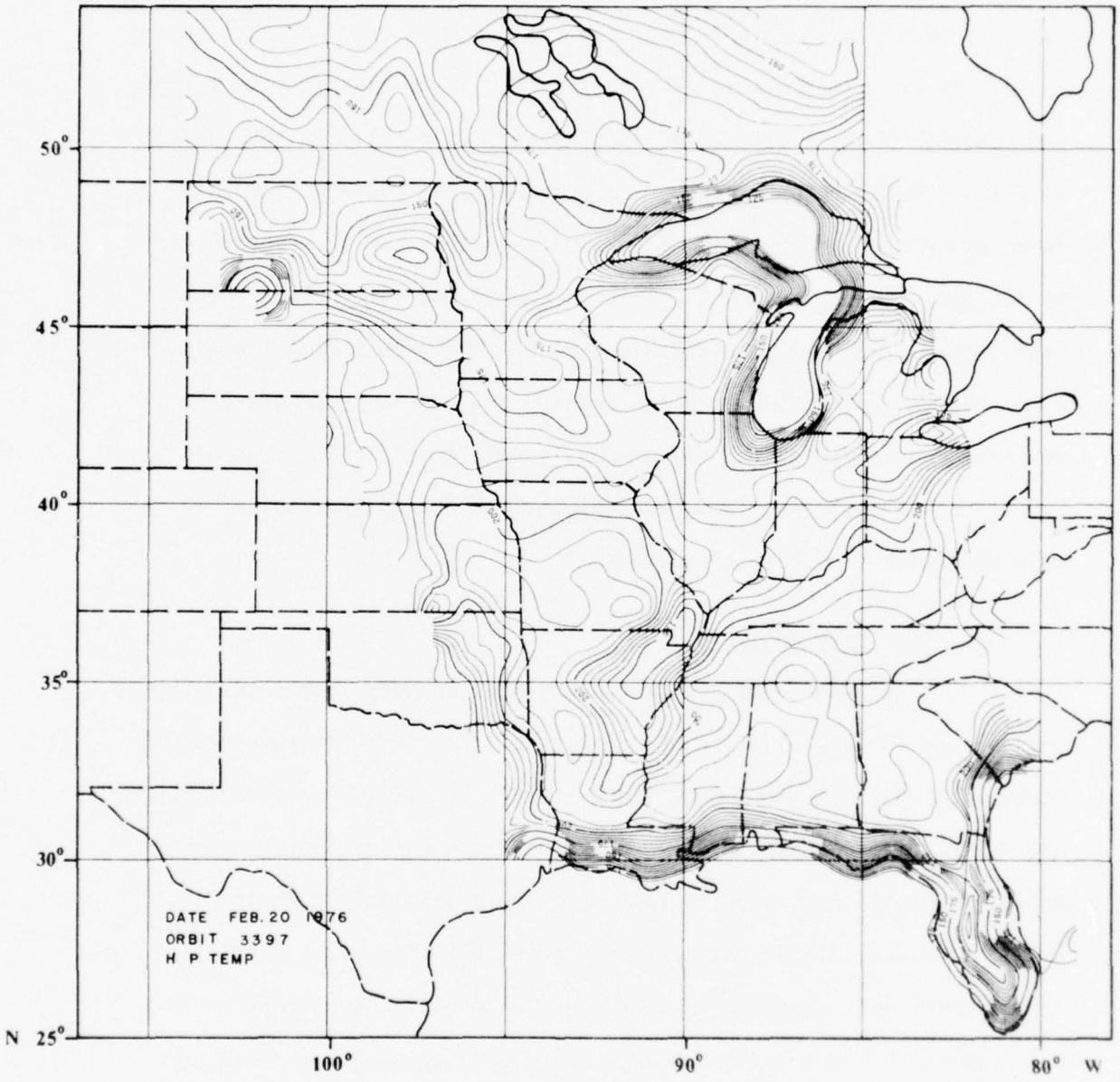

Figure 3.2.13. Brightness temperatures of the horizontally polarized component in the 37GHz band from the ESMR experiment on Nimbus VI.

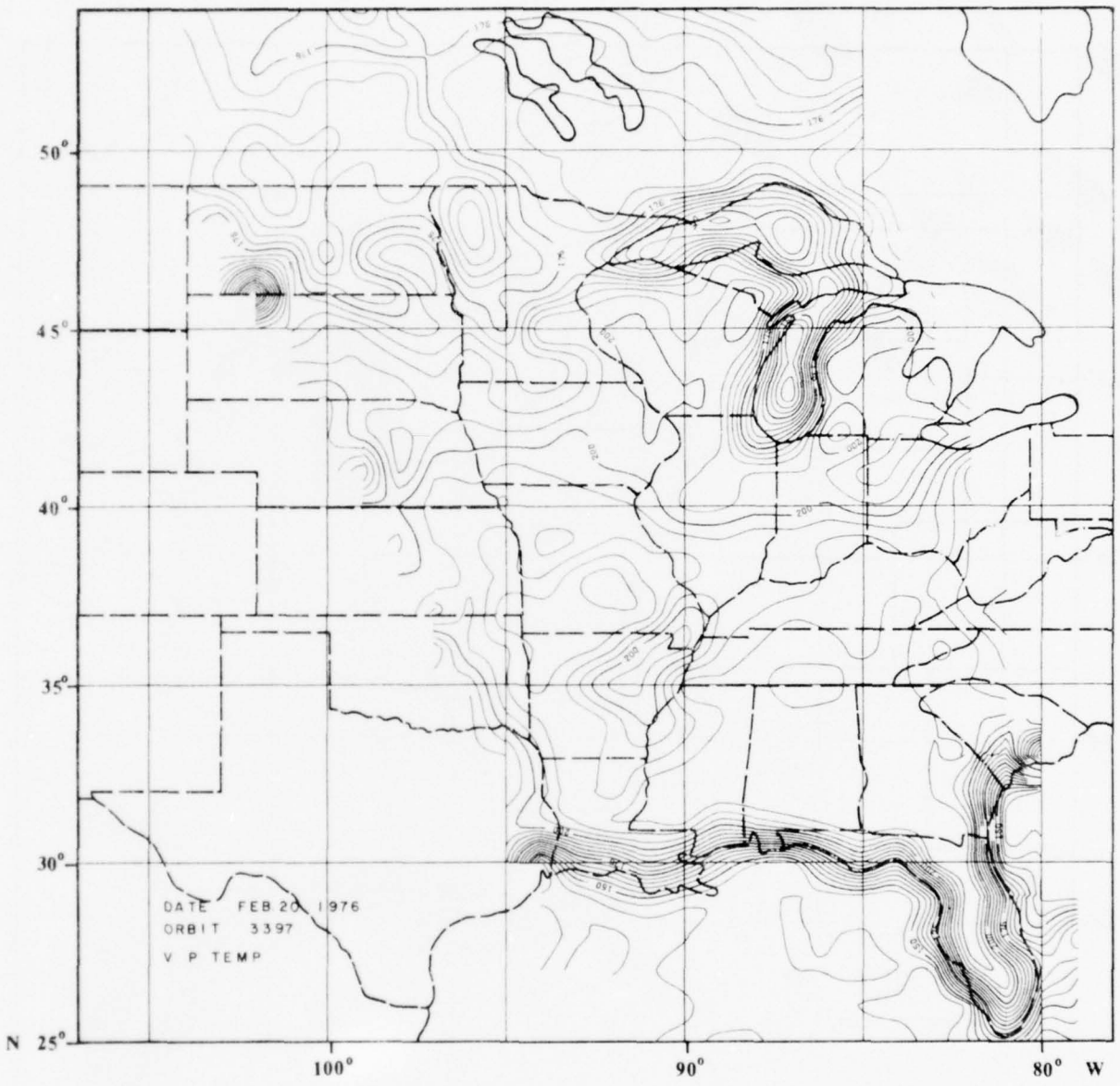

Figure 3.2.14. Brightness temperatures of the vertically polarized component in the 37 GHz band from the ESMR experiment on Nimbus VI.

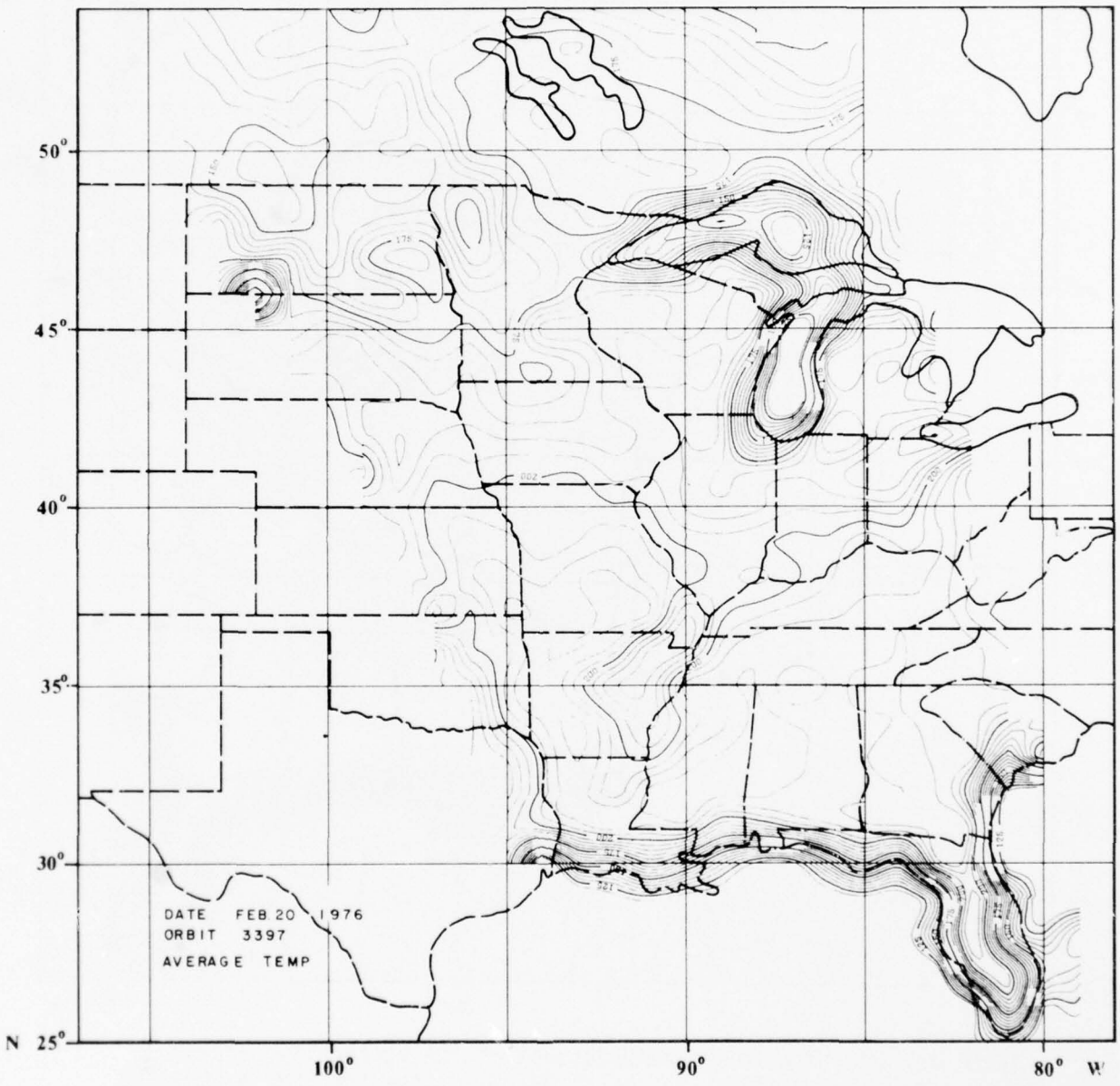

Figure 3.2.15. Average Brightness temperature of the horizontal and vertical components in the 37 GHz band from the ESMR experiment on Nimbus VI.

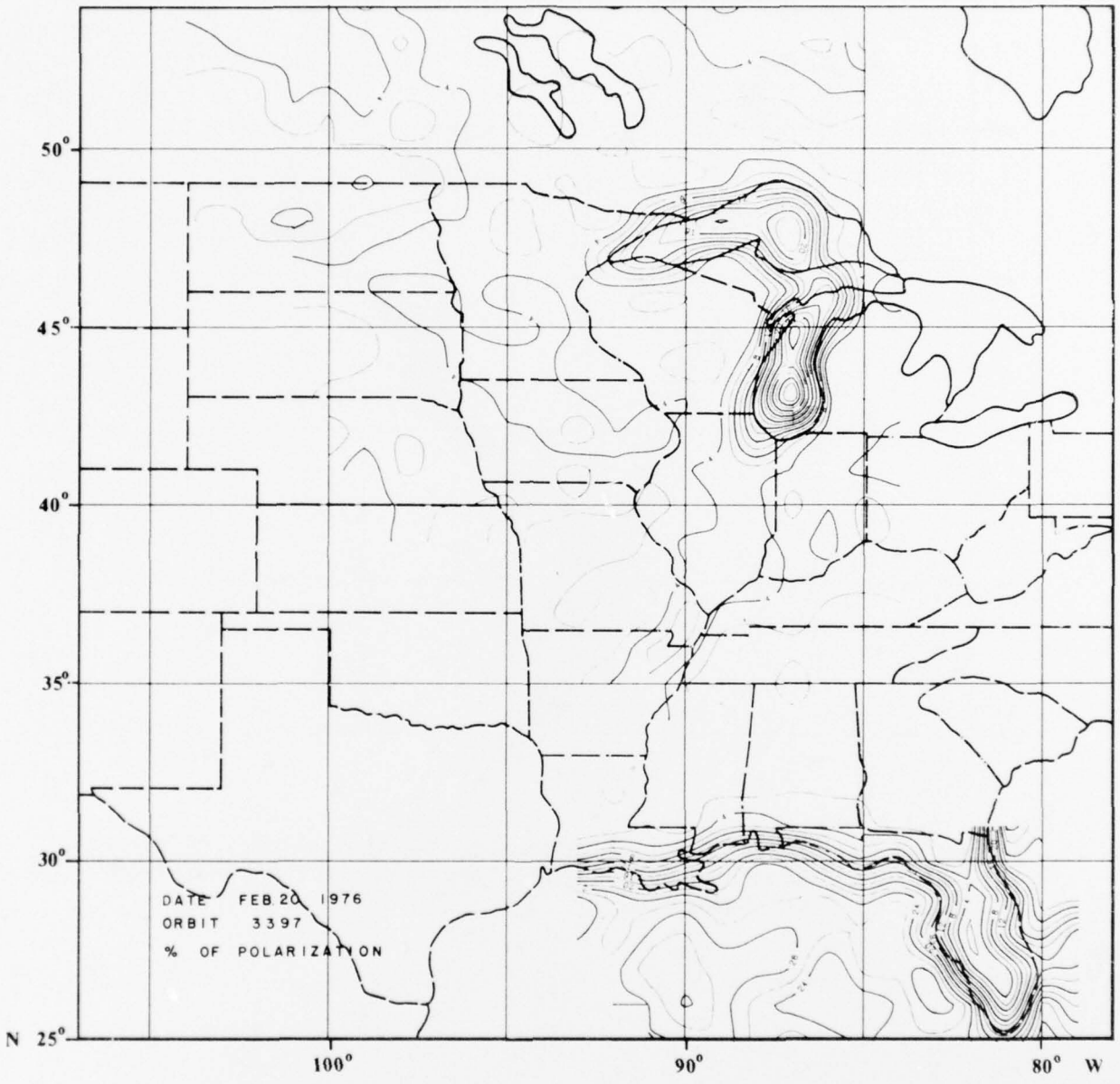

Figure 3.2.16. Percentage of polarization in the 37 GHz band from the ESMR experiment on Nimbus VI.

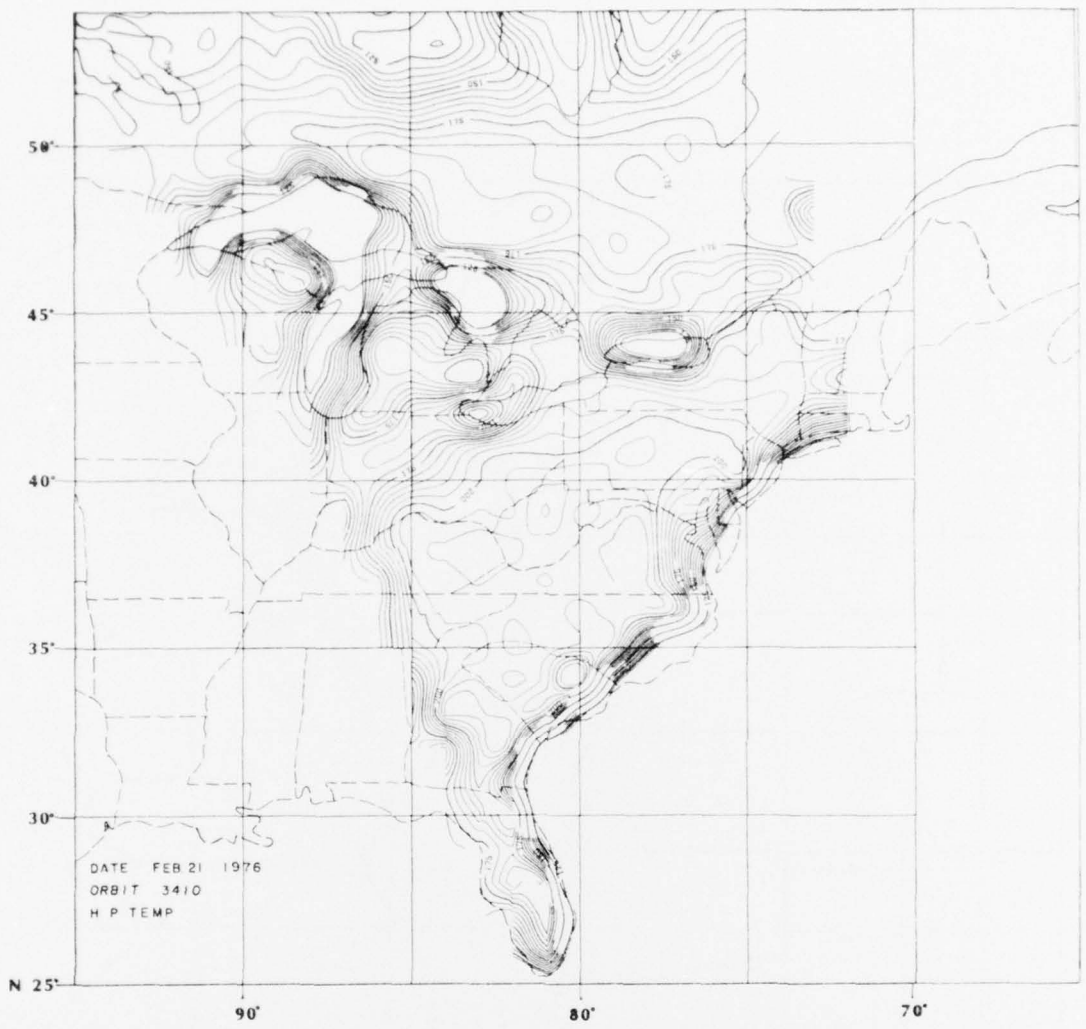

Figure 3.2.17. Brightness temperatures of the horizontally polarized component in the 37GHz band from the ESMR experiment on Nimbus VI.

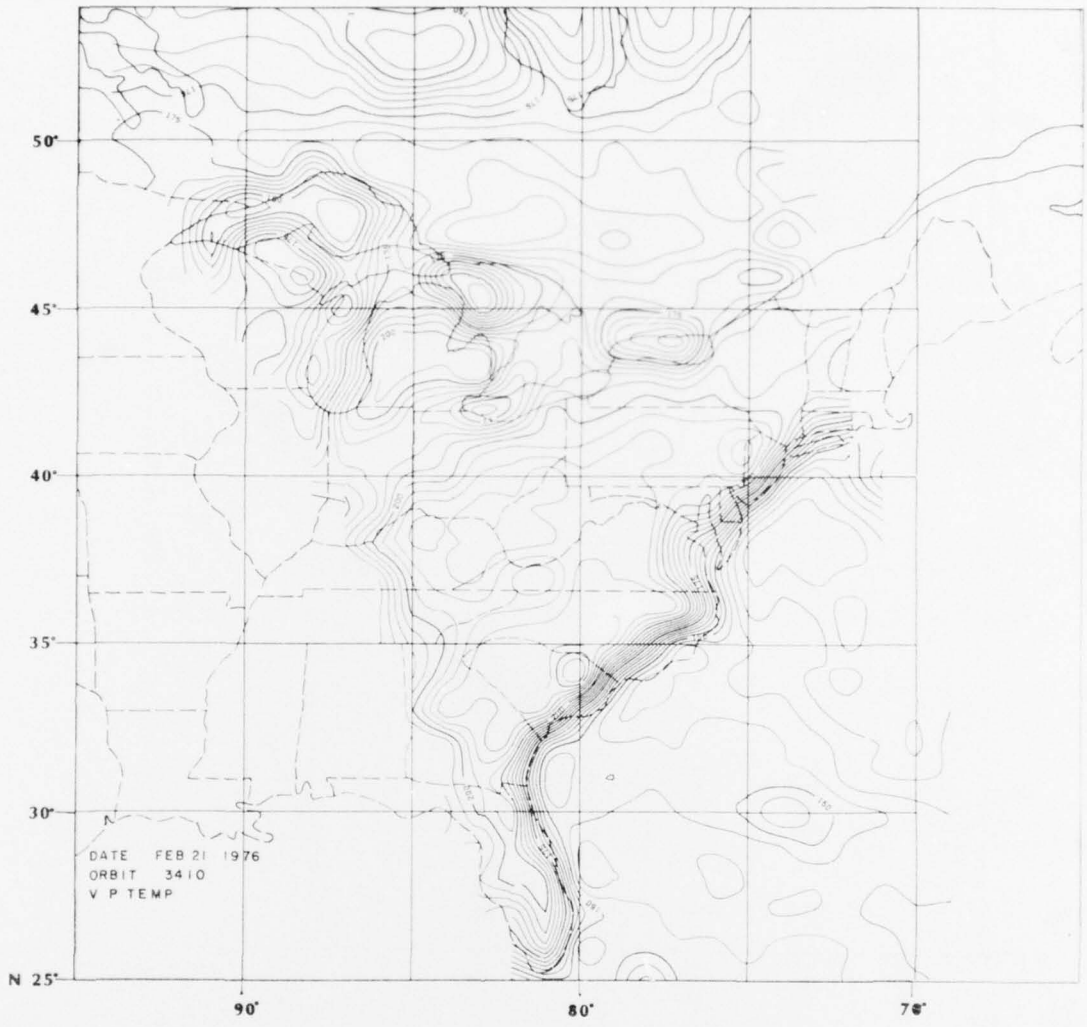

Figure 3.2.18. Brightness temperatures of the vertically polarized component in the 37 GHz band from the ESMR experiment on Nimbus VI.

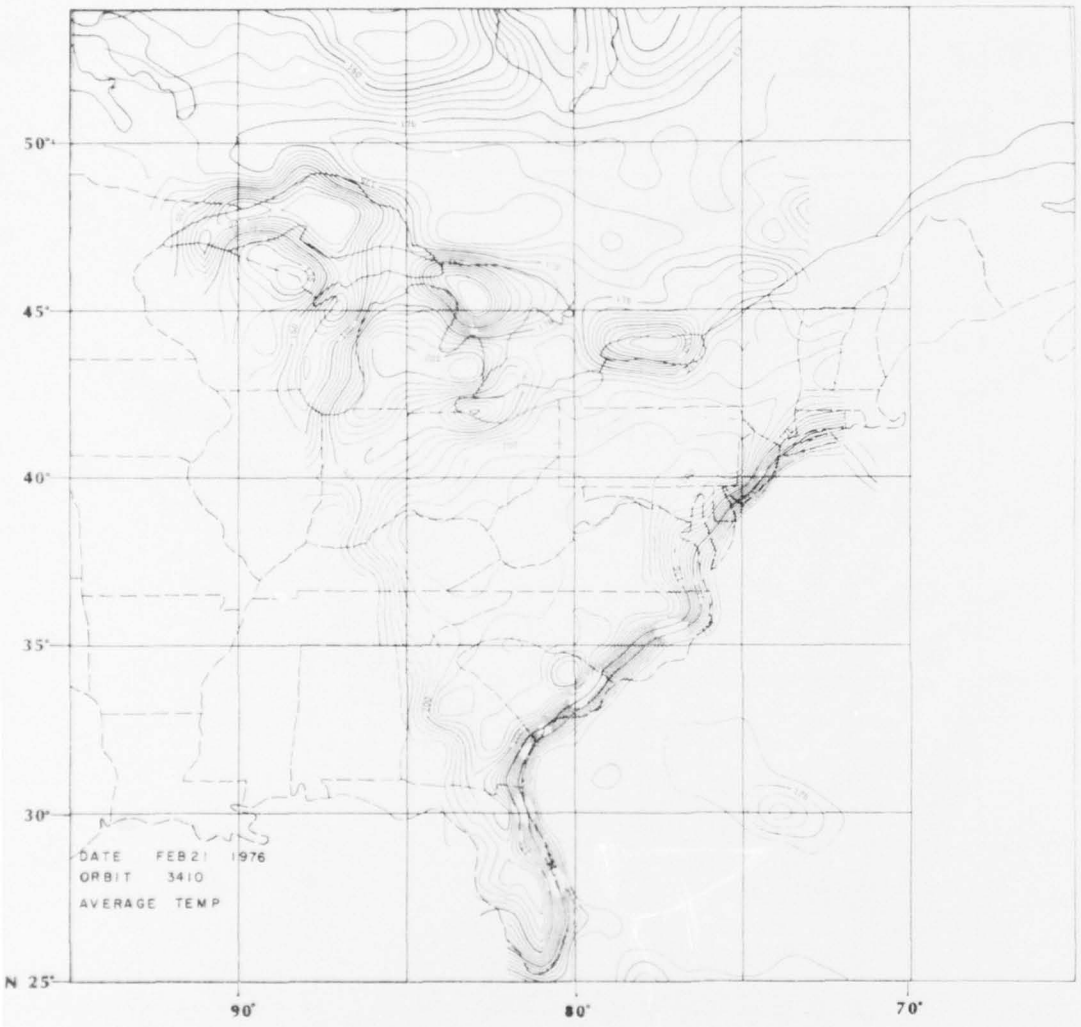

ure 3.2.19. Average Brightness temperature of the horizontal and vertical components in the 37 GHz band from the ESMR experiment on Nimbus VI.

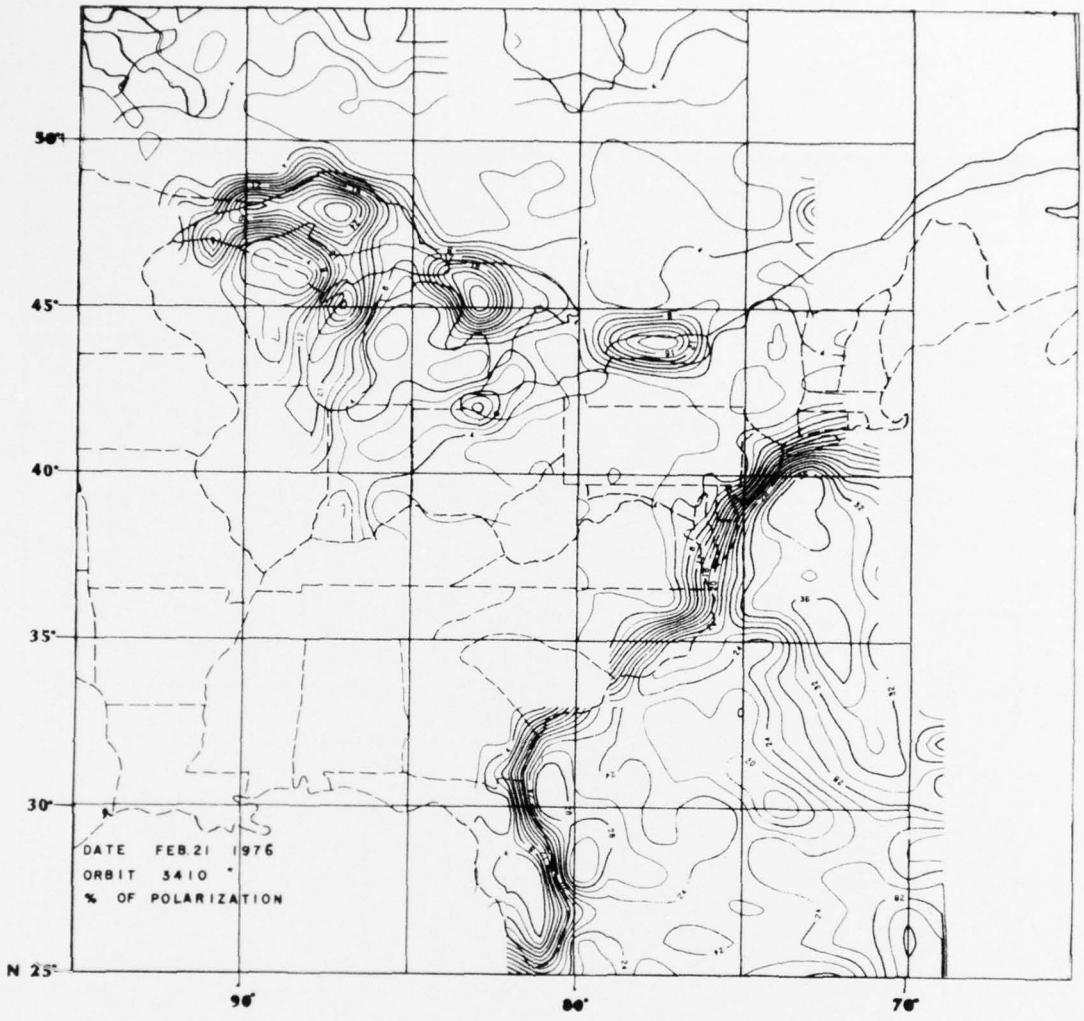

Figure 3.2.20. Percentage of polarization in the 37 GHz band from the ESMR experiment on Nimbus VI.

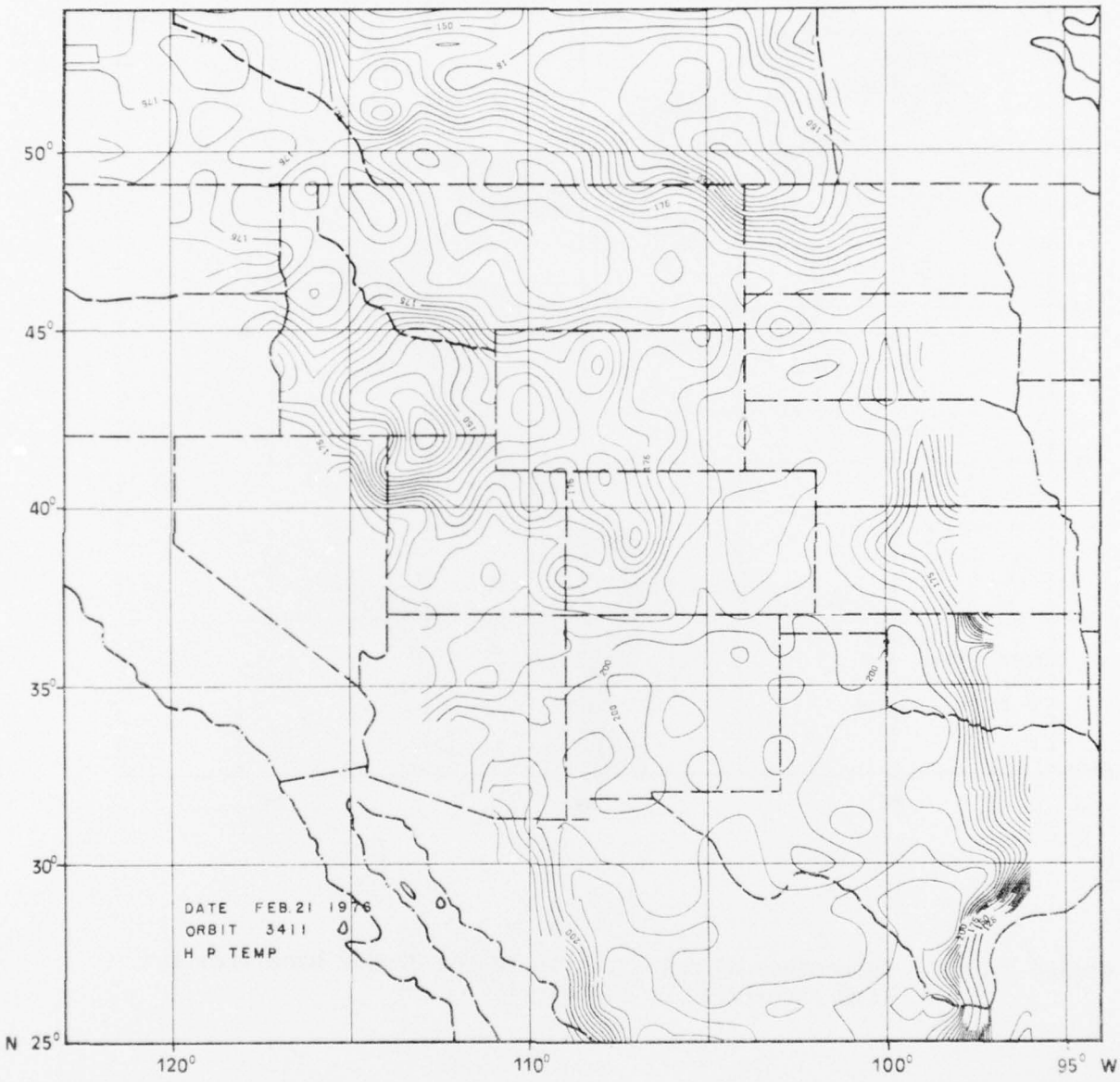

Figure 3.2.21. Brightness temperatures of the horizontally polarized component in the 37GHz band from the ESMR experiment on Nimbus VI.

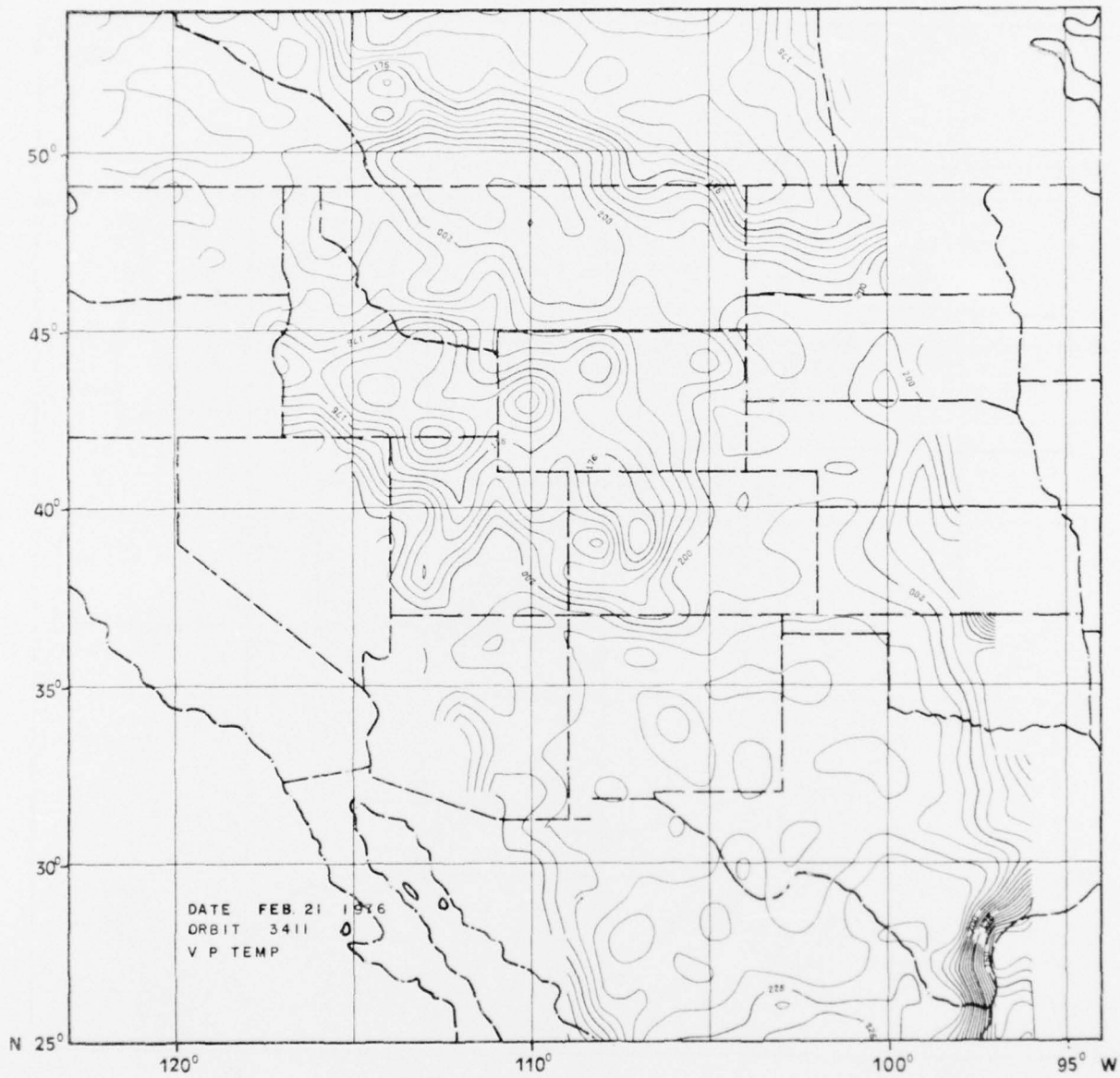

Figure 3.2.22. Brightness temperatures of the vertically polarized component in the 37 GHz band from the ESMR experiment on Nimbus VI.

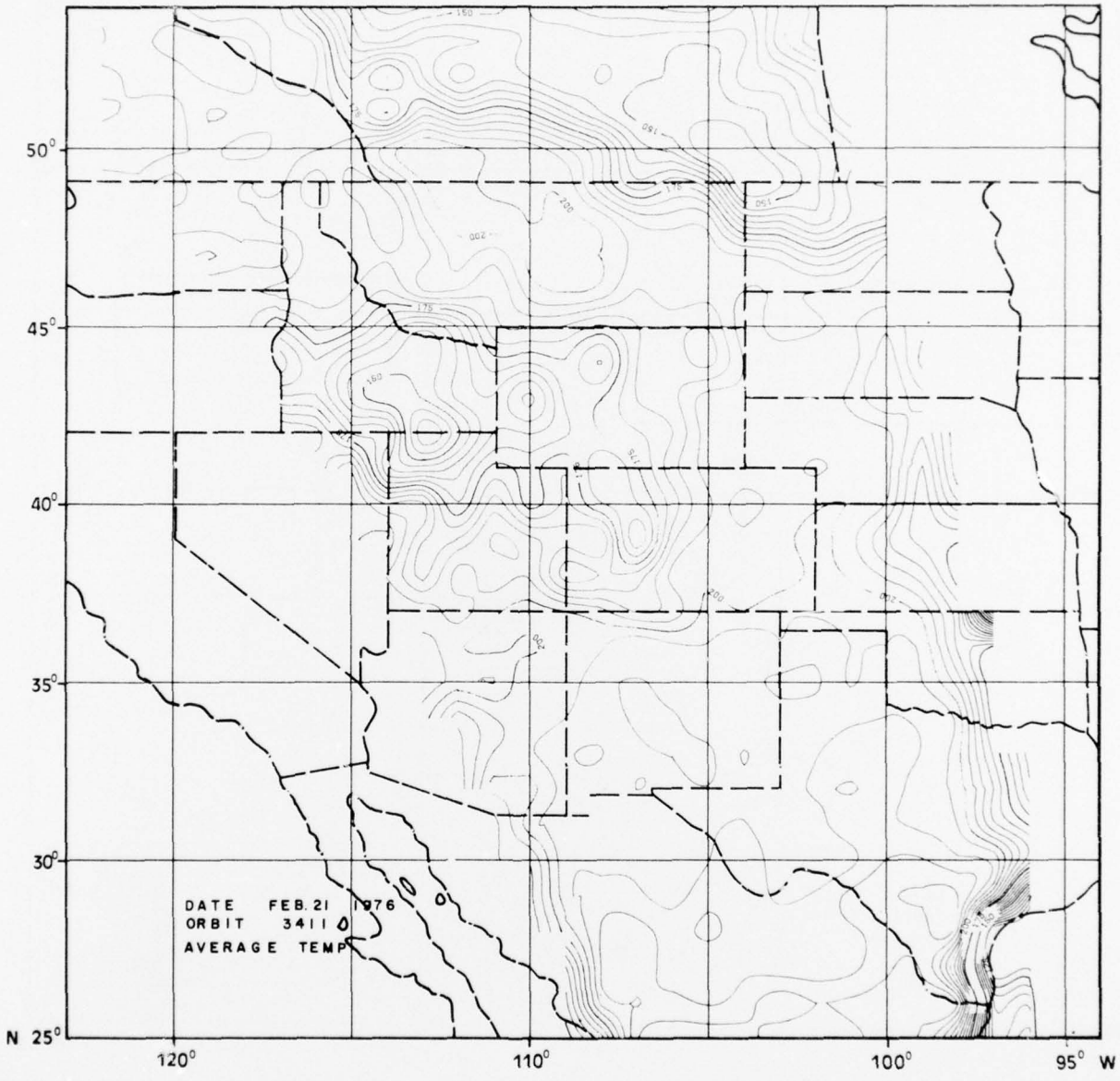

Figure 3.2.23. Average Brightness temperature of the horizontal and vertical components in the 37 GHz band from the ESMR experiment on Nimbus VI.

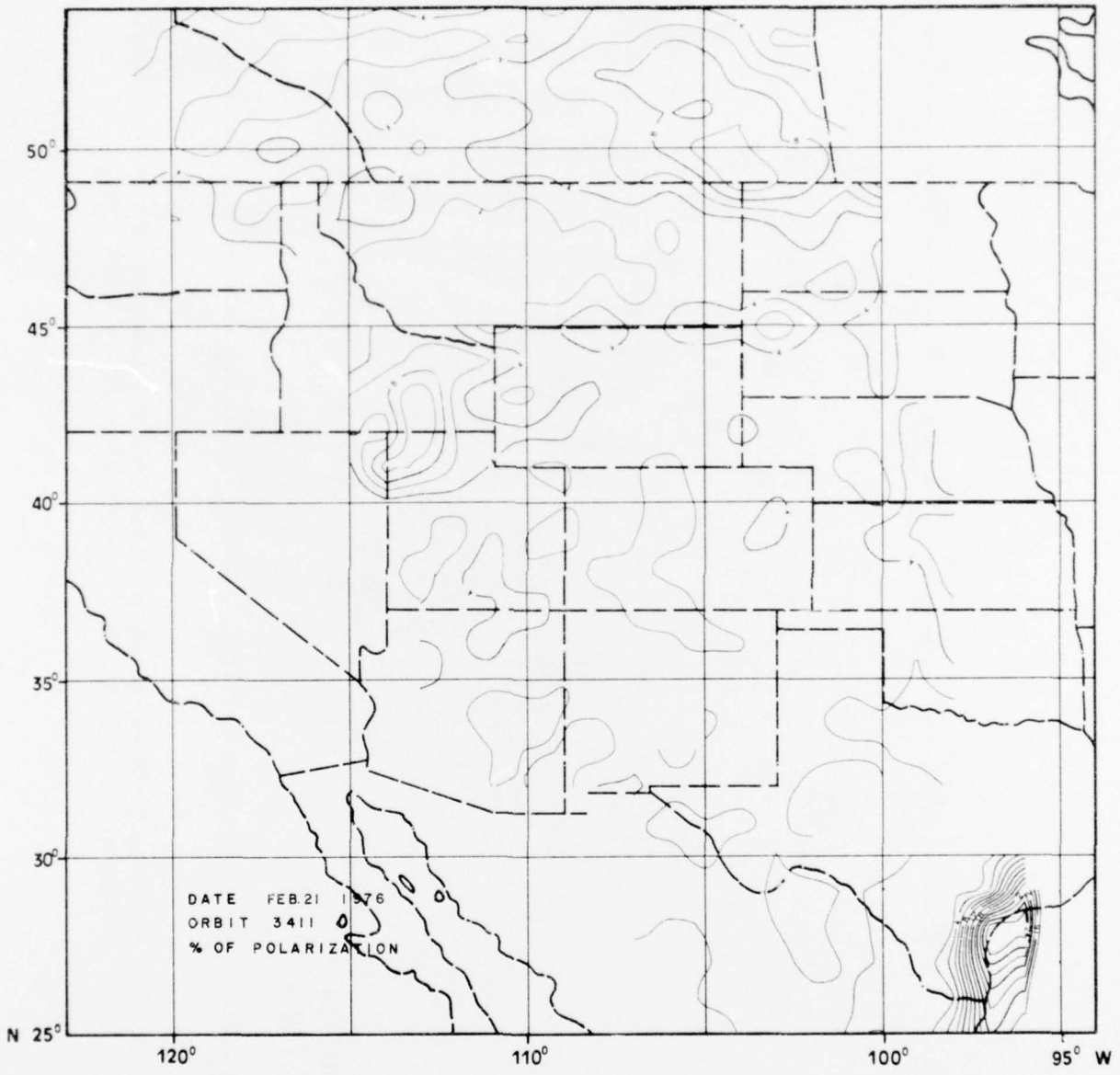

Figure 3.2.24. Percentage of polarization in the 37 GHz band from the ESMR experiment on Nimbus VI.

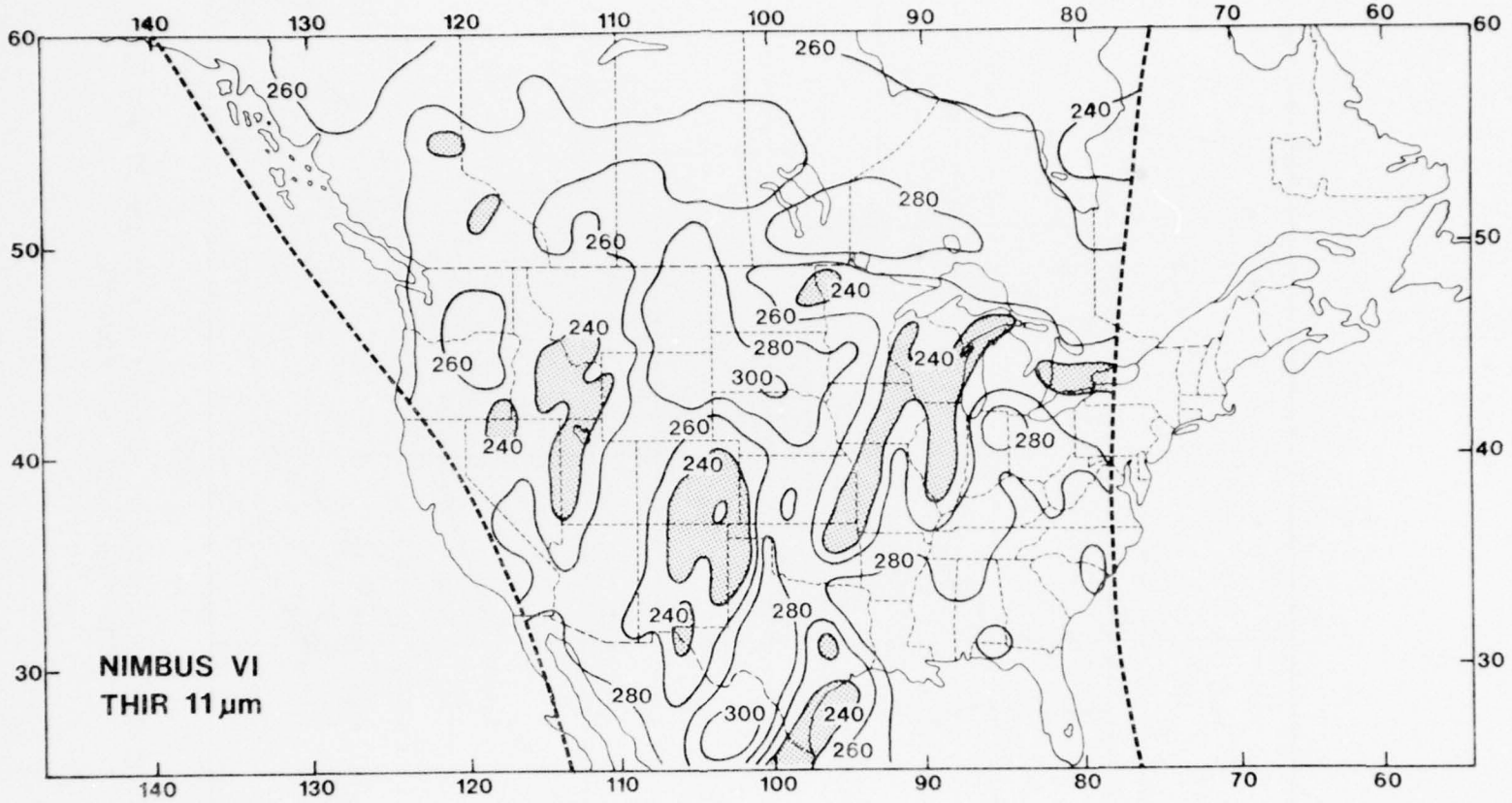

Figure 3.3.1. Equivalent blackbody temperatures from the atmospheric window channel of THIR on Nimbus VI for orbital pass 4134 at 1745 GMT 15 April 1976.

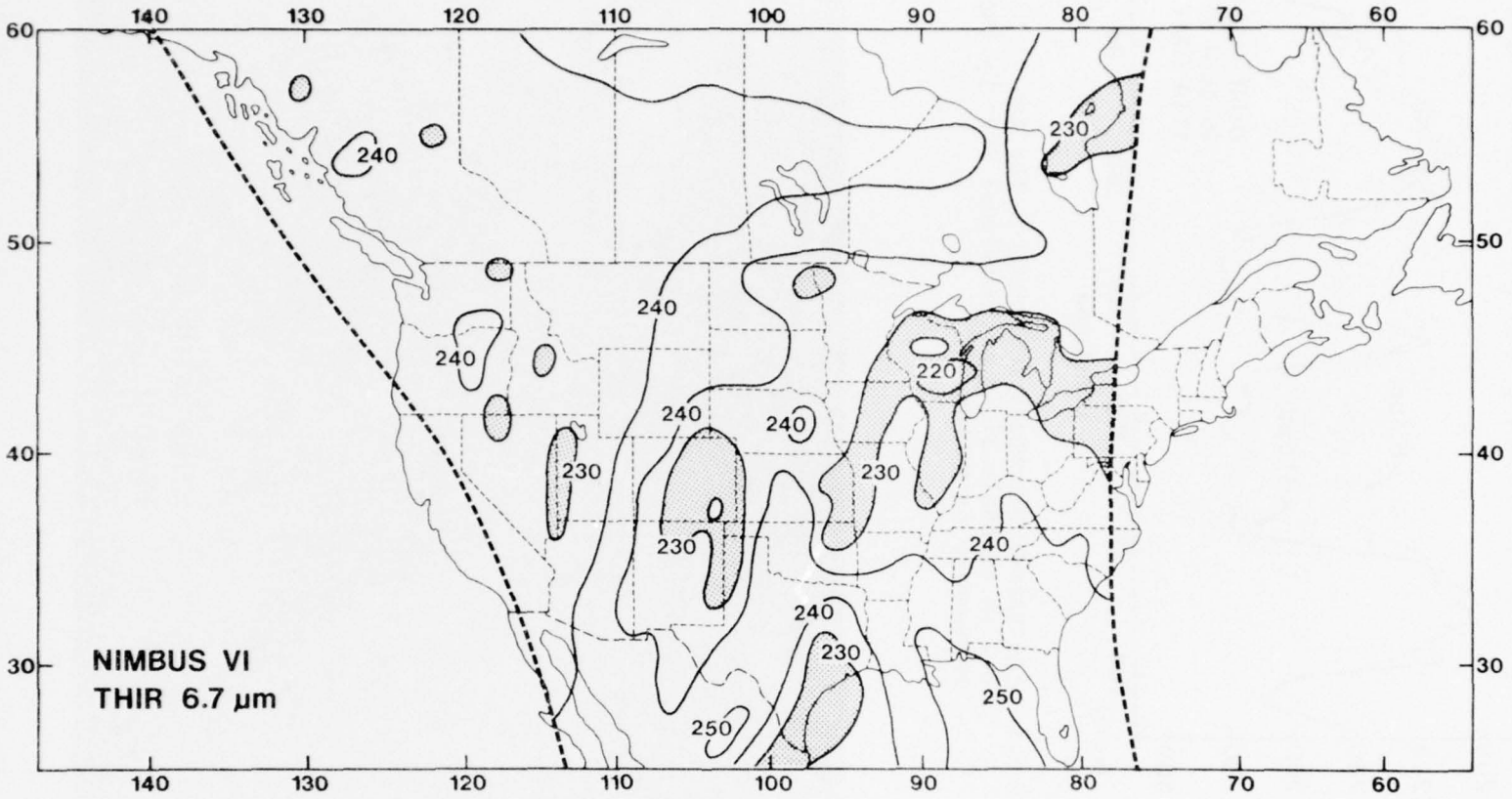

Figure 3.3.2. Equivalent blackbody temperatures from the water vapor channel of THIR on Nimbus VI for orbital pass 4134 at 1745 GMT 15 April 1976.

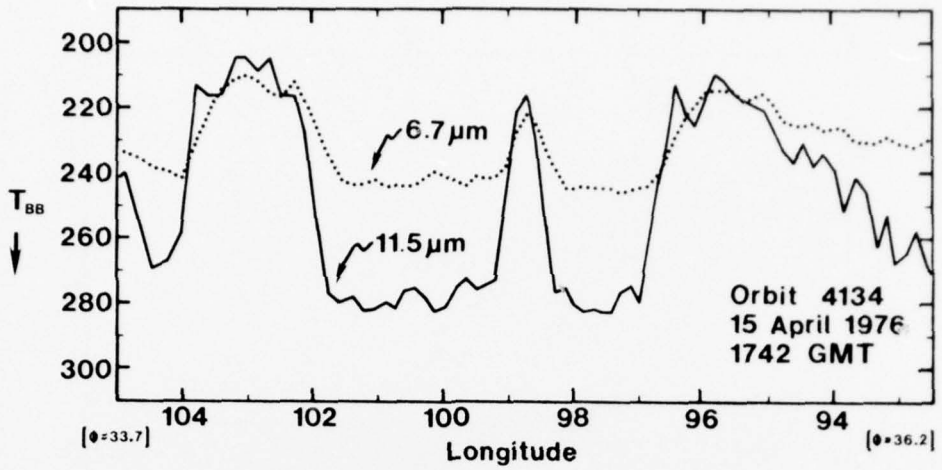

Figure 3.3.3. Equivalent blackbody temperatures for the 11.5 μm and 6.7 μm channels along an individual scan by the THIR radiometer on Nimbus VI.

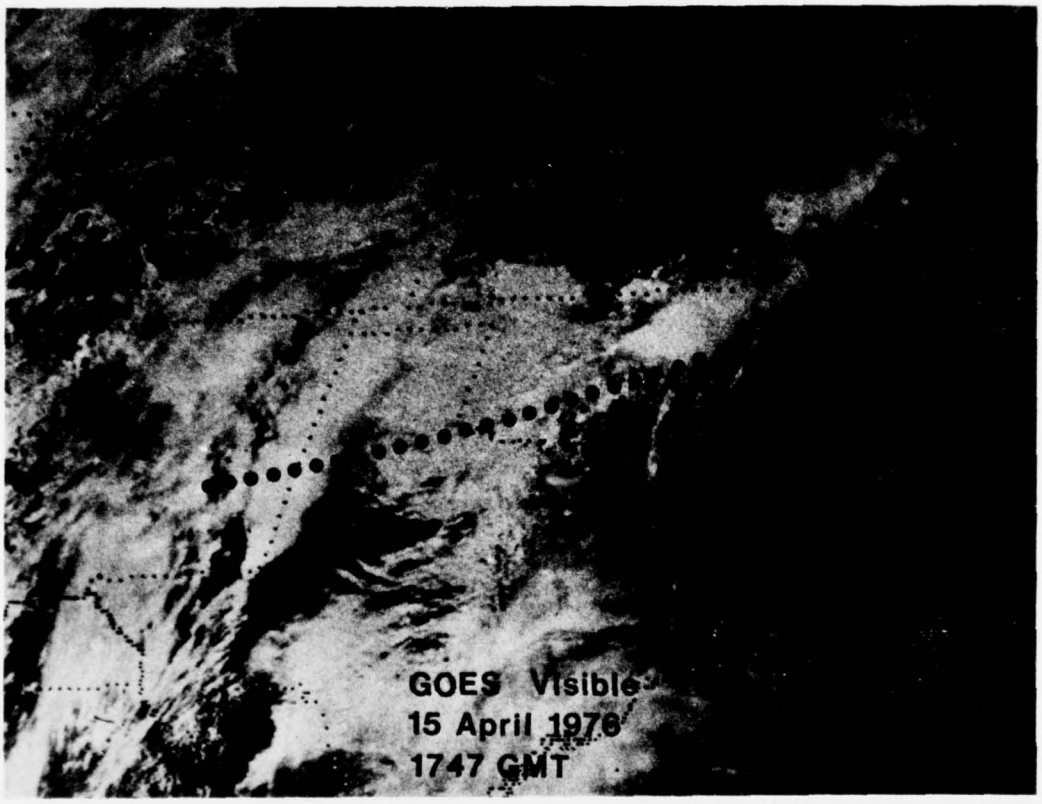

Figure 3.3.4. GOES visible image for the time nearest to the THIR data shown in Figure 3.3.3. The dotted line depicts the location of the individual scan swath.

Individual THIR scans were studied in order to examine the small scale variations of equivalent blackbody temperatures. Figure 3.3.3 shows an example of one swath of data across Oklahoma and Texas where convective and low level clouds were present. For comparison, a GOES visible image is shown in Figure 3.3.4 with the location of the individual THIR scan superimposed. Much detail was found in the THIR data because of the relatively high resolution compared to SCAMS.

It was interesting to note in Figure 3.3.3 that equivalent blackbody temperatures in the 11.5 μm channel were as much as 8°K colder than in the 6.7 μm channel in convective cloud regions near 96°W, 99°W, and 103°W longitudes. It is possible that the 6.7 μm water vapor channel detected moisture injected into the lower stratosphere by the convective activity. Water vapor above the tropopause would have a higher temperature than the cloud top temperatures detected by the 11.5 μm window channel. At higher temperatures and in the absence of inversions, the 11.5 μm equivalent blackbody temperatures are always warmer than the 6.7 μm temperatures. This was evident between 99° and 102°W longitudes in Figure 3.3.3.

REFERENCES

Corbell, R. P., C. J. Callahan, and W. J. Kotsch, Eds., 1977: The GOES/SMS User's Guide. NOAA/NASA Publication, Washington, D. C., 118 pp.

Cressman, G. P., 1959: An operational objective analysis system. Monthly Weather Review, 87, 367-374.

Feddes, R. G. and K. N. Liou, 1978: Atmospheric ice and water content derived from parameterization of Nimbus 6 High resolution infrared sounder data. J. Appl. Meteor., 17, 536-551.

Liou, K. N., T. L. Stoffel, R. G. Feddes and J. T. Bunting, 1978: Radiative properties of cirrus clouds in NOAA 4 VTPR channels: Some explorations of cloud scenes from satellites. Pure and Appl. Geophy., 116, No. 6, 1007-1029.

Liou, K. N. and A. D. Duff, 1979: Atmospheric liquid water content derived from parameterization of Nimbus 6 Scanning Microwave Spectrometer data. J. Appl. Meteor., 18, 99-103.

Liou, K. N., R. G. Feddes, T. L. Stoffel, G. C. Aufderhaar, 1977: Remote sounding of cloud compositions from NOAA 4 and Nimbus 6 infrared sounders. Final report, Air Force Geophysics Laboratory, AFGL-TR-77-0252.

MacDonald, A. E., 1977: On a type of strongly divergent steady state. Monthly Weather Review, 105, 771-785.

Staff Members, 1975: The Nimbus VI User's Guide. Goddard Space Flight Center, Greenbelt, Maryland, 227 pp.

emperature of the horizontal and
in the 37 GHz band from the ESMR
VI.

5